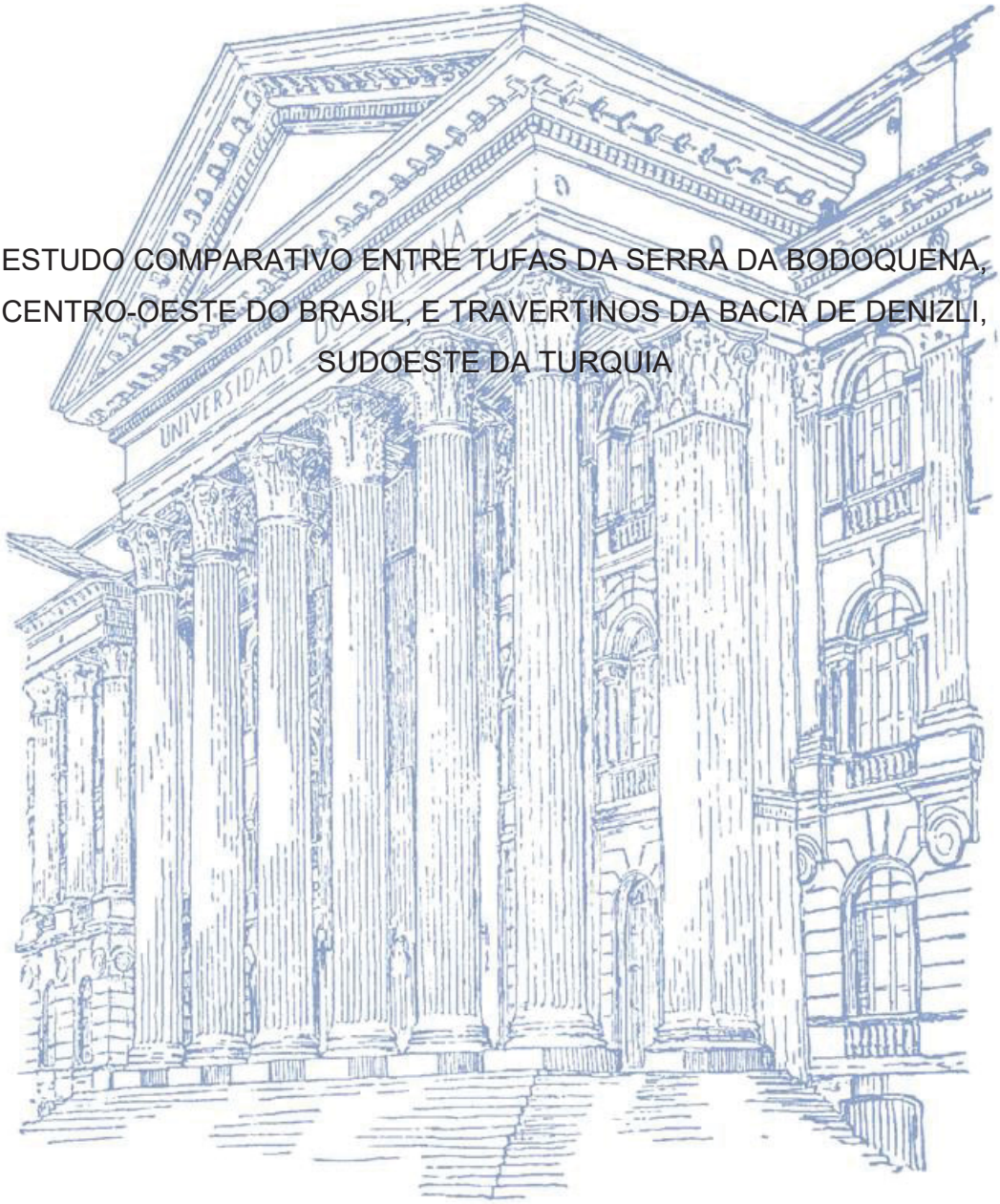
UNIVERSIDADE FEDERAL DO PARANÁ

VICTOR AMIR CARDOSO DORNELES



ESTUDO COMPARATIVO ENTRE TUFAS DA SERRA DA BODOQUENA, CENTRO-OESTE DO BRASIL, E TRAVERTINOS DA BACIA DE DENIZLI, SUDOESTE DA TURQUIA

CURITIBA

2021

VICTOR AMIR CARDOSO DORNELES

ESTUDO COMPARATIVO ENTRE TUFAS DA SERRA DA BODOQUENA, CENTRO-OESTE DO BRASIL, E TRAVERTINOS DA BACIA DE DENIZLI, SUDOESTE DA TURQUIA

Dissertação de Mestrado apresentada como requisito parcial à obtenção do grau de Mestre do Programa de Pós-graduação em Geologia, Setor de Ciências da Terra, Universidade Federal do Paraná.

Orientador: Dr. Ricardo Jorge Jahnert
Coorientador: Dr. Almério Barros França

CURITIBA

2021

Catalogação na Fonte: Sistema de Bibliotecas, UFPR
Biblioteca de Ciência e Tecnologia

D713e Dorneles, Victor Amir Cardoso
Estudo comparativo entre tufas da serra da Bodoquena, centro-oeste do Brasil, e travertinos da bacia de Denizli, sudoeste da Turquia [recurso eletrônico] / Victor Amir Cardoso Dorneles . – Curitiba, 2021.

Dissertação – Universidade Federal do Paraná, Setor de Ciências da Terra, Programa de Pós – Graduação em Geologia, 2021.

Orientador: Ricardo Jorge Jahnert. Coorientador: Almério Barros França.

1. Travertino. 2. Rochas. I. Universidade Federal do Paraná. II. Jahnert, Ricardo Jorge . III. França, Almério Barros. IV. Título.

CDD: 552.58

Bibliotecária: Vanusa Maciel CRB- 9/1928

TERMO DE APROVAÇÃO

Os membros da Banca Examinadora designada pelo Colegiado do Programa de Pós-Graduação GEOLOGIA da Universidade Federal do Paraná foram convocados para realizar a arguição da Dissertação de Mestrado de **VICTOR AMIR CARDOSO DORNELES** intitulada: **ESTUDO COMPARATIVO ENTRE TUFAS DA SERRA DA BODOQUENA, CENTRO-OESTE DO BRASIL, E TRAVERTINOS DA BACIA DE DENIZLI, SUDOESTE DA TURQUIA**, sob orientação do Prof. Dr. RICARDO JORGE JAHNERT, que após terem inquirido o aluno e realizada a avaliação do trabalho, são de parecer pela sua APROVAÇÃO no rito de defesa.
A outorga do título de mestre está sujeita à homologação pelo colegiado, ao atendimento de todas as indicações e correções solicitadas pela banca e ao pleno atendimento das demandas regimentais do Programa de Pós-Graduação.

CURITIBA, 24 de Setembro de 2021.

Assinatura Eletrônica
19/10/2021 13:58:43.0
RICARDO JORGE JAHNERT
Presidente da Banca Examinadora

Assinatura Eletrônica
19/10/2021 14:12:04.0
ANELIZE MANUELA BAHNIUK RUMBELSPERGER
Avaliador Interno (UNIVERSIDADE FEDERAL DO PARANÁ)

Assinatura Eletrônica
19/10/2021 13:38:14.0
PAULO CÉSAR BOGGIANI
Avaliador Externo (UNIVERSIDADE DE SÃO PAULO)

Documento assinado eletronicamente de acordo com o disposto na legislação federal Decreto 8539 de 08 de outubro de 2015.
Gerado e autenticado pelo SIGA-UFPR, com a seguinte identificação única: 120488
Para autenticar este documento/assinatura, acesse https://www.prppg.ufpr.br/siga/visitante/autenticacaoassinaturas.jsp e insira o codigo 120488

Dedico este trabalho à minha mãe, Marli.

AGRADECIMENTOS

À Universidade Federal do Paraná (UFPR) e ao Programa de Pós-Graduação em Geologia pela oportunidade de me formar Mestre em uma Universidade pública, gratuita e de qualidade, a qual vem mantendo a excelência acadêmica mesmo em tempos sombrios para a pesquisa e a ciência brasileira.

Aos meus orientadores Drs. Ricardo Jahnert e Almério França por toda a ajuda sobre os caminhos a seguir dentro desta pesquisa e por estarem sempre disponíveis para as discussões científicas.

À Coordenação de Aperfeiçoamento de Pessoal de Nível Superior - Brasil (CAPES) - Código de Financiamento 001, pelo apoio e concessão da bolsa de mestrado nos últimos seis meses.

Ao Projeto Microbial (Petrobras / FUNPAR-UFPR) pelo apoio financeiro da pesquisa, através de análises, viagem de campo e bolsa de mestrado.

Ao Instituto Laboratório de Análise de Minerais e Rochas (iLAMIR) pela infraestrutura e equipamentos disponibilizados e à equipe técnica pela prestatividade e auxílio nas análises.

À equipe da Estância Mimosa Ecoturismo de Bonito (MS), por todo o suporte e assistência durante a etapa de campo e coleta de amostras.

Ao Centro de Microscopia Eletrônica da UFPR (CME) pelo suporte técnico nas análises de Microscopia Eletrônica de Varredura.

Aos colegas da Geologia: Angela, Larissa, Kimberlym, Matheus, Midori e Rafaella, que me ajudaram em diversas etapas deste trabalho, seja por meio de mapas, fotografias, discussões ou auxílio em campo.

À minha mãe Marli, cujo o apoio e amor incondicional é a razão de tudo isso. Sem dúvidas qualquer caminho que eu escolher, por mais longo que seja, sempre será mais fácil de atravessar se eu tiver você por perto.

Aos amigos Gabriel, Giovana, Joana, Luís, Veleda e Wagner, obrigado por estarem comigo nesses dois anos e meio vivendo e sobrevivendo ao caos; obrigado pelos momentos prazerosos de descontrações e alívio mental.

Aos demais familiares e amigos que me apoiaram e torceram por mim.

RESUMO

Este trabalho tem como objetivo caracterizar as rochas carbonáticas de ambientes modernos de tufa e travertino, buscando compreender os processos de formação desses litotipos, além de identificar diferenças diagnósticas quanto ao conteúdo de microrganismos, microtexturas e suas assinaturas geoquímicas. A área de estudo das tufas foi o Rio Mimoso, Bonito, Brasil, enquanto que para os travertinos, a área de estudo foi a pedreira Faber, Denizli, Turquia. Foram descritas seções delgadas de tufas e travertinos para análises petrográficas; Microscopia Eletrônica de Varredura para a investigação de microtexturas e microrganismos; nos estudos geoquímicos, foram utilizadas as técnicas de Difratometria de Raios-X, Fluorescência de Raios-X e Isótopos Estáveis de Carbono e Oxigênio. Foram caracterizadas seis fácies de tufas e seis de travertinos. A principal diferença entre os litotipos de tufa e travertino está relacionada à presença de micrita na matriz. As fácies de travertino possui micrita primária e secundária, preenchendo os poros por micritização, garantindo menos porosidade para o travertino em comparação com a tufa. Além disso, dois tipos de micritas foram reconhecidos para fácies travertino: micrita maciça e peloidal. Em todas as fácies de tufas, foram identificadas organominerais como um produto da mineralização biologicamente influenciada. No entanto, para o travertino, apenas a fácies caliche e travertino junco apresentaram estruturas biogênicas associadas à organomineralização. Essas micro e nanoestruturas variam em tamanho e forma de acordo com o conteúdo de EPS presente na fácies. Em condições de baixo EPS, apenas esferoides nanométricos e tríades fibrosas foram formadas; notou-se que quanto mais EPS, mais desenvolvidos os produtos de organomineralização, como calcitas romboédricas lisas. Portanto, sugere-se que a produção de EPS é muito mais eficaz em sistemas de tufas do que em travertinos. Quanto ao fluido formador de tufas, os valores isotópicos de $\delta^{18}O$ corresponde a uma origem exclusivamente meteórica. Os valores isotópicos de $\delta^{13}C$ sugerem controle da fotossíntese neste sistema, dada a predominância de bactérias, algas e briófitas, além da influência de plantas C3. Os valores de $\delta^{18}O$ dos travertinos sugerem uma mistura do fluido como água meteórica aquecida por meio de fraturas e falhas, gerando um fluido termometeogênico. Os valores de $\delta^{13}C$ dos travertinos foram atribuídos quase que exclusivamente à fácies caliche, sugerindo uma maior influência da matéria orgânica, ou ainda, a ação da fotossíntese relacionada ao processo pedogenético. Por fim, os dados de DRX e FRX mostraram uma composição pura e restrita em ambos os sistemas, onde apenas calcita e quartzo foram identificados, sendo CaO e SiO_2 os principais óxidos. Os sistemas de tufas e travertinos representam importantes produtores de sedimentos carbonáticos no contexto de depósitos continentais.

Palavras-chave: carbonatos continentais, organomineralização, *spring deposits*

ABSTRACT

This work aims to characterize the carbonate rocks of modern environments of tufa and travertine, seeking to understand the formation processes of these lithotypes, in addition to identifying diagnostic differences regarding the content of microorganisms, microfabrics, and its geochemical signatures. The study area of the tufas was the Mimoso River, Bonito, Brazil. The travertine study area was the Faber quarry, Denizli, Turkey. Thin sections of tufa and travertine were described; the investigation of microfabrics and associated microorganisms was carried out by Scanning Electron Microscopy analysis; in the geochemical studies were used X-Ray Diffractometry, X-Ray Fluorescence and Carbon and Oxygen Stable Isotopes. Tufa and travertine were both characterized each with six facies. The main difference between tufa and travertine lithotypes is related to the presence of micrite in the rock matrix. Travertine facies have both primary and secondary micrite, this one filling pores by micritization, ensuring less porosity for travertine compared to tufa. In addition, two types of micrites have been recognized for travertine facies: massive micrite and granular peloidal. In all tufa facies, organomineral features were identified as a product of biologically influenced mineralization, such as smooth rhombohedral microcrystals and fibrous triads. However, for travertine, only caliche and reed travertine showed biogenic structures associated with organomineralization. These micro and nanostructures vary in size and shape according to the EPS content present in the facies. In conditions of low EPS, only nanometric spheroids and fibrous triads were formed; the more EPS, the more developed the products of organomineralization, such as smooth rhombohedral calcites. Therefore, it is suggested that EPS production is much more effective in tufa systems than in travertine. Concerning the tufa forming-fluid, the isotopic values of $\delta^{18}O$ it was found to be of exclusively meteoric origin. The isotopic values of $\delta^{13}C$ suggest control of photosynthesis in this system, given the predominance of cyanobacteria, algae and bryophytes, in addition to the influence of C3 plants. Travertine $\delta^{18}O$ values suggest that the fluid was meteoric water heated through fracture and fault infiltration, generating a thermo-meteogenic fluid. The $\delta^{13}C$ the negative values of travertines are attributed almost exclusively to Caliche facies, suggesting a greater influence of organic matter in this system, or even, the action of photosynthesis related to the pedogenic process. Finally, XRF and XRF data showed a pure and restrict composition in both systems, which only calcite and quartz were identified, and the main oxides presented were CaO and SiO2. Tufa and travertine systems represent important producers of carbonate sediments in the context of continental deposits.

Keywords: continental carbonates, organomineralization, spring deposits

LISTA DE FIGURAS

Figura 1 - Exemplos de ambientes deposicionais continentais não marinhos de carbonatos. Os carbonatos continentais se originam em ambientes terrestres e aquáticos sem influência marinha, podendo ser formados por processos abióticos ou bióticos, que os diferem em muitos aspectos dos carbonatos marinhos (Flugel, 2010). 18
Figura 2 - Mapa geológico e de localização da área de estudo das tufas do Rio Mimoso na fazenda Estância Mimosa, em Bonito, Brasil. 22
Figura 3 - Mapa de localização da bacia hidrográfica do Rio Formoso, na qual encontra-se inserido o Rio Mimoso, constituindo a área de estudo deste trabalho (Torres et al., 2006). 23
Figura 4 - Desenho esquemático mostrando os sítios de ocorrência de tufas da Estância Mimosa e a trilha de acesso aos afloramentos. Dez pontos de ocorrência de tufas ativas são encontradas ao longo do trecho do Rio Mimoso (em azul), além de depósitos inativos nas margens do rio. 24
Figura 5 - Mapa geológico e de localização da área de estudo dos travertinos na Bacia de Denizli. A Pedreira Faber encontra-se destacada em vermelho no quadro à direita, localizada à nordeste da cidade de Denizli, no sudoeste da Turquia (França et al., 2017). 26
Figura 6 - Pedreira Faber, local de amostragem do testemunho estudado neste trabalho, é uma das pedreiras de travertinos da região de Ballik, na Bacia de Denizli, que são exploradas atualmente (Foto: Almério França). 27
Figura 7 - Mapa geológico da porção sudoeste da Faixa Paraguai, mostrando o Domínio Sul-Mato-Grossense, composto por rochas do Grupo Corumbá que formam o Planalto da Bodoquena ao sul, localizado a sudeste da Planície do Pantanal (Oliveira, 2013). 30
Figura 8 - Seções verticais das sucessões carbonáticas da Serra da Bodoquena, na região da Faixa Paraguai, representada pela sequência 1 (pleistocênica) e sequência 2 (holocênica), cujo o topo apresenta ocorrências de tufas associadas ao sistema fluvial e de ressurgências (Modificado de Oliveira et al., 2017). 32
Figura 9 - Mapa de ocorrência da Formação Serra da Bodoquena, abrangendo a região do município de Bonito (Adaptado de Sallun Filho et al., 2009). 33
Figura 10 - Mapa de contexto geotectônico da região do Mar Egeu e oeste da Turquia (Alçiçek et al., 2007). A) localização da área de estudo em relação à Província Extensional da Anatólia Ocidental, mostrando as grandes estruturas tectônicas da região; B) Bacia de Denizli (polígono tracejado), situada à leste do *graben* Buyuk Menderes, identificado como BMB (Buyuk Menderes Basin), e demais grabens do sistema. 35
Figura 11 - Desenho esquemático do processo de formação dos depósitos de travertinos de Denizli através de fissuras e falhas, reativadas por atividades sísmicas locais, mostrando fluidos hidrotermais ascendentes (flechas vermelhas) e águas meteóricas (flechas brancas) que descem e percolam no subsolo, e se misturam (flechas laranjas) fornecendo águas ricas em íons de carbonatos oriundos

das rochas carbonáticas do embasamento da bacia que servem como rocha fonte (Adaptado de Ozkul et al., 2013). 37
Figura 12 - Mapa da região de Ballik, localizada a nordeste de Denizli, mostrando algumas pedreiras ativas de exploração dos travertinos, dentre elas a Pedreira Faber, as quais estão situadas em uma área dômica formada topograficamente devido aos prolongamentos dos mergulhos das falhas normais e transcorrentes que limitam a região do flanco norte do *graben* de Denizli (De Boever et al., 2016). ... 38
Figura 13 - Exemplos de depósitos ativos de tufas em corredeiras de água, formando barragens, cascatas e piscinas, associados a musgos, folhas e material vegetal transportado, na região norte da Itália (Adaptado de Perri et al., 2012). .. 39
Figura 14 - Imagem de microscópio eletrônico de varredura mostrando a influência de macro e microrganismos na precipitação mineral dos depósitos de tufas, tais como folhas, briófitas incrustadas, EPS e diatomáceas (Adaptado de Turner & Jones, 2005). 41
Figura 15 -Exemplo de construções de tufas precipitadas por ação de insetos aquáticos. Os casulos do estágio larval de insetos da família Philopotamidae (ordem Trichoptera), foram calcificados de forma in situ formando uma fácies de tufas (Plant, 2019). 42
Figura 16 -Modelos deposicionais de tufas apresentados por Pedley (1990), aplicáveis aos sistemas ativos ou inativos (Oste, 2017). 45
Figura 17 - Modelo de variação das assinaturas isotópicas de ^{13}C e ^{18}O em escala regional dos sistemas de precipitação de tufas (Andrews, 2006). 46
Figura 18 - Exemplos de depósitos ativos de travertinos de fonte hidrotermal associados a vulcanismo, como piscinas, barragens e terraços, em Mammoth Hot Spring, no Parque Nacional de Yellowstone, EUA (Fouke, 2011). 47
Figura 19 - Exemplos de depósitos microbianos gerando as fácies de travertinos de Mammoth Hot Spring (EUA), mostrando uma variedade de pigmentação e morfologia da microbiota associada às diferentes fácies (Adaptado de Fouke., 2011). 49
Figura 20 - Esquema unificado de classificação de travertinos proposto por Pentecost & Viles (1994), levando em conta critérios de geoquímica, morfologia e fábrica da rocha. 50
Figura 21 - Modelo de classificação de depósitos de travertinos da Bacia de Denizli, propostos por Ozkul et al., (2002), apresentando os cinco ambientes deposicionais e seus subambientes (França et al., 2017). 54
Figura 22 - Exemplos de amostras de tufa coletadas na Estância Mimosa, em Bonito (Brasil). A) amostra de depósito ativo, mostrando associação com folha de árvore; B) amostra de depósito inativo, essencialmente mais consolidada e com associação de diferentes fácies. 56
Figura 23 - Testemunho de travertinos amostrado na pedreira Faber, em Denizli, na Turquia, e utilizado no presente trabalho. Contém 28,5 m de material recuperado. 57

Figure 24 - Localization maps of the study areas. A) Image showing the Bodoquena Plateau and Estancia Mimosa, Brazil; B) Denizli city and the location of Faber quarry and Pamukkale travertine, Turkey. 67
Figure 25 - Different tufa morphologies in the Mimoso River. A) cascades, waterfalls, dams, and pools of different sizes in the same site, showing the deeper portions in the center of the pools, and shallow portions close to the edges; B) ramp deposit with carbonate mud deposition in the shallow portion of larger pools..... 72
Figure 26 - Travertine deposits identified within the quarries of the Denizli Basin. A) quarry wall showing deposits such as smooth ramps, waterfalls, and caves with stalactites (red narrows) formed by calcification of plant walls; B) the high-slope ramps with > 40º of slope, preserved pools and waterfalls; C) highlight the paleosol layer between the travertine layers; D) reeds that are common in the region and responsible for the formation of travertine reed lithofacies. (Photos by Almerio Franca) 74
Figure 27 - Tufa facies in the Mimoso River, Bonito, Brazil. A) bryophyte phytoherm tufa, active and in situ precipitation of bryophytes; B) tufa fabric reflecting the dendriform plant structure, interleaved with millimeter layers of micrite (red arrow); C) preservation of phylloides as original fine plant structure (dark organic matter) and the association of the micrite facies; D) tree phytoherm tufa, in situ precipitation of roots and trunks of superior vascular plants, located at the edge of rivers and waterfalls; E) mineral growth around woody material, that occurs as concentric layers or as shrubs (yellow arrow); F) thin concentric laminar growth around the woody material that decomposes, the thickness of the laminae may vary, followed by spatic palisade growth in a perpendicular direction; G) algal tufa, in situ occurrence of green algae which was calcified in shallow pools; H) algal tufa level lithified, showing excellent porosity; I) calcified green algae tallus with evident micrite trapping; J) bioherm tufa facies, outcrop showing the bioherm facies as a cluster of calcified larval tubes; K) the facies fabric with thin layers forming the tube walls, showing the difference in sizes of the larval cases in relation to root tubes or branches of bryophyte structure (yellow arrow); L) precipitation of organic tissues as sparite and microsparite, showing the exceptional preservation of the layered walls of the larval cases; M) micrite tufa, outcrop with micrite deposition on calcified bryophyte, forming a micrite crust; N) thick micrite tufa layer showing continuous internal lamination; O) sub-horizontal to horizontal laminar inner structure, with continuous and localized levels of palisade sparite growth; P) phytoclast tufa, active deposit of woody material where the facies formation occurs; Q) sample showing phytoclastic material, such as leaves, small trunks, and roots, trapped and calcified as phytoclast tufa facies; R) examples of phytoclasts such as fragments of bryophytes and other small calcified plants, leaf molds, basal sections of small trunks, roots, and associated organic matter. 80
Figure 28 - Travertine facies described from Faber quarry, Denizli, Tukey. A) micrite travertine, core sample showing the massive structure and predominant composition of micritic calcite; B) thin section overview of the facies showing dark and massive

micritic calcite; C) gastropod mold porosity preserved in micritic calcite matrix; D) granular travertine, core sample showing a granular facies texture with calcite granules created by filling pores; E) photomicrograph of overview showing the composition of dark peloid micrite as a rock framework and with microsparite surrounding, as a pore-filling cement; F) another type of micrite with a lumpy appearance and microsparite cement filling the dissolution pores totally or partially; G) reed travertine, core sample with phytoporosity represented by fragments of reeds in a living position (sub-vertical) and other round pores, possibly of charophytes or even reed roots, highlighting the calcified reed tube and preserved in a porous cavity; H) photomicrograph with an overview of the rock whose reed phytoclasts occur in a dark micritic matrix and microsparite cement, forming high phytoporosity of basal and longitudinal sections of their stems; I) highlighting oogonia phytoclasts, the reproductive organ of charophyte algae, whose mold was completely filled with sparite calcite, forming a mosaic cement, in addition to a pore by dissolution partially filled with calcite equant cement; J) caliche, in a core sample distinguishing micrite travertine lithoclasts reworked and cemented by a granular matrix with intense oxide percolation; K) photomicrograph with an overview of the rock composed of reworked material, with percolation of yellowish oxides within irregular pores; L) emphasis on vadose silt infiltrations, which are intercalated with dark micrite and sparite films filling fractures; M) pisolith travertine, core sample with glass lithoclasts of rounded and laminated circular pisoliths (red arrow); N) photomicrograph of the general view with a framework consisting of pisoliths and ooids, in a dark micrite matrix; O) emphasis on spherical pisolith with continuous internal laminae and carbonate lithoclast core; P) breccia, core sample whose framework is composed of angular clasts and supported by the granular micritic matrix; Q) photomicrograph showing a micritic and massive matrix supporting the framework of angular grains of carbonate lithoclasts from other facies or reworked; R) framework composed of angular lithoclasts of varying sizes, the interparticle porosity is preserved without effective posterior cementation, in addition to the preservation of the pisolith clast, in a matrix-supported by the framework, an occurrence located in the facies. 86

Figure 29 - SEM images from tufas facies microfabrics and biological contents associated. A) fossil remains of filamentous bacteria (yellow arrow) and EPS largely disseminated in the tufa facies; B) well-developed calcite microcrystal as triangular polyhedral shape, neoformed by the coalescence of nanocrystals (yellow line highlighted), and the association of this facies with diatoms in the Bioherm Tufa; C) anhedral calcite grains showing not completed development of the crystal in the tree Phytoherm Tufa; D) nanocrystals of tetrahedrons (yellow highlight) in a coalescence process to form a larger rhombohedral crystal in the Bryophyte Phytoherm Tufa; E) basal section of the microtubes in Bryophyte Phytoherm Tufa, due to the probable decomposition of organic matter vegetable; F) tree phytoherm facies showing a rich content of fossil EPS and mucus-like material; G) calcified algal tallus in algal tufa, with organominerals formed by on the algae organic tissue, besides the trapping

neoformed rhombohedral micrite crystals and diatoms (yellow arrow); H) imprint of cyanobacteria on microsparite crystals and hollow microtubes in the Micrite Tufa, an evidence of the activity of filamentous cyanobacteria in pools where this facies was deposited; I) larval cases with its inner layers preserved in the Bioherm Tufa Facies, suggesting that the silk excreted by the organism also serves as an organic matrix for organomineralization; J) calcite grains forming the layers of the larval cases, with similar sizes and subhedral to euhedral shapes of soft rhombohedrons with an internal triangular structure; K) microcolumns formed by coalescence of calcite nanospherulites in the Bioherm Tufa Facies; L) trapped diatoms between calcite micrite grains as an ubiquitous content in the bioherm tufa, but they also occur on other facies. 90
Figure 30 - SEM images from travertine facies microfabrics and some biological contents associated. A) densely packed cryptocrystalline micrite aphanitic to sub-aphanitic slightly laminated texture, in the Micrite Travertine Facies; B) granular micrite, with grain size ranging from 1 to 2 μm, that occurs in the micrite and pisolith travertine; C) peloid as another type of micrite (pl) in Travertine Facies, occurring in the Granular Travertine, as rounded grains reaching up to 222 μm in diameter, surrounded by sparry calcite filling the pore spaces; D) pores partially filled with secondary crystals of calcite equant in the Granular Travertine Facies; E) total filling pores with mosaic sparry calcite cement, also in the Granular Travertine Facies and in the Micrite Travertine; F) acicular microsparry calcite crystals of about 5 μm long, in the Granular Travertine Facies; G) best-developed organomineral in the Reed Travertine Facies as euhedral crystal of rhombohedral calcite neoformed by the junction of smaller triangular polyhedrons, identified as the internal structure of the larger crystals (yellow highlighted); H) structures of calcified charophyte algae, such as the tallus and the algae reproductive organ, showing exceptional preservation in the Reed Travertine Facies; in the Caliche Facies there is the occurrence of I) clusters of neoformed calcite nanospheres in an organic matrix, which will coalesce to form larger structures, such as pinnacles, J) pseudo microcolumns, and fibrous triads, but without the formation of larger and well-defined crystals; K) possible fossils of coccoid bacteria, characterized by colony-like aggregates of ovoid and spherical carbonate nanocrystals, forming a distributed granular viscous texture irregularly on the crystal surface; L) bacterial rods as isolated solid calcite tubes and associated with mucus-like material. 93
Figure 31 - Geochemical analysis data. A) and B) graphs with the oxide contents obtained by X-ray fluorescence, with values presented in an ascending order of the CaO content, the main chemical component found in both tufa and travertine samples, and the volatile content was calculated based on the loss to fire, and the composition of trace oxides was not considered; C) and D) X-ray diffraction results, with the main mineral phases found in the samples of both lithotypes, calcite and quartz, which have an inversely proportional relationship, so that calcite occurs mostly in facies where there is a decrease in quartz content. 96

Figure 32 - Carbon and oxygen stable isotope data. Tufas from the Mimoso river showed negative ranges for either $\delta^{13}C$ and $\delta^{18}C$ values; whilst travertines from the Faber quarry presented $\delta^{13}C$ signature lightly enrichment only in the caliche facies, and also a negative range for $\delta^{18}O$..... 98
Figure 33 - Comparison between tufa and travertine active systems. Tufa deposits in the Mimoso River are controlled by the river bed geometry, showing a width of tens of meters, while the travertine deposits in Pamukkale correspond to the pre-existing relief, covering hundreds of meters in extension. 101
Figure 34 - Hand samples of tufas from the Mimoso River showing the massive association of facies on centimeter scales, identified in most of the collected samples. 102
Figure 35 - Representative vertical section of the Faber core, in the scale of 1:200, showing the great intercalation of the travertine facies described in the quarry. . 104
Figure 36 - Tufas from the Mimoso River showing plant material such as A) leaf mold, from which microsparite crystals grow; and B) bryophytes calcified also by precipitation of microsparite from the remaining organic filaments, slightly obliterating the porosity of the rock. Travertine facies reed from Faber quarry with C) reed and charophyte algae remain surrounded by microsparitic cement completely filling the pores; and D) travertine facies with reed mold in basal and transversal cut, partially filled with microsparite, in addition to micrite forming the rock matrix (upper left portion of the thin section). 108
Figure 37 - Types of cement in the Faber travertine facies. A) dog-tooth cement, in which equant calcite crystals grow perpendicular to the pore wall surface, in plane-polarized light; B) image with crossed polarizers; C) fibrous to acicular calcite cement partially filling pores of the Travertine Reed Facies, in plane-polarized light; D) image with crossed polarizers; E) pore completely filled with mosaic-type cement, in Granular Travertine Facies, in plane-polarized light; F) image with crossed polarizers.…..... 111
Figure 38 - Occurrences of shrub structures in tufas and travertines of the present study. A-B) examples of tree phytoherm tufa facies shrubs in the Mimoso River as ray-crystal crusts, in which the radial development of the crystals takes place on remain organic matter; C-D) in Faber travertines only the Caliche Facies present the incipient occurrence of bacterial shrubs, with precipitation mediated by microbes. 112
Figure 39 - Bioherm Tufa Facies of the Mimoso River. A-B) aquatic insects in their immature stage as larvae that live fixed in the substrate, the yellow arrow indicates the beginning of the construction of a single larval case; the white arrows show the dense community of larval insects living fixed and submerged in waterfalls, with emphasis on cases in early stages of formation in the area demarcated with a dashed line; C) inactive deposit in the Mimoso River with densely compacted Bioherm Tufa; D) active occurrence of Bioherm Tufa in waterfall showing a spare arrangement. 114

Figure 40 -Comparison of the main organomineralization products of the tufas and travertines facies. A) gentle rhombohedral calcite formed in Bioherm Tufa Facies, showing tetrahedrons (highlighted) as a remnant structure of grain coalescence; B) neoformed crystal in Bryophyte Phytoherm Tufa Facies, in which, despite being large, it is not well developed as a polyhedron; highlighting the association of EPS and filaments (yellow arrow) around the crystal; C) calcite nanospheres in caliche facies, as the initial product of organomineralization in an organic matrix; D) pseudo fibrous triads neoformed by the coalescence of nanospheres also in the travertine Caliche Facies, but without forming larger crystals. 117

LISTA DE TABELAS

Tabela 1 - Classificação das fácies de tufas conforme a origem dos depósitos, proposto por Pedley (1990). 43
Tabela 2 - Litofácies de travertinos da região de Denizli, descritas por Ozkul et al. (2002). 52
Table 3 - Classification of tufa facies by Pedley (1990) and its adaptations related to the present study, including the bioherm facies of Leggitt & Cushman (2001). 76
Table 4 - Travertine classifications from literature, and adaptations related to this study. 82
Table 5 - Comparison of tufas from Mimoso River and travertines from Faber quarry, according to the parameters analyzed in this study, following a decreased scale. 106

SUMÁRIO

CAPÍTULO 1 – INTRODUÇÃO ... 18
1.1 CONTEXTO E PROBLEMA ... 18
1.2 JUSTIFICATIVA ... 19
1.3 OBJETIVOS ... 20
1.4 ESTRUTURA DA DISSERTAÇÃO ... 21
CAPÍTULO 2 – FUNDAMENTAÇÃO TEÓRICA ... 21
2.1 ÁREAS DE ESTUDOS ... 21
2.1.1 Estância Mimosa, Bonito (Brazil) ... 21
2.1.2 Pedreira Faber, Denizli (Turquia) ... 25
2.2 CONTEXTO GEOLÓGICO ... 28
2.2.1 Tufas da Serra da Bodoquena ... 28
2.2.2 Travertinos da Bacia de Denizli ... 33
2.3 ESTADO DA ARTE ... 39
2.3.2 Tufas ... 39
2.3.3 Travertinos ... 46
CAPÍTULO 3 – MATERIAIS E MÉTODOS ... 55
3.1 AMOSTRAGEM ... 56
3.2 MICROSCOPIA ELETRÔNICA DE VARREDURA ... 58
3.3 DIFRATOMETRIA DE RAIOS X ... 59
3.4 FLUORESCÊNCIA DE RAIOS X ... 59
3.5 ISÓTOPOS ESTÁVEIS DE CARBONO E OXIGÊNIO ... 60
CAPÍTULO 4 – RESULTADOS E DISCUSSÕES ... 61
PETROGRAPHIC AND GEOCHEMISTRY CRITERIA FOR DISTINGUISHING TUFAS AND TRAVERTINES: CASE STUDY OF BODOQUENA PLATEAU, BRAZIL, AND DENIZLI BASIN, TURKEY ... 61
ABSTRACT ... 61
INTRODUCTION ... 62
LOCATIONS AND GEOLOGICAL SETTING ... 65
METHODS ... 69
RESULTS ... 70

SITE DESCRIPTIONS 70
TUFAS FACIES 74
TRAVERTINES FACIES 81
MICROFABRICS 88
GEOCHEMICAL ANALYSIS 94
DISCUSSIONS 98
MORPHOLOGY OF THE ACTIVE DEPOSITS 98
COMPARISON BETWEEN TUFAS AND TRAVERTINES FACIES 105
ORGANOMINERALIZATION PROCESSES AND ITS INFLUENCE IN THE TUFAS AND TRAVERTINES MICROFABRICS 115
GEOCHEMICAL CONDITIONS OF THE TUFAS AND TRAVERTINES FORMATION 119
CONCLUSIONS 123
ACKNOWLEDGMENTS 124
CAPÍTULO 5 - CONSIDERAÇÕES FINAIS 125
REFERÊNCIAS 127

CAPÍTULO 1 – INTRODUÇÃO

1.1 CONTEXTO E PROBLEMA

Os carbonatos continentais englobam os espeleotemas, calcretes, calcários lacustres, tufas e travertinos, e são principalmente precipitados sob condições subaéreas de águas ricas em bicarbonato de cálcio, carbonato e cálcio, sem influência marinha (Gandin & Capezzuoli, 2008; Flugel, 2010; Capezzuoli et al., 2014). São rochas com uma grande variedade de configurações deposicionais e diagenéticas (Figura 1), portanto, entender os processos de formação desses carbonatos facilita o reconhecimento e a delimitação de suas fácies (Flugel, 2010).

Dentre os processos de formação de carbonatos continentais têm-se principalmente a desgaseificação de CO_2, causada pela variação na temperatura, pressão e turbulência da água; a concentrações de íons de bicarbonato e carbonato de cálcio; e atividades biológicas indutoras e influenciadoras da precipitação (Chafetz & Folk, 1984; Pedley, 1990; Pentecost, 1993; Pedley et al., 2009).

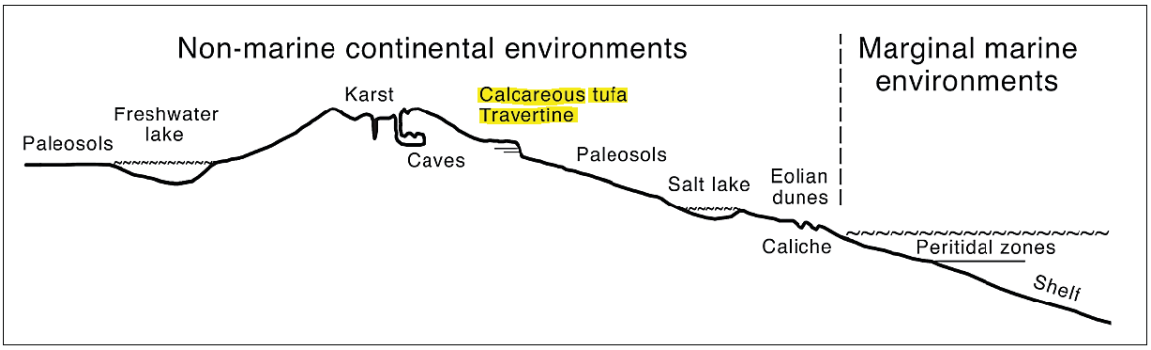


Figura 1 - Exemplos de ambientes deposicionais continentais não marinhos de carbonatos. Os carbonatos continentais se originam em ambientes terrestres e aquáticos sem influência marinha, podendo ser formados por processos abióticos ou bióticos, que os diferem em muitos aspectos dos carbonatos marinhos (Flugel, 2010).

Os eventos de deposição desses tipos de carbonatos possuem curta duração no registro geológico, entretanto, são capazes de transformar rapidamente a paisagem e influenciar na geomorfologia (Ford & Pedley, 1996). Os processos

abióticos e bióticos de acumulação são responsáveis por uma rápida taxa deposicional, variando em escala de milímetros a centímetros por ano, para tufas, e de centímetros a metros por ano, para travertinos (Capezzuoli, et al., 2014).

Travertinos e tufas são termos amplamente utilizados para designar os carbonatos lacustres e fluviais de água doce, todavia, a dificuldade de distinção entre estas rochas existe há muitas décadas (Pentecost & Viles, 1994; Claes et al., 2015). Os travertinos são referidos comumentemente como precipitados em águas quentes (acima de 30ºC, podendo exceder 60ºC) de origem hidrotermal. Em contrapartida, as tufas são precipitados de águas em temperatura ambiente, geralmente em torno de 20ºC (Pedley, 1990; Ford & Pedley, 1996; Pedley, 2009; Capezzuoli et al. 2014). Algumas variações ocorrem quando a temperatura do fluido formador decresce na medida que se distancia da fonte hídrica, resultando assim em depósitos proximais de travertinos e depósitos distais de tufas, em um mesmo sistema (Claes et al., 2015).

Portanto, a comparação de litofácies e isotópicas de carbono e oxigênio relacionadas aos depósitos ativos ainda conectados com a água e o sistema de origem, podem fornecer critérios para a identificação litológica inequívoca de suas contrapartes fósseis de modo que sejam facilmente detectados, mesmo em escala de campo, como tufas, se controladas pelo clima, ou travertinos, controlados por processos tectônicos (Gandin & Capezzuoli, 2008). Além disso, aspectos como textura, mineralogia, geoquímica, a associação com a biota e a química das águas de formação, bem como o contexto geomorfológico, hidrológico e tectônico devem ser considerados, sobretudo em estudos de caracterização de depósitos antigos de carbonatos continentais (Capezzuoli et al., 2014).

1.2 JUSTIFICATIVA

As tufas e travertinos tem apresentado uma grande importância para os estudos paleoclimáticos ao longo das últimas décadas (Capezzuoli et al., 2014), bem como uma notável relevância geoturística devido ao seu valor paisagístico (Boggiani et al., 2002). Os carbonatos continentais podem ainda configurar

importantes reservatórios para óleo e gás devido a sua alta porosidade e permeabilidade, portanto, a compreensão dos sistemas modernos de precipitação de carbonatos é aplicável na interpretação dos ambientes e o modelo de distribuição destes depósitos (Terra et al., 2010; Wright, 2012; Della Porta, 2015).

Desde a descoberta da seção Pré-sal na margem continental brasileira, cujos reservatórios de idade Aptiana foram descritos, em parte, como travertinos e tufas, expandiu-se o interesse em melhor conhecer a gênese e distribuição destas rochas carbonáticas precipitadas em sistemas modernos para utilizá-los como análogos aos reservatórios petrolíferos de subsuperfície (Wright, 2012).

A caracterização de reservatórios carbonáticos continentais é dificultada, uma vez que amostras de subsuperfície são pontuais e localizadas, e podem apresentar características litológicas semelhantes em macro e mesoescala. Dessa maneira, surge a necessidade de um estudo comparativo detalhado, em micro e nanoescala, a fim de contribuir para a distinção e aprimoramento do conhecimento acerca desses litotipos.

1.3 OBJETIVOS

O presente trabalho tem como **objetivo geral** caracterizar as rochas carbonáticas oriundas de ambientes modernos de tufas e travertinos, buscando entender a gênese e os processos de formação desses litotipos, além de investigar a influência orgânica na precipitação mineral destes depósitos e sua relação com a porosidade e a textura das fácies

Em vista disso, os **objetivos específicos** são:

a) Definir as fácies de ambos os sistemas deposicionais;
b) Determinar a composição mineralógica, as formas e arranjos cristalinos;
c) Caracterizar as diferentes microtexturas;
d) Investigar a presença de biofilmes, substâncias exopoliméricas (EPS) e microrganismos, como influenciadores da precipitação;
e) Interpretar as características geoquímicas dos precipitados.

1.4 ESTRUTURA DA DISSERTAÇÃO

A presente dissertação foi dividida em cinco capítulos descritos a seguir. O Capítulo 1 é correspondente à parte introdutória da pesquisa, como conceitos sobre os objetos de estudo, a justificativa da pesquisa e os objetivos propostos. Ao Capítulo 2 foi reservado as informações necessárias como base teórica para esse trabalho, como a caracterização das áreas de estudo, o contexto geológico regional e o estado da arte a respeito das tufas e travertinos. No Capítulo 3 foram discutidos os materiais, métodos e técnicas utilizados neste estudo. Enquanto que o Capítulo 4 apresenta os principais resultados e as discussões da pesquisa, elaborado em formato de artigo, no qual será discutido as diferenças e semelhanças entre os sistemas de tufas e travertinos, bem como o registro da ocorrência da fácies de tufa bioerma, descrita pela primeira vez nos depósitos da Serra da Bodoquena em Bonito, no Brasil. Por fim, o Capítulo 5 traz algumas considerações finais desta pesquisa de mestrado, reiterando as principais conclusões obtidas.

CAPÍTULO 2 – FUNDAMENTAÇÃO TEÓRICA

2.1 ÁREAS DE ESTUDOS

2.1.1 Estância Mimosa, Bonito (Brazil)

A área de estudo das tufas situa-se em um trecho do Rio Mimoso, localizado na fazenda Estância Mimosa Ecoturismo, no município de Bonito, estado do Mato Grosso do Sul, no Brasil (Figura 2). Coordenadas UTM da área: 7.679.706.09 S e 550.289.44 O (WGS84). O acesso ao local pode ser feito a partir da rodovia MS-382 e depois MS-345, vindo do Sul, ou pela rodovia MS-345, pelo Norte, além das estradas locais.

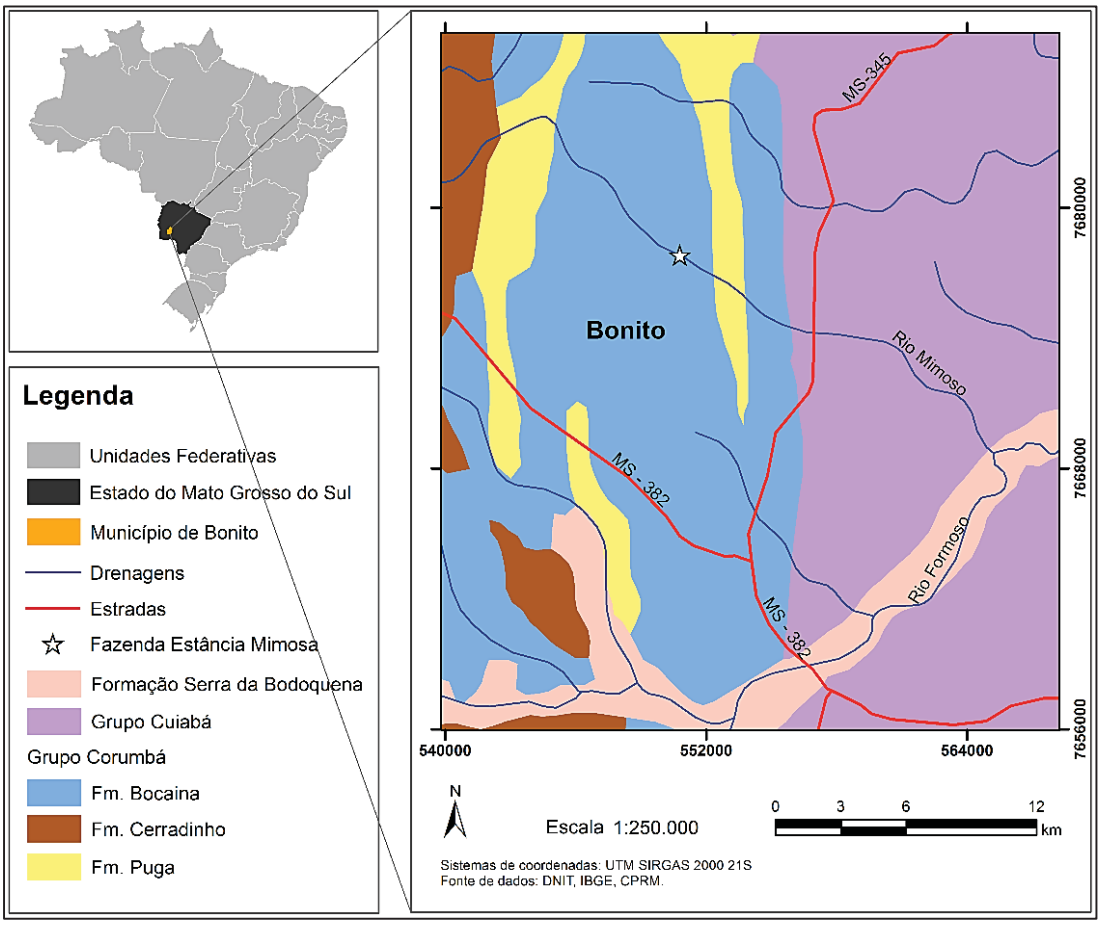


Figura 2 - Esquema geológico e de localização da área de estudo das tufas do Rio Mimoso na fazenda Estância Mimosa, em Bonito, Brasil.

O Rio Mimoso tem seu curso principalmente para sudeste como o principal afluente do Rio Formoso, e situa-se sobre um relevo cárstico ondulado, formado pela serra da Bodoquena (Torres et al., 2006; Sallun Filho & Karmann, 2007). A bacia do Rio Formoso está inserida na sub-bacia do Rio Miranda, a qual juntamente com outras seis sub-bacias formam a grande Bacia Hidrográfica do Rio Paraguai, que drena toda a extensão do Pantanal Sul-mato-grossense (Figura 3).

No trecho em que o Rio Mimoso percorre uma área de desníveis de aproximadamente 150 m, o relevo acidentado com presença de cascatas e cachoeiras promove a precipitação de tufas, a partir de águas ricas em íons de carbonato provenientes das rochas carbonáticas proterozóicas do Grupo Corumbá subjacentes (Sallun Filho et al., 2009).

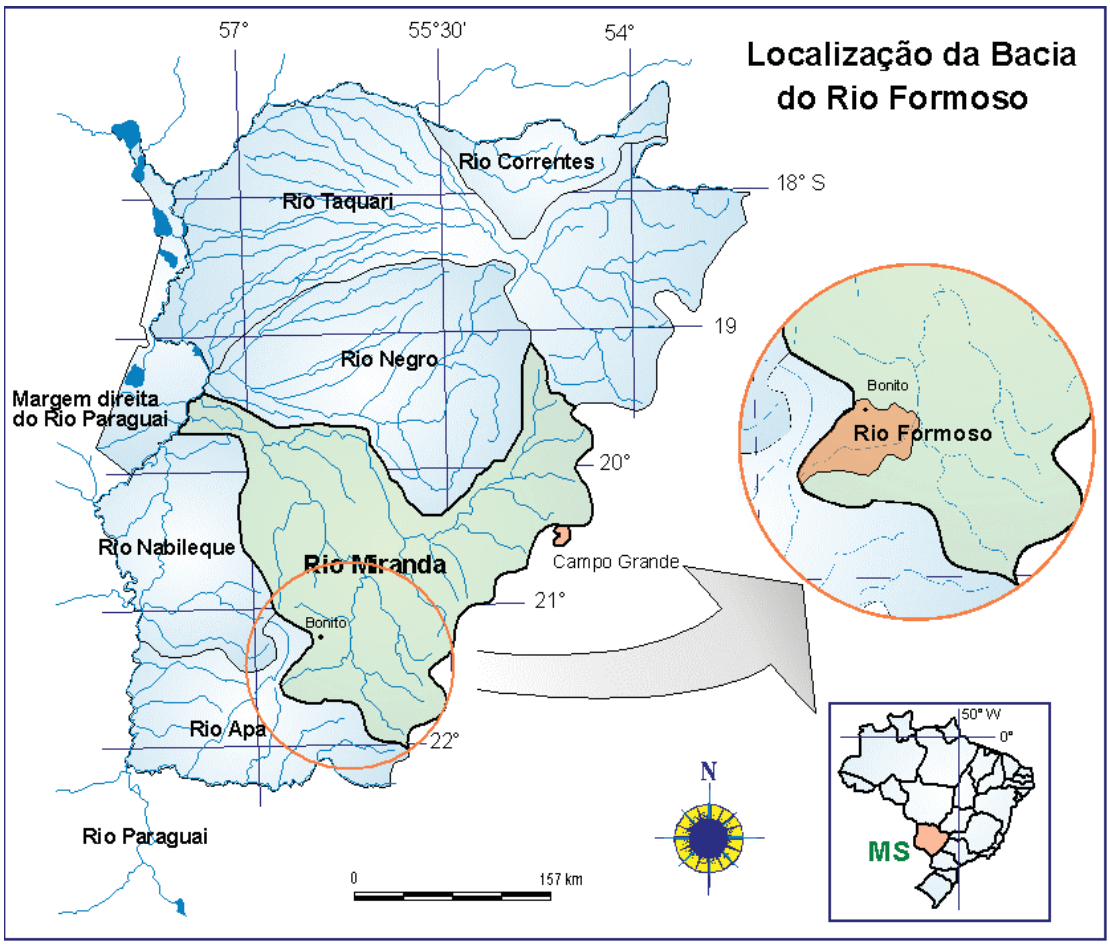


Figura 3 - Mapa de localização da bacia hidrográfica do Rio Formoso, na qual encontra-se inserido o Rio Mimoso, constituindo a área de estudo deste trabalho (Torres et al., 2006).

Na Estância Mimosa são encontradas uma série de cachoeiras dispostas em um trecho de 2 km onde ocorrem tufas ativas nas drenagens e inativas nas margens, as quais podem ser acessadas por uma trilha construída para atividade turística (Figura 4).

Em campanha de campo realizada setembro de 2019, durante a estação seca da região, as quedas de água apresentavam menor fluxo e o nível do rio encontrava-se baixo. O pH da água do Rio Mimoso no trecho estudado variou de 8,1 a 8,5, com temperatura média de 24º C e alta concentração de íons.

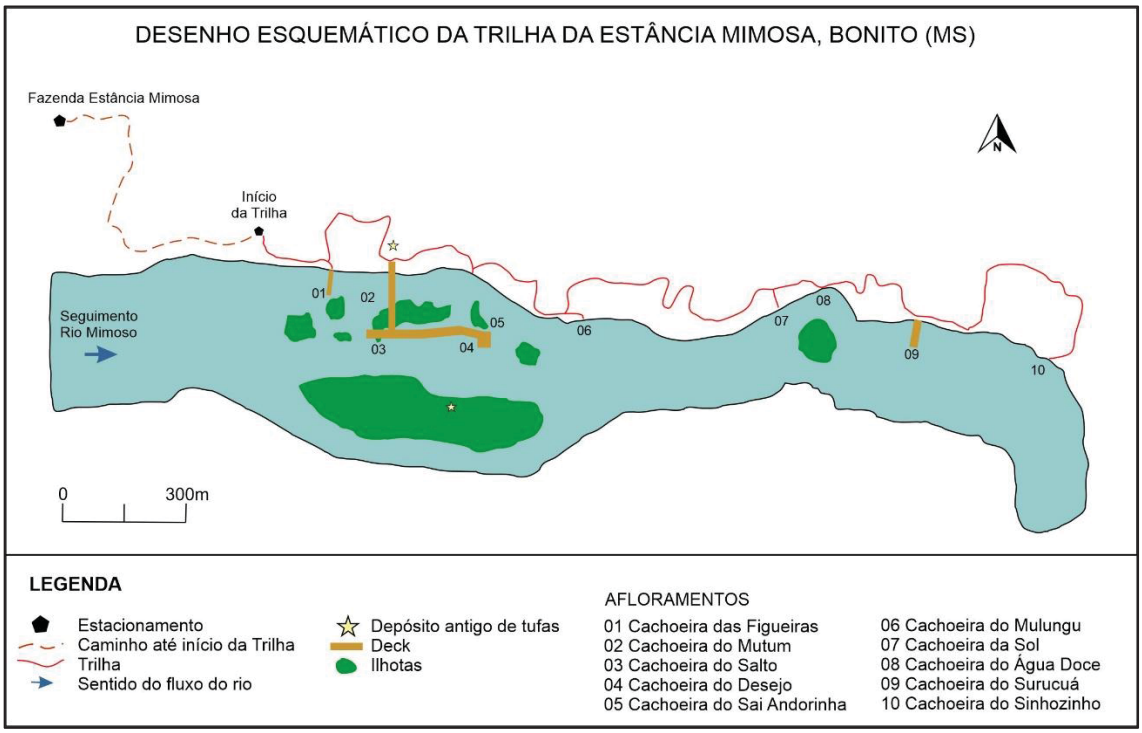


Figura 4 - Desenho esquemático mostrando os sítios de ocorrência de tufas da Estância Mimosa e a trilha de acesso aos afloramentos. Dez pontos de ocorrência de tufas ativas são encontradas ao longo do trecho do Rio Mimoso (em azul), além de depósitos inativos nas margens do rio.

A área de estudo está inserida no Parque Nacional Serra da Bodoquena, com área de 76.400 hectares, foi criado no ano de 2000, como forma de proteger um dos últimos remanescentes da vegetação de mata estacional semidecídual, no Planalto da Bodoquena, bem como os reservatórios subterrâneos de água, que brotam em diversas ressurgências cársticas e são fundamentais para a manutenção das condições ambientais, preservação da biodiversidade e preservação das tufas da Serra (Boggiani et al., 2002).

As tufas do Rio Mimoso foram descritos pela primeira vez por Almeida (1965), e os depósitos de tufas da Serra da Bodoquena foram registrados como um dos sítios Geológico e Paleontológico do Brasil (Boggiani et al., 2002). Posteriormente, os referidos depósitos foram estudados por Sallun Filho et al. (2009) para proposta de definição da Formação Serra da Bodoquena. Por fim, trabalhos mais recentes realizados nas tufas do Rio Mimoso focaram na caracterização palinológica e

quimioestratigráfica (Oste et al., 2018); além da investigação dos controles ambientais e deposicionais na formação desses depósitos (Oste et al., 2021).

2.1.2 Pedreira Faber, Denizli (Turquia)

A área de estudos de travertinos foi a Pedreira Faber, local de amostragem dos testemunhos usados no presente trabalho, a qual localiza-se a nordeste da cidade de Denizli, província homônima, no sudoeste da Turquia (Figura 5). As coordenadas UTM da área são 4.193.476.64 N e 705.736.74 E (WGS84).

Os depósitos de travertinos da Pedreira Faber estão inseridos no contexto deposicional da Bacia de Denizli, a qual ocupa uma área total de cerca de 100 km^2 de depósitos antigos e recentes, cujas espessuras podem chegar até 60 m (Ozkul et al., 2002). Os travertinos daquela região apresentam grande importância para o estudo desses sistemas carbonáticos, pois são acessíveis aos pesquisadores.

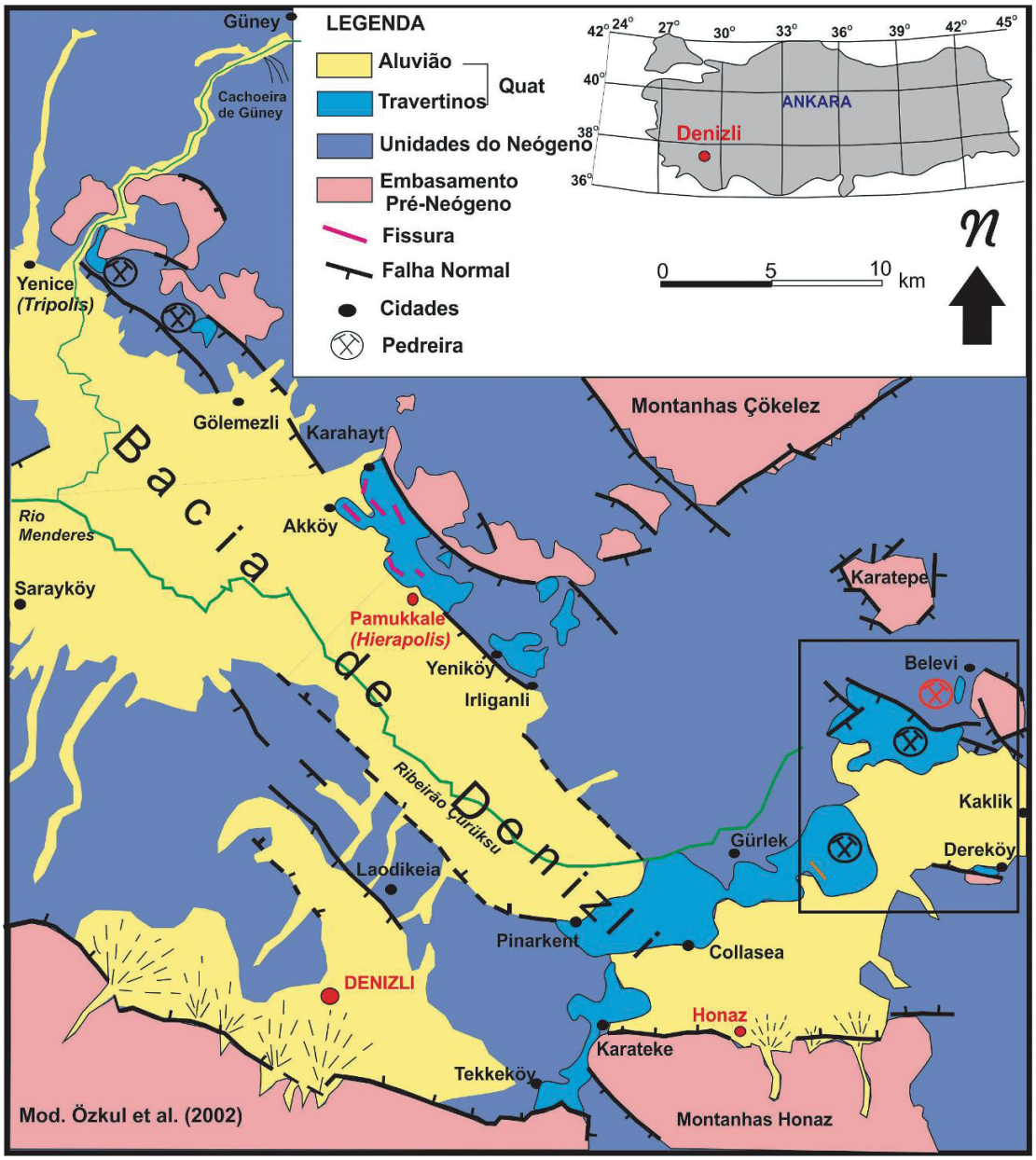


Figura 5 - Mapa geológico e de localização da área de estudo dos travertinos na Bacia de Denizli. A Pedreira Faber encontra-se destacada em vermelho no quadro à direita, localizada à nordeste da cidade de Denizli, no sudoeste da Turquia (França et al., 2017).

Os depósitos mais antigos são explorados em uma área de pedreiras ativas, principalmente nas proximidades das cidades de Kaklik e Kocabas, por empresas de marmoraria (Ozkul et al., 2013; Claes et al., 2015). A pedreira Faber tem dimensões de cerca de 200 m de comprimento e 400 m de largura, com

aproximadamente 70 m de altura, apresentando excelente condição de exposição em larga escala, devido às atividades de escavação (Figura 6).



Figura 6 - Pedreira Faber, local de amostragem do testemunho estudado neste trabalho, é uma das pedreiras de travertinos da região de Ballik, na Bacia de Denizli, que são exploradas atualmente (Foto: Almério França).

Os travertinos da província de Denizli são mundialmente reconhecidos principalmente pelas ocorrências modernas de Pamukkale, onde a atividade turística é amplamente desenvolvida devido aos seus extraordinários depósitos de carbonatos brancos em forma de piscinas e terraços (Altunel & Hancock, 1993; Erten et al., 2005), cuja temperatura média das águas é de 35,20 °C e pH 6,67.

Especificamente na Pedreira Faber, os trabalhos científicos se iniciaram com a descrição e datação de fósseis de mamíferos encontrados na pedreira (Erten et al., 2005) e usados na investigação da idade dos depósitos de travertinos de Denizli. Recentemente, a pedreira foi bastante estudada visando a caracterização de litofácies e reconstruções sedimentológicas (Claes et al., 2015); a compreensão dos controles genéticos sobre a arquitetura deposicional (De Boever et al., 2016);

estudos petrofísicos e classificação de porosidades (Claes et al., 2017); e ainda, em reconstruções tectônicas da região com base na análise estrutural das feições deformacionais rúptil dos depósitos da pedreira (Van Noten et al., 2013; 2019).

2.2 CONTEXTO GEOLÓGICO

2.2.1 Tufas da Serra da Bodoquena

O Planalto da Bodoquena é uma feição geomorfológica localizada a sudeste da Planície do Pantanal, apresentando altitudes de até 800 m, e comprimento de cerca de 200 km com alongamento norte-sul (Boggiani et al., 2002; Sallun Filho et al., 2004; Sallun Filho & Karmann, 2007; Sallun Filho et al., 2009). O relevo da Bodoquena caracterizado por escarpas a oeste e leve inclinação a leste, onde transiciona para a planície de inundação do Rio Miranda, foi influenciado pelas estruturas tectônicas da Faixa Paraguai (Boggiani et al., 2002; Sallun Filho et al., 2004; Sallun Filho & Karmann, 2007).

A Faixa Paraguai compreende o segmento sudoeste do Sistema Orogênico Tocantins, estendendo-se entre os estados de Mato Grosso e Mato Grosso do sul, às margens do Cráton Amazônico (Hasui, 2012). A porção sul da Faixa Paraguai é definida pelo Domínio Sul-Mato-Grossense, com direção NNW, onde se expõe entre o limite da bacia do Pantanal e bacia do Paraná (Figura 7).

As rochas metamórficas de baixo grau neoproterozoicas do Cinturão de Dobramentos Paraguai compõem ainda o embasamento da Planície do Pantanal, esta por sua vez encontra-se localizada na margem esquerda do Rio Paraguai, e faz parte da bacia hidrográfica do Rio Paraguai, sendo delimitada por uma série de planaltos denominados de Serras Residuais do Rio Paraguai, dentre eles o Planalto da Bodoquena (Assine, 2004; Assine & Soares, 2004).

Assine & Soares (2004) propuseram que, além das mudanças climáticas e da dinâmica sedimentar, outro fator que condiciona a sedimentação e a inundação da Planície do Pantanal é a atividade tectônica associada às tensões derivadas do contexto andino do *foreland*. Além disso, a paisagem pantaneira tem sido

modificada desde o final do Pleistoceno devido às mudanças paleoclimáticas e paleogeográficas registradas, como a instalação de um ambiente mais quente e úmido no Holoceno.

A principal exposição do Domínio Sul-Mato-Grossense da Faixa Paraguai é o Planalto da Bodoquena, cuja composição intercala rochas carbonáticas e terrígenas do Grupo Corumbá (Boggiani et al., 2002; Sallun Filho et al., 2004).

O Grupo Corumbá é composto, da base para o topo, pelas formações Cadineus (conglomerados e arenitos); Cerradinho (arenitos, arcósios, dolomitos e pelitos); Bocaina (dolomitos estromatolíticos e fosforitos); Tamengo (calcários escuros e pelitos carbonosos); e Guaicurus (pelitos), como proposto por Boggiani, (1997). O registro sedimentar do Grupo Corumbá data de 500 a 544Ma (Ediacarano), representando uma das mais importantes unidades da transição neoproterozoico-cambriana na América do Sul (Boggiani et al., 2010).

Campanha et al. (2011) mostraram que as formações Bocaina e Tamengo, de composições carbonáticas, são as mais representativas nas porções mais altas do Planalto da Bodoquena, inclusive na porção oeste de Bonito. Dessa forma, o Grupo Corumbá esteve exposto e submetido ao desenvolvimento do relevo cárstico da Bodoquena, se tornando a fonte de carbonato de cálcio disponível naquele sistema (Boggiani et al., 2002).

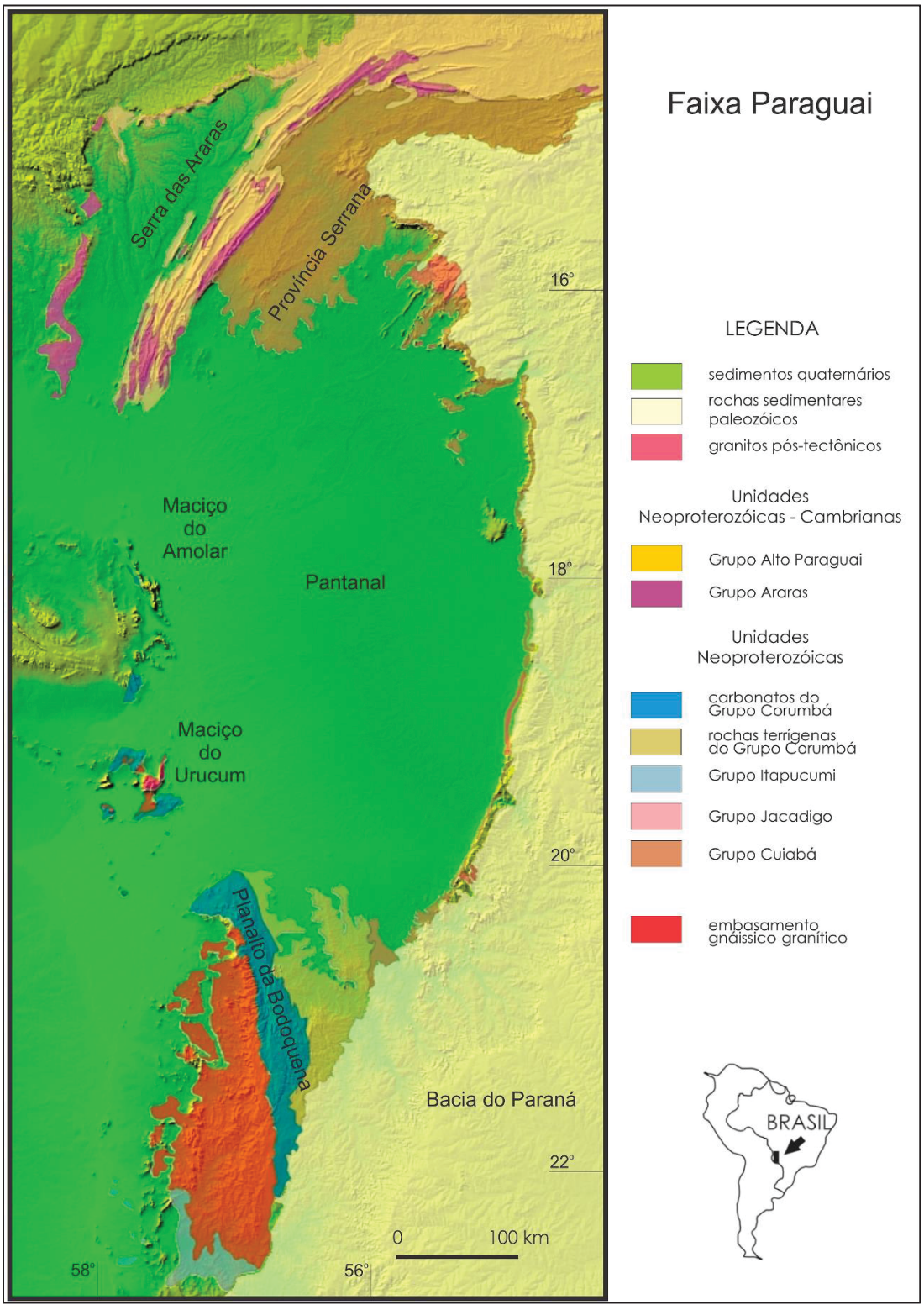


Figura 7 - Mapa geológico da porção sudoeste da Faixa Paraguai, mostrando o Domínio Sul-Mato-Grossense, composto por rochas do Grupo Corumbá que formam o Planalto da Bodoquena ao sul, localizado a sudeste da Planície do Pantanal (Oliveira, 2013).

O Planalto da Bodoquena apresenta ainda ocorrências superficiais de carbonatos continentais recentes depositados sobre as rochas mais antigas (Boggiani et al., 2002). Trata-se de uma região cujas drenagens apresentam alta limpidez da água, alto teor de carbonato de cálcio dissolvido, recarga autogênica do sistema cárstico e ausência de sedimentos siliciclásticos, favorecendo assim a atividade biológica e uma ampla deposição de tufas (Sallun Filho et al., 2009).

Boggiani et al. (2002) descreveram dois principais tipos de tufas na Serra da Bodoquena, de acordo com o tipo do depósito: como *tufas acamadadas* que formam as represas e cachoeiras; ou como *micritas inconsolidadas*. Oliveira et al. (2017) reconheceram uma sucessão de carbonatos com dois estágios deposicionais, sendo a parte basal no Pleistoceno Tardio, cujas idades são de 118 mil anos AP e de 75 a 51 mil anos AP; e o topo no Holoceno, com idades que vão de 5,6 a 2,1 mil anos AP e de 800 anos até o presente.

Os estágios pleistocênicos e holocênicos da Serra da Bodoquena são delimitados por um contato erosivo entre si e com o embasamento (Oliveira et al., 2017). Além disso, suas composições também diferem, apresentando tufas e wackestones brechados na base; packstones oncolíticos, wackestones fossilíferos e depósitos ativos de tufas no topo (Figura 8).

Em relação aos depósitos de tufas da Bodoquena, Oliveira et al. (2017) descreveram duas litofácies principais que podem ocorrer associadas entre si, estando relacionadas aos canais fluviais ativos ou não:

a) Laminadas (Lt), para tufas com laminação estromatolítica, composta por calcita microesparita, e ricas em fósseis de micróbios, macrófitas incrustadas e icnofósseis, com presença de argilominerais;
b) Maciças (Mt), são tufas compostas por caules, sementes e folhas, com incrustação ou substituição de calcita microesparita.

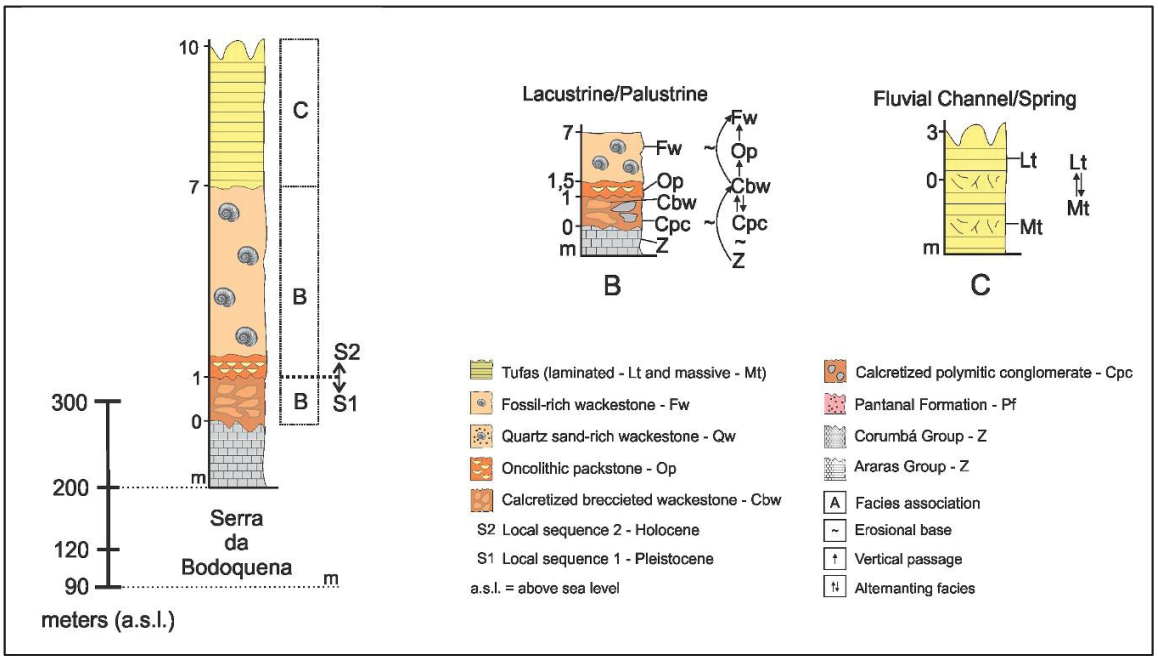


Figura 8 - Seções verticais das sucessões carbonáticas da Serra da Bodoquena, na região da Faixa Paraguai, representada pela sequência 1 (pleistocênica) e sequência 2 (holocênica), cujo o topo apresenta ocorrências de tufas associadas ao sistema fluvial e de ressurgências (Modificado de Oliveira et al., 2017).

Desde a década de 1940 os depósitos de tufas do Planalto da Bodoquena foram definidos pelos trabalhos pioneiros de Almeida na região como pertencentes à Formação Xaraies, descrita na Escarpa de Corumbá-Ladário, nos arredores do Maciço do Urucum (Boggiani et al., 2002). Posteriormente, Sallun Filho et al. (2009) propuseram o termo Formação Serra da Bodoquena para delimitar os depósitos ativos e inativos das tufas quaternárias da região homônima (Figura 9).

A Formação Serra da Bodoquena, portanto, diz respeito aos depósitos de tufas formados em ambiente fluvial e de clima úmido, cujos sedimentos são pouco ou não litificados, e mais recentes que aqueles da Fm. Xaraies, além de ocorrerem em sistemas cársticos e bacias hidrográficas distintas (Sallun Filho et al., 2009).

A presente unidade foi dividida em dois membros: Mb. Rio Formoso, correspondente aos depósitos de represas e cachoeiras, ativas ou não; e Mb. Fazenda São Geraldo, correspondendo aos depósitos inativos de micritas, reconhecidos na base da Formação.

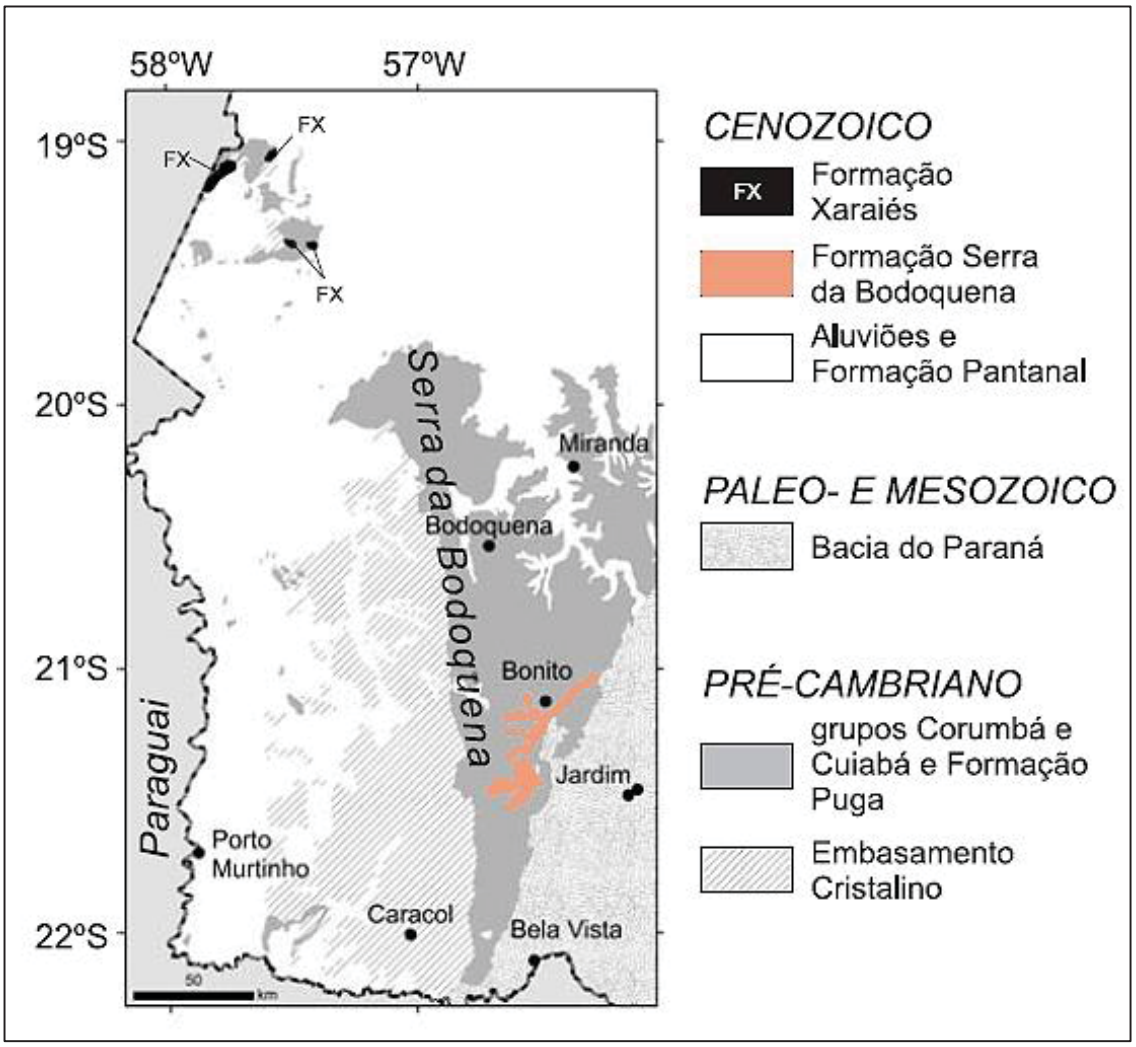


Figura 9 - Mapa de ocorrência da Formação Serra da Bodoquena, abrangendo a região do município de Bonito (Adaptado de Sallun Filho et al., 2009).

As amostras de tufas utilizadas no presente trabalho foram identificadas como pertencentes à unidade estratigráfica Membro Rio Formoso da Fm. Serra da Bodoquena.

2.2.2 Travertinos da Bacia de Denizli

A Bacia de Denizli é uma depressão com 50 km de comprimento e cerca de 25 km de largura, com trend WNW-ESSE, caracterizada como um pequeno graben assimétrico, formado a leste do graben Buyuk Menderes (Figura 10B), no sudoeste

da Turquia, a cerca de 250 km da costa do Mar Egeu (Westaway, 1993; Ozkul et al., 2002; Westaway et al., 2005). Em ambas as margens a bacia é limitada por escarpas associadas a falhas normais de extensão N-S.

A Bacia de Denizli faz parte da grande Província Extensional da Anatólia Ocidental (Figura 10A), que cobre desde o oeste da Turquia, o Mar Egeu até parte da Grécia, configurando uma das maiores zonas de extensão crustal ativas do mundo, acomodada por falhas normais que formam sistemas *horst-graben,* como resultado do aumento do ângulo de subducção da placa oceânica (*slab rollback)* do Norte da África sob a placa da Anatólia, no pós Mioceno Médio (Westaway, 1993; Alçiçek et al., 2007; Özpolat et al., 2020).

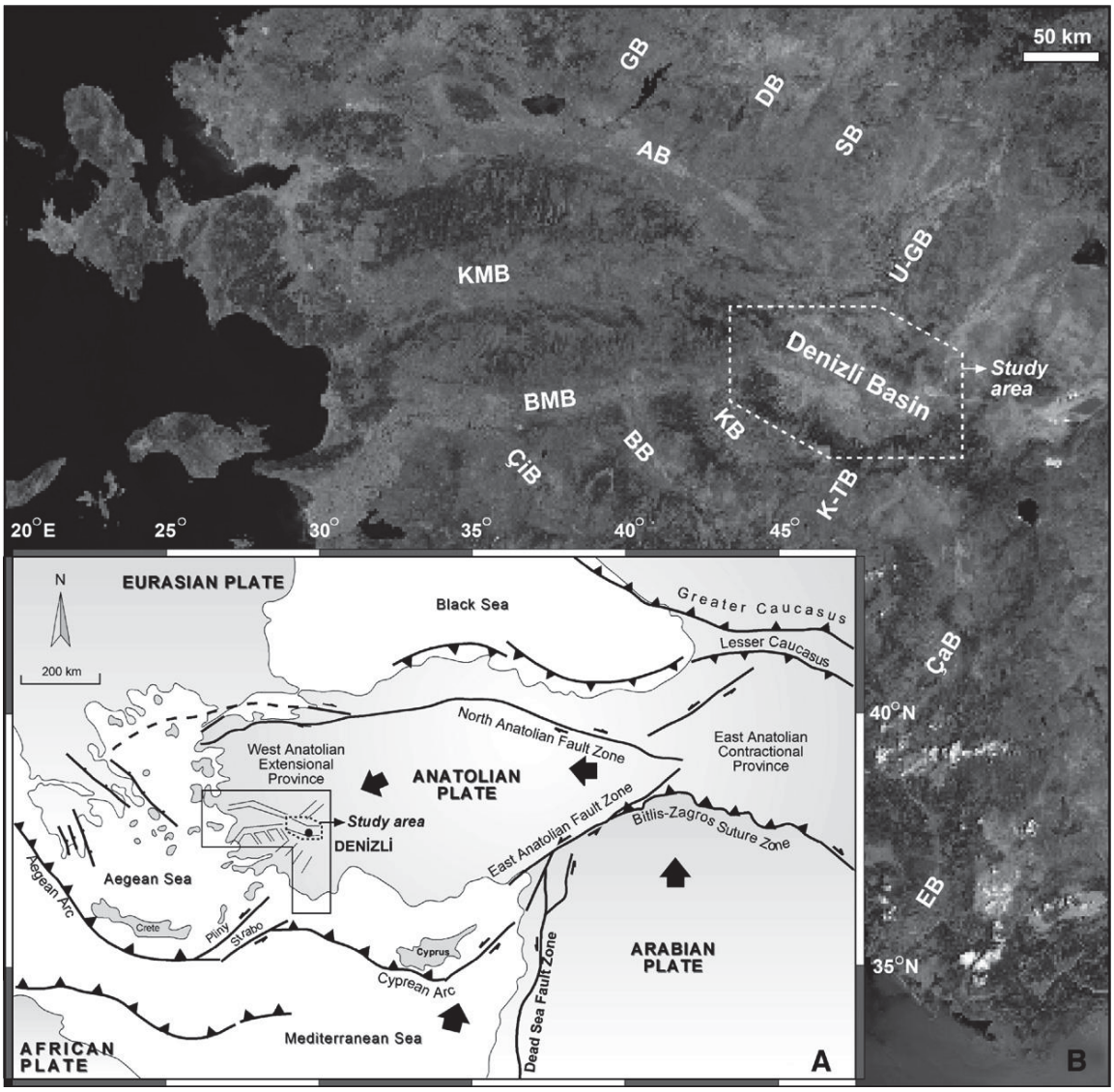


Figura 10 - Mapa de contexto geotectônico da região do Mar Egeu e oeste da Turquia (Alçiçek et al., 2007). A) localização da área de estudo em relação à Província Extensional da Anatólia Ocidental, mostrando as grandes estruturas tectônicas da região; B) Bacia de Denizli (polígono tracejado), situada à leste do *graben* Buyuk Menderes, identificado como BMB (Buyuk Menderes Basin), e demais grabens do sistema.

O embasamento da Bacia de Denizli é composto por rochas pré-Neógenas, que afloram nas regiões de *horsts*, e são representadas por litotipos metamórficos autóctones do Maciço de Menderes, de idades paleozoica-mesozoicas, e carbonatos mesozoicos alóctones (Ozkul et al., 2002; Alçiçek et al., 2007).

O Maciço de Menderes é cortado de leste a oeste por três *grabens*: Gediz, mais ao norte; Kuçuk Menderes, central; e o graben Buyuk Menderes, mais ao sul

(Lips et al., 2001). Esse sistema de *grabens* subdivide o Maciço em três submaciços, sendo o setor do sul e o central aqueles que compõem o embasamento da Bacia, cuja composição é dada, respectivamente, por sequência de gnaisses, xistos e mármores de diferentes graus (Lips et al., 2001; Alçiçek et al., 2007).

O preenchimento da Bacia de Denizli, a partir de depósitos Neógeno-Quaternários, está relacionado à fase atual da deformação extensional do oeste da Turquia, iniciada a cerca de 7,0 Ma (Westaway et al., 2005). A sequência basal (Neógeno) foi depositada em ambiente fluvio-lacustre, sendo predominantemente composta por calcários e margas, em contraste com as demais bacias neógenas daquela região, as quais registram sedimentação siliciclásticas de leques aluviais (Westaway, 1993). No entanto, existem porções da bacia onde os depósitos de travertino são assentados sobre sequências quaternárias de arenitos lacustres e flúvio-aluviais, lamitos, margas, conglomerados, arenitos e argilitos (Alçiçek et al., 2007).

Segundo Ozkul et al. (2002), os depósitos de travertinos quaternários se acumulam ao longo de fissuras extensionais e falhas normais, sobre os sedimentos neógenos de norte ao sul da bacia. São as rochas carbonáticas abaixo que servem como fonte de íons de carbonatos para a formação dos travertinos sobrejacentes (Ozkul et al., 2013).

Trabalhos como Ozkul et al. (2013) e Van Noten et al. (2013) demonstraram que as falhas e fraturas quaternárias que ocorrem ao longo das margens do graben são os caminhos naturais pelos quais a água meteórica se infiltra e percola no subsolo, onde a altas profundidades é aquecida e se mistura com fluidos hidrotermais que ascendem à superfície por outras falhas e fraturas (Figura 11). O fluido gerado, comumente ácido, ressurge na superfície e, devido a diminuição da temperatura e pressão, perde CO_2 rapidamente, no processo de desgaseificação, que aumenta o pH e facilita a precipitação de travertino (Ozkul et al., 2013). Esse processo é favorecido pelos sistemas geotermais rasos e profundos da região, os quais influenciam na alta sismicidade local da Bacia de Denizli (Westaway et al., 2005; Alçiçek et al., 2007).

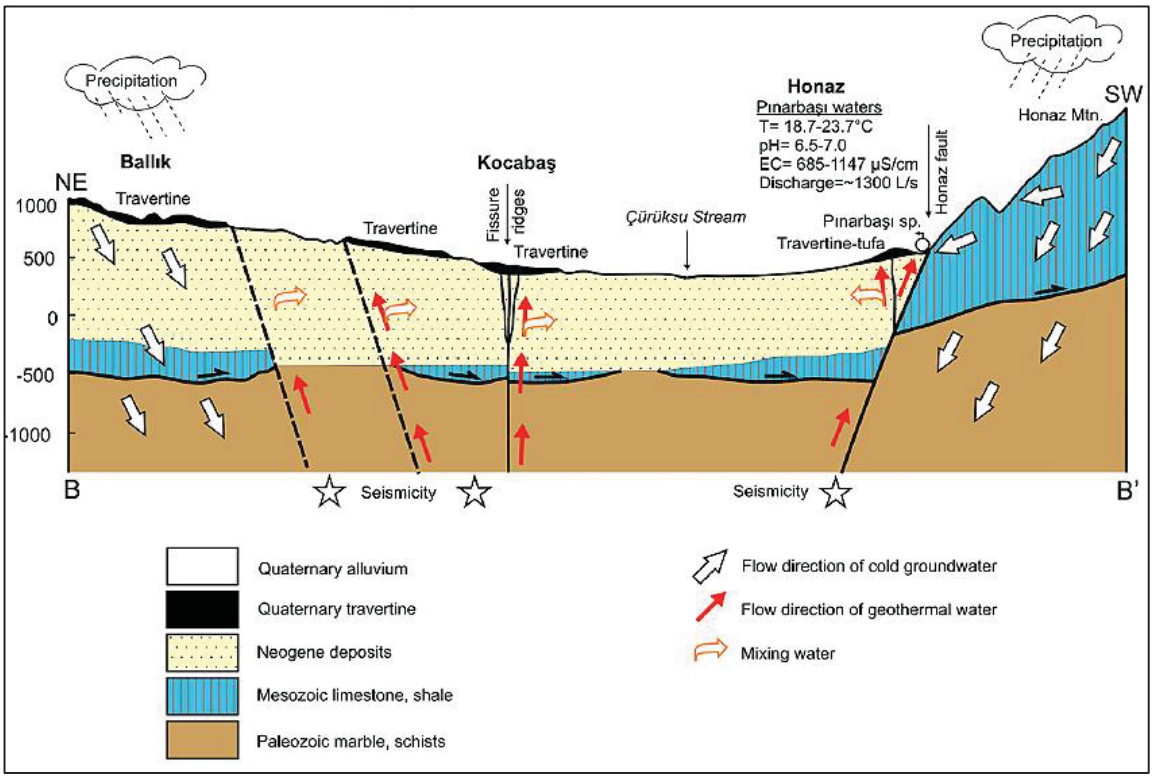


Figura 11 - Desenho esquemático do processo de formação dos depósitos de travertinos de Denizli através de fissuras e falhas, reativadas por atividades sísmicas locais, mostrando fluidos hidrotermais ascendentes (flechas vermelhas) e águas meteóricas (flechas brancas) que descem e percolam no subsolo, e se misturam (flechas laranjas) fornecendo águas ricas em íons de carbonatos oriundos das rochas carbonáticas do embasamento da bacia que servem como rocha fonte (Adaptado de Ozkul et al., 2013).

Os depósitos antigos e modernos de travertinos de Denizli são bastante expressivos na região de Ballik, situada no flanco norte do graben de Denizli, onde são extraídos atualmente blocos de rochas em cerca de 50 pedreiras, dentre elas a Pedreira Faber (Claes et al., 2015; De Boever et al., 2016). De Boever et al. (2016) descreverem a região de Ballik como sendo um domo topográfico de 2,0 km de comprimento e cerca de 70 m de espessura, formado pelo prolongamento de mergulho para sul das falhas normais Cal e Baklan e pela falha Kaklık de mergulho para norte (Figura 12).

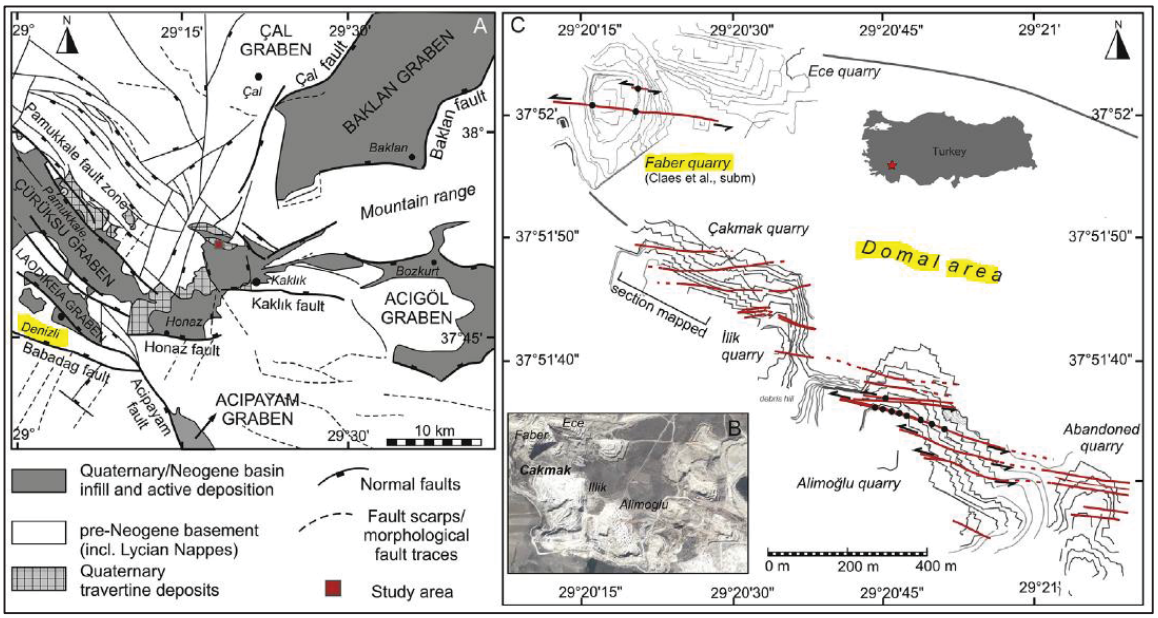


Figura 12 - Mapa da região de Ballik, localizada a nordeste de Denizli, mostrando algumas pedreiras ativas de exploração dos travertinos, dentre elas a Pedreira Faber, as quais estão situadas em uma área dômica formada topograficamente devido aos prolongamentos dos mergulhos das falhas normais e transcorrentes que limitam a região do flanco norte do *graben* de Denizli (De Boever et al., 2016).

Ozkul et al. (2013) usando análises de U-Th investigaram as idades de travertinos de diversas localidades da Bacia de Denizli, e relataram que a deposição se torna mais jovem a partir das margens do graben ao norte e ao sul em direção ao centro; desconsiderando que em localidades como Pamukkale a deposição esteve ativa durante intervalos de tempo diferentes. Desse modo, a idade mais antiga datada para os travertinos da Bacia é de 611 mil anos, em uma região de denominada de Gölemezli, enquanto que a idade mais jovem é de 18 mil anos, proveniente do cume Akköy.

Especificamente na Pedreira Faber, Erten et al. (2005) descreveram dois fragmentos de chifres e uma mandíbula de pequenos cervídeos identificados como semelhantes às espécies de referência da fauna do Pleistoceno Médio na Europa Central.

Os dados geocronológicos indicam que a deposição de travertinos na Bacia de Denizli se iniciou durante períodos glaciais e interglaciais do Pleistoceno Médio;

ao passo que a deposição durante o final do Quaternário não foi fortemente influenciada pelas variações climáticas (Ozkul et al., 2013).

2.3 ESTADO DA ARTE

2.3.2 Tufas

Tufas são caracterizadas como carbonatos continentais precipitados em águas de temperatura ambiente, ricas em bicarbonato de cálcio, carbonato e cálcio, e comumente associadas a vegetais, microrganismos e invertebrados (Pentecost, 1981; Pedley, 1990; Ford e Pedley, 1996; Capezzuoli et al., 2014). Estes depósitos fazem parte de sistemas de carste, que ocorrem associados a fontes hídricas, corredeiras, cachoeiras e quedas de água de sistemas fluviais, palustres ou lacustres (Figura 13).

O termo tufa foi firmado no início do século XIX, como "*kalktuff*", "*tuf calcaire"* e "*calcareous tufa"*, do alemão, francês e inglês, respectivamente, em referência à tufa calcária, como forma de distingui-las dos depósitos de cinzas vulcânicas, chamados de tufo (Pedley, 1990; Pentecost & Viles, 1994).



Figura 13 - Exemplos de depósitos ativos de tufas em corredeiras de água, formando barragens, cascatas e piscinas, associados a musgos, folhas e material vegetal transportado, na região norte da Itália (Adaptado de Perri et al., 2012).

A deposição de tufas está frequentemente relacionada à presença de macrófitas, cianobactérias, bactérias autotróficas e heterotróficas e algas, o que

sugere uma menor temperatura de precipitação em relação aos depósitos de travertinos (Guo & Riding, 1998; Capezzuoli et al., 2014). Além disso, a taxa de deposição é mais baixa, os depósitos apresentam-se pobremente laminados e acamadados, com alta porosidade, compostos predominantemente por calcita, com razão isotópica $^{13}C/^{12}C$ baixa e fortemente negativa (Capezzuoli et al., 2014).

Segundo Pedley (1990) o crescimento de tufas é retardado por condições frias e semiáridas, já que estas não sustentam um alto volume de água perene, ou durante fases de congelamento. Climas quentes e úmidos são, portanto, mais favoráveis ao desenvolvimento de tufas. Essas constatações são valiosas informações para as interpretações paleoambientais de sequências antigas de tufas.

As tufas configuram sistemas autorreguláveis, pois seus depósitos geram os próprios sedimentos carbonáticos, e o material detrítico é derivado da degradação local das próprias tufas, resultando em um equilíbrio dinâmico, onde a taxa de erosão equivale à formação de novas tufas (Pentecost, 1981; Ford & Pedley, 1996).

Organismos como bactérias e algas, bem como a substância polimérica extracelular (EPS) associada, podem induzir a precipitação do carbonato ou servir de substrato para o crescimento dos cristais (Figura 14), e esses fatores podem influenciar na morfologia das tufas (Dupraz et al., 2009; Pedley et al., 2009). Dessa forma, o sistema de tufas é um exemplo efetivo de que a precipitação de carbonatos pode ser um produto compartilhado de processos físico-químicos e de biomediação microbiológica (Capezzuoli et al., 2014).

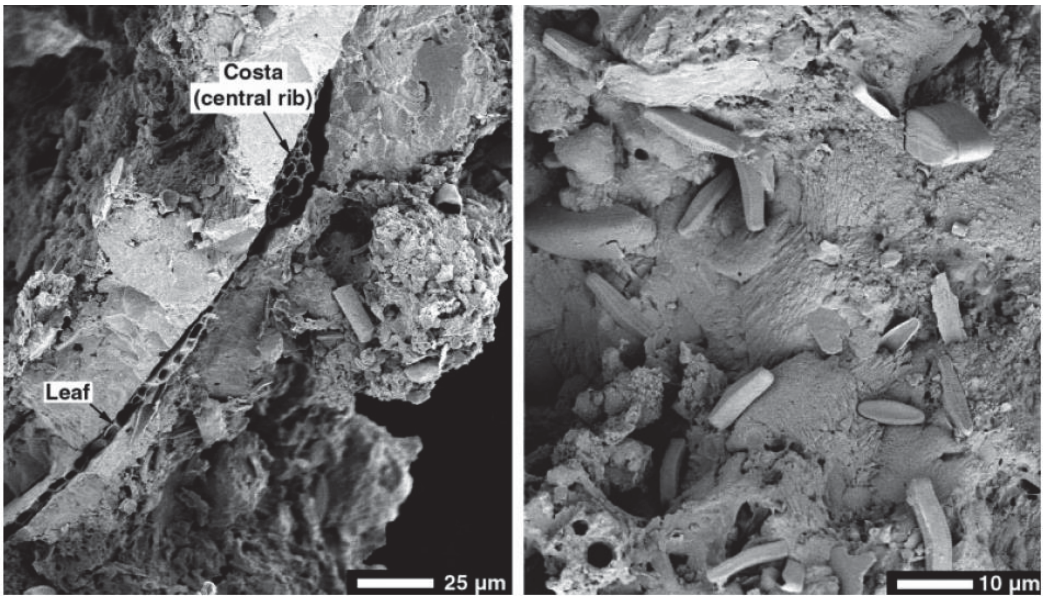


Figura 14 - Imagem de microscópio eletrônico de varredura mostrando a influência de macro e microrganismos na precipitação mineral dos depósitos de tufas, tais como folhas, briófitas incrustadas, EPS e diatomáceas (Adaptado de Turner & Jones, 2005).

Pentecost (1981) já relatava a rica variação de flora e fauna associada aos depósitos de tufa do norte de Yorkshire, no Reino Unido. Entretanto, além da grande variedade de algas, briófitas e diatomáceas, o autor reconheceu a presença de animais invertebrados da espécie *Rhyacophila* (Trichoptera), gerando como produto uma fácies de tufas formadas pela calcificação dos casulos destes organismos.

Recentemente novos trabalhos registraram a influência de metazoários invertebrados na construção de depósitos de tufa. Seard et al. (2013) descreveram na formação Green River (EUA) a presença de carbonatos compostos por agregados de casulos, que foram conectados e preservados por calcificação, com crescimento vertical e perpendicular às camadas, descritos como "*caddisfly cases"* relacionados a atividade de insetos da ordem Trichoptera. He et al. (2015) mostraram uma preservação excepcional de casulos de larvas de insetos *caddisfly* do Cretáceo Inferior, no oeste da China. Ahmed et al. (2018) investigaram construções larvais de insetos aquáticos das ordens Trichoptera, Diptera e Lepidoptera, em depósitos pleistocênicos de tufa no sul da Tunísia. Plant (2019) descreveu formas de acreção em redor de tubos compostos por calcita, oriundos da

calcificação de casulos das larvas de insetos da família *Philopotamidae* (ordem Trichoptera), em depósitos no norte da Tailândia (Figura 15).

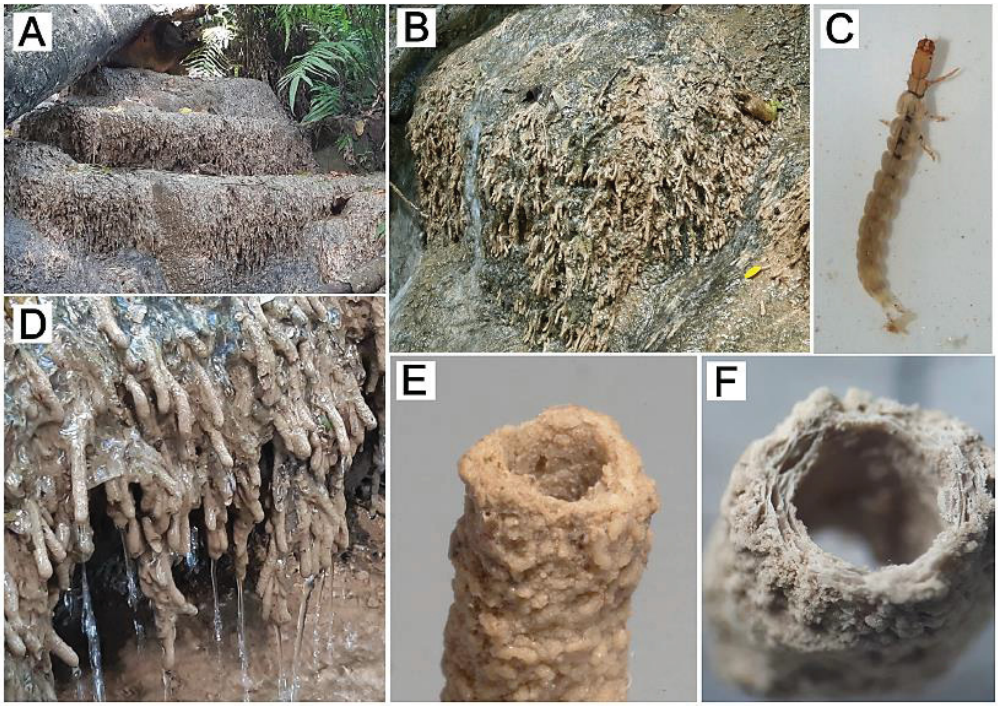


Figura 15 -Exemplo de construções de tufas precipitadas por ação de insetos aquáticos. Os casulos do estágio larval de insetos da família Philopotamidae (ordem Trichoptera), foram calcificados de forma in situ formando uma fácies de tufas (Plant, 2019).

A classificação das fácies de tufa mais utilizada atualmente foi criada por Pedley (1990), na qual o autor propôs um esquema coerente de classificação a partir de observações petrográficas e ambientais, separando os depósitos em autóctones, cujas fácies são *Phytoherm framestone* e *Phytoherm boundstone*; ou depósitos alóctones, com as fácies *Phytoclast tufa*, *Cyanolith oncoidal tufa*, *Intraclast tufa*, *Microdetrital tufa* e *Palaeosoils* (Tabela 1). As fácies de tufas podem ocorrer separadas ou em associação dentro de um mesmo depósito.

Tabela 1 - Classificação das fácies de tufas conforme a origem dos depósitos, proposto por Pedley (1990).

Depósitos Autóctones	*Phytoherm framestone* (tufa fitoerma)	Formada por macrófitas eretas ou reclinadas, colonizadas por cianobactérias, bactérias, fungos e diatomáceas.
	Phytoherm boundstone (tufa estromatolítica)	Formada por cabeças de estromatólitos esqueletais, associadas a cianobactérias.
Depósitos Alóctones	*Phytoclast tufa* (tufa fitoclasto)	Formada por fragmentos de plantas, folhas e galhos que foram transportados e cimentados.
	Cyanolith oncoidal tufa (oncólitos)	Estromatólitos sub-esféricos compostos por cianobactérias e cimento em franja.
	Intraclast tufa (tufa intraclasto)	Formada por fragmentos de tufas detríticas derivadas da erosão de depósitos acima.
	Microdetrital tufa (tufa microdetrítica – tufa peloidal)	Formada pela deposição de micrita em lagos, piscinas e pântanos, podendo ser micrita peloidal ou não.
	Palaeosoils (paleossolos)	Formada pela variação hidrológica e fatores erosivos em condições subaéreas.

Ford & Pedley (1996) atualizaram essa classificação acrescentando aos depósitos autóctones as tufas do tipo *shrubs*, cuja textura está associada ao crescimento de colônia de bactérias; e aos depósitos alóctones, adicionaram as tufas litoclásticas, formada por litoclastos polimíticos em cimento carbonático.

Diversas formas de classificar os depósitos de tufas foram propostas levando em conta diferentes abordagens, como configurações geomorfológicas, petrográficas e até a associação botânica dos depósitos. Dessa forma, Pedley (1990) apresentou cinco modelos deposicionais caracterizados por uma combinação de fatores como geometria do depósito, característica do leito do rio, agrupamento de fácies e associação da biota. Segundo o autor a maioria dos depósitos de tufas seguem os seguintes modelos (Figura 16):

1) *Perched springline model* (modelo elongado de surgência): em regiões mais inclinadas as fontes ricas em carbonato ressurgem nas encostas íngremes (> 30º), formando um aglutinado de degraus. Os depósitos proximais são dominados por briófitas colonizadas por cianobactérias e diatomáceas. Enquanto que os depósitos distais consistem em camadas finas de intraclastos de tufas provenientes dos depósitos proximais;
2) *Cascate model* (modelo de cascata): ocorrem quando cortinas de briófitas crescem nas bordas das quedas de água e ficam sepultadas em camadas íngremes de carbonato precipitado pela água rica em carbonato que fluí por ali. Cavernas escondidas podem se formas atrás das tufas e formar estalactites;
3) *Fluvial models* (modelos fluviais): depósitos formados nos leitos dos rios, sendo a) *braided fluvial model* (modelo fluvial entrelaçado), os depósitos espessos de oncólitos; b) *barrage model* (modelo de barragem), ocorre quando a tufa fitoerma cresce formando uma barreira para o fluxo de água, podendo se formar nos leitos ou em lagos;
4) *Lacustrine model* (modelo lacustrino): onde se desenvolvem corpos de águas grandes e profundos, tem-se a colonização de macro e micrófitas nas bordas e porções mais rasas, e com o leve aquecimento da água a saturação do carbonato de cálcio na água aumenta, podendo formar tufas de bioerma algal e estromatólitos;
5) *Paludal model* (modelo palustre): em águas alimentadas por nascentes que escoam lentamente por uma área plana com tapete de briófitas, formando camadas superficiais de carbonato em toda a vegetação.

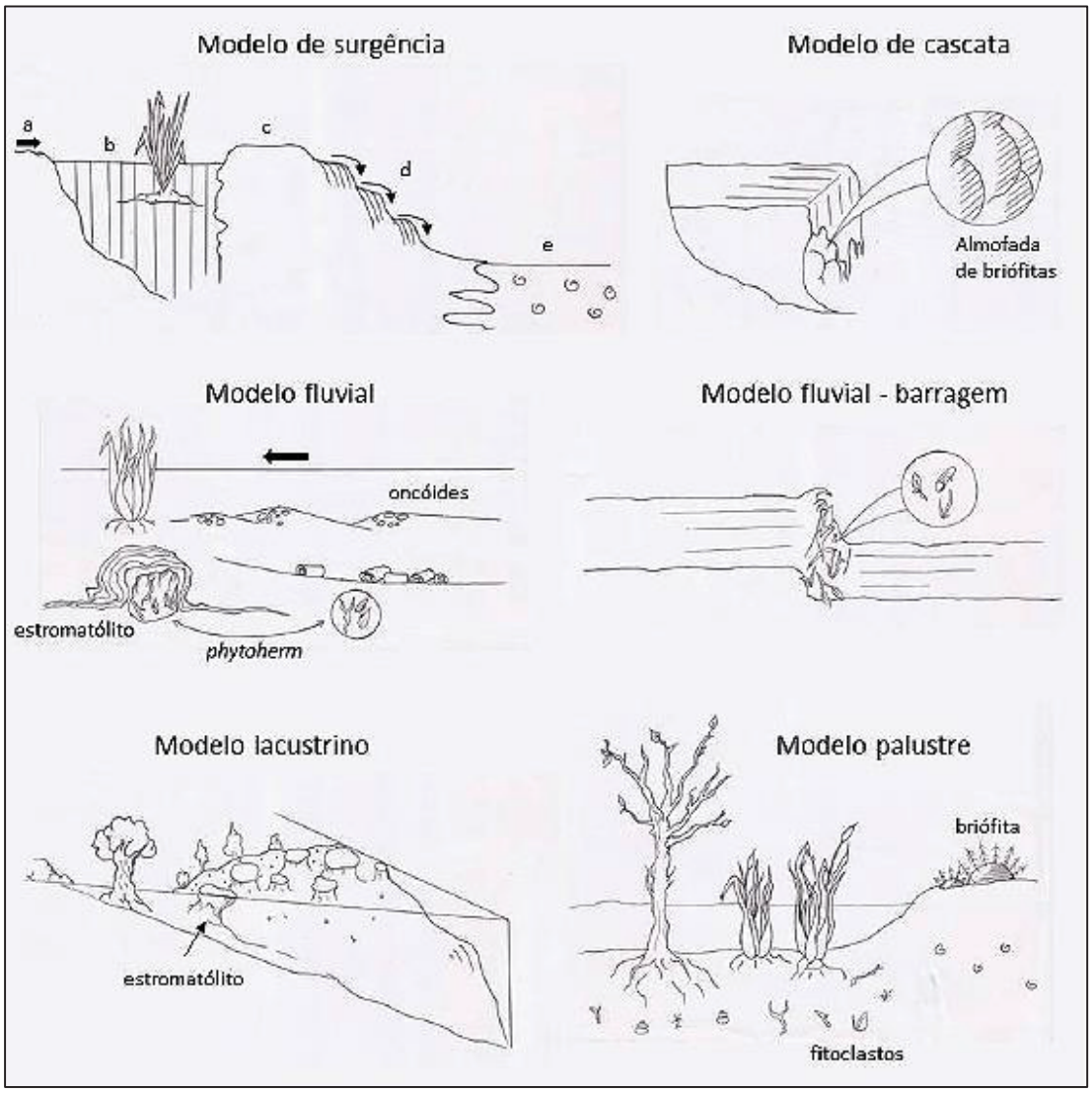


Figura 16 -Modelos deposicionais de tufas apresentados por Pedley (1990), aplicáveis aos sistemas ativos ou inativos (Oste, 2017).

Os depósitos de tufas apresentam ainda assinaturas geoquímicas muito características. Andrews (2006) sugeriu que os valores isotópicos de carbono e oxigênio são depletados em $\delta^{13}C$, ou seja, ligeiramente negativos, correspondendo a um sistema hidrologicamente aberto (por exemplo, o sistema cárstico) e com alta taxa de evaporação ou desgaseificação de CO_2. Portanto, o controle sobre a composição isotópica da água em depósito de tufas deriva do controle sobre a água meteórica responsável por alimentar todo esse sistema (Figura 17). Ademais, a variação dos valores de carbono derivados do CO_2, especificamente, pode estar

relacionada com a decomposição da matéria orgânica do solo, dissolução do carbonato do aquífero ou da atividade biológica no canal de drenagem.

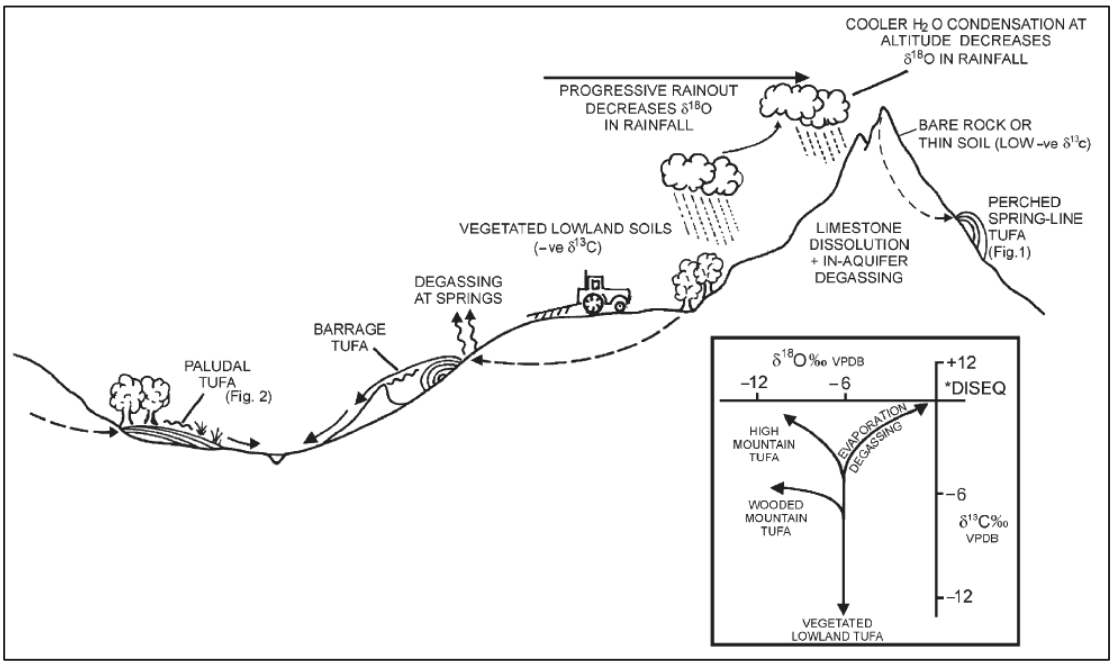


Figura 17 - Modelo de variação das assinaturas isotópicas de carbono e oxigênio em escala regional dos sistemas de precipitação de tufas (Andrews, 2006).

Oliveira et al. (2017) relatou as composições isotópicas das tufas da Serra da Bodoquena, no Brasil, variando entre -9,44 ‰ e -4,20 ‰ VPDB para $\delta^{18}O$, e entre -9,26 ‰ e -1,39 ‰ VPDB para $\delta^{13}C$. Os autores discutiram que os valores médios para as tufas do Pleistoceno da região da Bodoquena são mais negativos que as amostras do Holoceno, possivelmente devido ao aumento das chuvas e da vegetação na época mais recente.

2.3.3 Travertinos

Travertinos são carbonatos continentais formados por processos inorgânicos ou orgânicos, em águas saturadas em bicarbonato, carbonato e cálcio, oriundas de fontes termais ou hidrotermais com efetiva desgaseificação do CO_2 (Chafetz & Folk, 1984; Pedley, 1990; Guo & Riding, 1998; Capezzuoli et al., 2014). São típicos de

áreas tectonicamente ativas e de vulcanismo, estando associados a falhas, as quais servem de condutos para a água quente viajar até a superfície (Figura 18).

O termo travertino tem origem do latim "*lapis tiburtinus"*, que significa a pedra de Tibur, referência à antiga cidade italiana de Tibur, atual Tivoli, usada há mais de 2000 anos para a construção de diversos monumentos históricos de Roma (Chafetz & Folk, 1984; Pentecost & Viles, 1994; Ford & Pedley, 1996).



Figura 18 - Exemplos de depósitos ativos de travertinos de fonte hidrotermal associados a vulcanismo, como piscinas, barragens e terraços, em Mammoth Hot Spring, no Parque Nacional de Yellowstone, EUA (Fouke, 2011).

Depósitos de travertinos geralmente apresentam: alta taxa de deposição; bandeamento regular e fina laminação; baixa a alta porosidade; baixa a alta permeabilidade; textura cristalina inorgânica; microorganismos do domínios Bactéria e Archea e cianófitas são tipicamente os únicos organismos associados, devido aos fatores inadequados para o crescimento de plantas e árvores, como alta temperatura, pH e presença de enxofre; maior presença de aragonita em detrimento da calcita; e razão isotópica do $\delta^{13}C$ regularmente alta, com valores positivos ou

ligeiramente negativos (Chafetz & Folk, 1984; Pedley, 1990; Gandin & Capezzuoli, 2008; Capezzuoli et al., 2014).

A influência orgânica na precipitação de travertinos não é tão diversa como nas tufas, os componentes biológicos nesse caso são comumente microrganismos. Em áreas de águas quentes das fontes hidrotermais as condições de vida são extremas, por isso os organismos envolvidos são em sua maioria colônias de bactérias termofílicas, amantes do calor, instaladas em microhabitats e nichos de baixa energia, onde desempenham um papel passivo na bioprecipitação de carbonatos pela incorporação de partículas minerais em seus biofilmes (Gandin & Capezzuoli, 2008).

Fouke (2011) demonstrou que os depósitos ativos de travertinos de Mammoth Hot Spring (EUA) são dominados por uma extensa variedade de comunidades bacterianas nas fácies deposicionais de travertinos, conferindo distintas pigmentações e morfologias aos tapetes microbianos e gerando diferentes fácies (Figura 19). Segundo o autor existe uma relação na diversidade da microbiota associada às fácies de travertinos de acordo com o tipo do depósito, temperatura, geoquímica e fluxo do fluido.

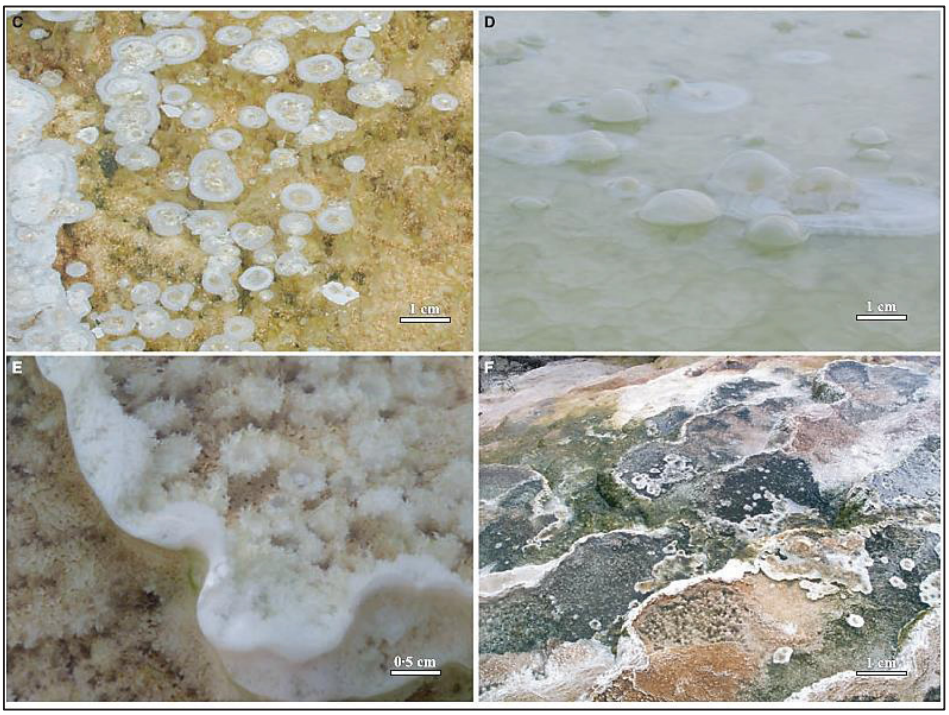


Figura 19 - Exemplos de depósitos microbianos gerando as fácies de travertinos de Mammoth Hot Spring (EUA), mostrando uma variedade de pigmentação e morfologia da microbiota associada às diferentes fácies (Adaptado de Fouke., 2011).

A precipitação de travertinos é rápida, sendo marcada por uma grande variação lateral e vertical de suas fácies. Guo & Riding (1998) demonstraram que um fator importante na definição das fácies de travertinos é a topografia, a qual atua como um controlador da energia, temperatura, pH e energia das águas. Quando a surgência ocorre em encostas e elevações, acontece a formação dos terraços e depósitos de encostas suaves até alcançar as áreas mais baixas e formar os depósitos de depressão.

Pentecost & Viles (1994) apresentaram uma classificação unificada de travertinos usando como principais critérios a geoquímica, a morfologia dos depósitos e a textura dos carbonatos, os quais não são exclusivos, mas podem ser usados separadamente (Figura 20). A escala de estudo desses sistemas carbonáticos pode influenciar no reconhecimento de seus depósitos, portanto, o tipo de classificação usada vai depender do tipo de investigação a ser feita.

Nessa classificação **geoquímica**, o fluido de formação deve ser considerado, pois a sua fonte pode ser termogênica ou meteogênica. No contexto **morfológico**,

considera-se os processos autóctones ou alóctones envolvidos na deposição e suas associações com o relevo. Por fim, a **textura** fornecerá informações de organismos como plantas e bactérias associadas à deposição, além do grau de diagênese.

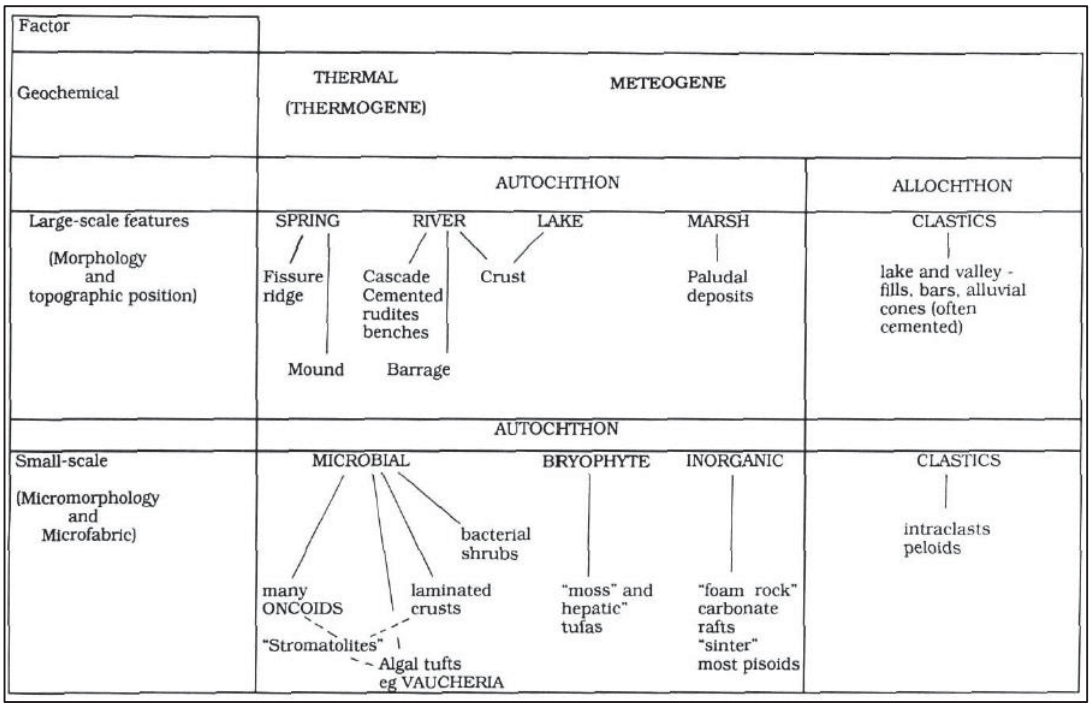


Figura 20 - Esquema unificado de classificação de travertinos proposto por Pentecost & Viles (1994), levando em conta critérios de geoquímica, morfologia e textura da rocha.

Pentecost (1995) agrupou os travertinos da Europa em três tipos de depósitos de acordo com a origem do fluido de formação:

a) **meteogênicos**: aqueles formados por água fria em equilíbrio com a atmosfera do solo; possui baixo valor de TDIC (carbono inorgânico total dissolvido); baixa taxa de deposição; valor isotópico do $\delta^{13}C$ depletado (-2 a -12 ‰), devido à respiração do solo; laminação sazonal nas fácies, exibindo combinação de micrita-esparita; e as texturas influenciadas por briófitas e espermatófitas;
b) **termogênicos**: cuja formação se dá em água quente, com alta pressão parcial do CO_2; alto teor de TDIC; maior taxa de deposição, e alta taxa de *degassing*; com $\delta^{13}C$ levemente enriquecido (-2 a 10‰); apresentam cristais

grandes radiados formados por rápida deposição; e a textura é mais influenciada por assembleia microbiana;

c) **termometeogênicos**: quando a água fria de origem meteórica circula em altas profundidades da crosta, se aquecendo, e ressurge para formar travertinos.

Conforme os travertinos precipitam em diferentes contextos deposicionais, diferentes características são expressadas em relação à cor, acamamento, porosidade, textura e composição (Ozkul et al., 2002). Estes autores investigaram nove principais litofácies nos travertinos da região de Denizli, na Turquia, baseados em escala de campo e nas características petrográficas (Tabela 2).

Tabela 2 - Litofácies de travertinos da região de Denizli, descritas por Ozkul et al. (2002).

Crystalline crust travertine (crosta cristalina)	Textura densa e grosseiramente fibrosa, de cor clara, consistindo em cristais alongados de calcita, crescidas perpendicularmente à superfície de deposição.
Shrub travertine (travertino shrubs)	Textura formada por estruturas de cor creme clara, cujo crescimento é semelhante a pequenos arbustos, limitados por camadas micríticas na parte inferior e superior.
Pisolith travertine (pisólitos)	Formados por grãos esféricos a discoidais revestidos por carbonatos pelo controle da agitação da água e da atividade microbiana.
Paper-thin raft travertine	Formado por finas camadas cristalinas precipitadas na superfície da água de piscinas ou aberturas de fissuras preenchidas por água quente.
Coated bubble travertine (bolhas de gás revestidas)	Textura de bolhas de gás revestidas por carbonato de cálcio, oriundas de atividade microbiológica nos sedimentos das piscinas, que ficam aprisionadas sob as p*aper-thin raft travertine*, entre as plantas e nos cristais.
Reed travertine (travertino junco)	Textura formada por moldes de juncos, grama e plantas aquáticas que crescem nas áreas por onde as águas termais fluem. As raízes estabilizam os sedimentos e são incrustadas por micrita.
Lithoclast travertine (travertino litoclasto)	Formados por fragmentos (litoclastos) penecontemporâneos, angulares a subangulares de travertino de diferentes tamanhos, derivados da erosão das encostas superiores.
Pebbly travertine (travertino seixoso)	Formados por seixos arredondados esparsos de calcário, mármore, *cherts* e serpentinito derivados de inundações efêmeras das unidades de embasamento Neógeno.
Paleosoil (paleossolo)	Horizontes de paleossolo formados pela exposição da superfície do travertino à água da chuva, dessecação subaerial, atividades biológicas e processos pedogenéticos.

Ainda considerando os exemplos de travertinos de Denizli, Claes et al. (2015) refinaram a classificação das litofácies adicionando: *dark coloured peloidal travertine,* cuja composição é de micrita peloidal rodeada, intercalada ou coberta

por outra micrita e/ou microesparita; e *monomictic travertine*, no qual os litoclastos do arcabouço consistem exclusivamente em fragmentos de travertinos, geralmente em uma matriz de carbonato micrítico peloidal.

Em relação à classificação dos depósitos de travertinos, várias propostas foram descritas anteriormente para depósitos ao redor do mundo por diversos autores como Chafetz & Folk (1984); Pentecost (1993); Pentecost (1995); Ford & Pedley (1996); Guo & Riding (1998); entre outros. Ozkul et al. (2002) reconheceram nos travertinos da região de Denizli cinco principais ambientes deposicionais com seus subambientes, levando em conta a geometria dos depósitos, o relevo e até a proximidade com a fonte do fluido (Figura 21):

1) *Slope depositional environmental* (depósitos de rampa): consiste em paredes verticais dos terraços, formando cachoeiras, piscinas, rampas suaves com terraços em declive variando de 10-40°, e rampas íngremes com piscinas;
2) *Depression depositional environmental* (depósitos de depressão): são áreas vazias horizontais ou sub-horizontais, associadas a inundações e riachos efêmeros, podendo ser divididas em subambientes de brejo ou shrubs;
3) *Mound depositional environmental* (depósitos de monte): normalmente associados aos depósitos de travertino junco, são aqueles em que as plantas aquáticas estão densamente localizadas em depressões e perto de encostas mais baixas, formando montes;
4) *Fissure ridge depositional environmental* (depósitos de crista de fissura): são montes lineares estreitos, cristas, formados onde as águas termais emergem ao longo de uma junta ou falha em uma elevação;
5) *Self-built channel depositional environmental* (depósitos de canal autoconstruído): são depósitos lineares de travertino formados por nascentes na direção do fluxo, apresentam formas sinuosas em vista plana, e de cone cortado ou em forma de 'M' quando em seção transversal.

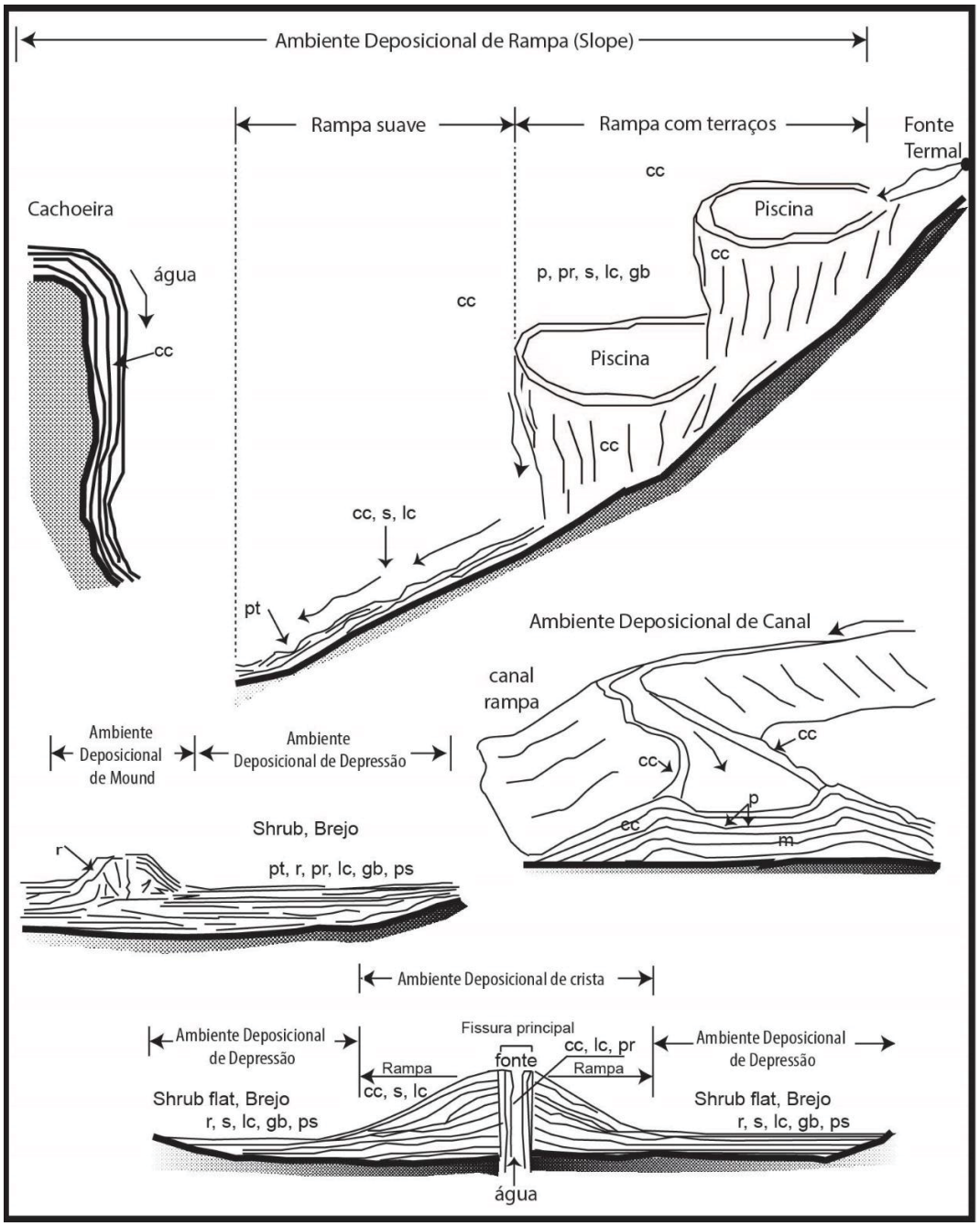


Figura 21 - Modelo de classificação de depósitos de travertinos da Bacia de Denizli, propostos por Ozkul et al., (2002), apresentando os cinco ambientes deposicionais e seus subambientes, com as suas respectivas fácies: cc: crosta cristalina; s: shrub; p: pisólito; pr: paper-thin raft: bg: coated gas bubble; r: junco; lc: litoclastos; pt: pebbly travertine, ps: paleossolo; m: lâmina micrítica (França et al., 2017).

Assim como no sistema de tufas, os travertinos apresentam uma variação isotópica estável típica, dadas as suas características deposicionais, as quais

registram o controle dominante dos parâmetros físico-químicos na precipitação carbonática. Gandin & Capezzuoli (2008) expuseram dados isotópicos estáveis obtidos de calcita precipitada de águas quentes ou mornas, onde o $\delta^{18}O$ varia de -4 ‰ a -30 ‰, sugerindo uma influência de altas temperaturas e níveis de supersaturação das águas; enquanto que a faixa típica de -2 ‰ a +8 ‰ de valores de $\delta^{13}C$, é interpretada como reflexo da derivação meteórica e em parte de proveniência geotérmica ou magmática juvenil reciclada.

Para o sistema hidrológico de Denizli, Forisz et al. (2011) demonstraram que a composição isotópica das águas termais, mornas e frias variam em uma faixa relativamente estreita, salvo os valores de $\delta^{18}O$ de algumas águas quentes que foram deslocados para valores mais positivos durante a interação rocha-água. Portanto, esses dados isotópicos, apoiados por dados radiométricos, indicam que todas as águas na Bacia de Denizli se infiltraram no Holoceno sob condições de mesmo clima, se tratando então de águas jovens com curto tempo de recarga seja por fluxo mais rápido sob a superfície ou caminho mais curto do fluxo subterrâneo.

CAPÍTULO 3 – MATERIAIS E MÉTODOS

A presente pesquisa de mestrado foi desenvolvida conforme quatro etapas integradas de trabalho. A primeira etapa consistiu em um minucioso levantamento bibliográfico acerca dos carbonatos continentais, com foco nas tufas e nos travertinos, seguido de uma seleção dos trabalhos mais relevantes para a discussão e comparação dos dois litotipos em relação às características morfológicas e estruturais dos depósitos; feições petrográficas; configurações geoquímicas de deposição; origem dos fluídos formadores; microestruturas e componentes biológicos associados. A segunda etapa correspondeu à coleta de amostras em campo, seguida pela etapa laboratorial da pesquisa, representada pela seleção e descrição das amostras, confecção de seções delgadas, descrições petrográficas, amostragem geoquímica e realização de análises laboratoriais. Por fim, a última etapa do trabalho foi marcada pela análise, integração e interpretação dos resultados, descritos na presente dissertação e elaboração dos artigos científicos.

O presente trabalho está inserido em um projeto *guarda-chuva* denominado “Projeto MICROBIAL: geoquímica de carbonatos microbiais continentais associados à precipitação de argilominerais” (Processo SIGITEC: 2016/00141-1, SAP: 4600538216), o qual é fruto de uma cooperação técnico-cientifica entre a UFPR/FUNPAR, o Instituto Laboratório de Minerais e Rochas (iLAMIR) e a empresa Petrobras.

3.1 AMOSTRAGEM

O estudo de campo dos depósitos de tufas, bem como a coleta de amostras, ocorreram em um trabalho de campo realizado em setembro de 2019, na Fazenda Estância Mimosa, no município de Bonito (Brasil), onde ocorre um segmento do Rio Mimoso com alta ocorrência de tufas e presença de cachoeiras com diferentes morfologias. Cerca de 42 amostras foram coletadas de oito depósitos ativos e um inativo, todas armazenadas no iLAMIR (Figura 22).

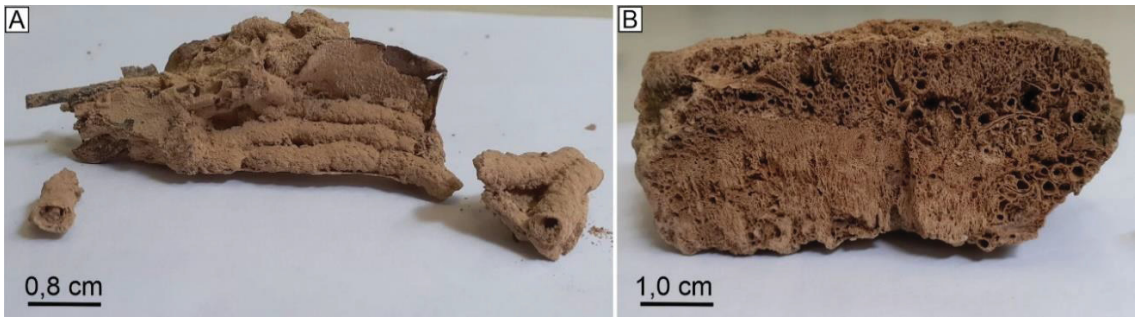


Figura 22 - Exemplos de amostras de tufa coletadas na Estância Mimosa, em Bonito (Brasil). A) amostra de depósito ativo, mostrando associação com folha de árvore; B) amostra de depósito inativo, essencialmente mais consolidada e com associação de diferentes fácies.

Em campanha de campo realizada em 2011 pela Petrobras, em parceria com a Universidade de Pamukkale (Turquia) e a Universidade Católica de Leuven (Bélgica), foram coletados três testemunhos de sondagem continua nas pedreiras ativas da região de Denizli, na Turquia. Os testemunhos Faber, Çinkaya e Simersan foram armazenados no iLAMIR. O testemunho da Pedreira Faber foi utilizado no

presente trabalho, e apresenta cerca de 40 m, em cota 605 m, com 28,5 m recuperados (71%) (Figura 23).



Figura 23 - Testemunho de travertinos amostrado na pedreira Faber, em Denizli, na Turquia, e utilizado no presente trabalho. Contém 28,5 m de material recuperado.

No que concerne às descrições das amostras, tanto de tufas quanto de travertinos, não foi possível aplicar as classificações de rochas carbonáticas consideradas clássicas e bastante difundidas até hoje, por exemplo Folk (1962) ou Dunham (1962), essencialmente composicional ou embasada na textura deposicional, respectivamente.

Ambos os litotipos abordados neste trabalho necessitam de classificações específicas para carbonatos microbiais continentais, visto que suas características peculiares estão associadas ao conjunto de fatores que envolvem os processos de formação, ambientes deposicionais, composição e influência biogênica (Ver Capitulo 2 – Seção 2.3). Desse modo, os depósitos de tufas e travertinos, foram descritos macroscopicamente e suas litofácies caracterizadas baseando-se, principalmente, nos trabalhos de Pedley (1990), Ford & Pedley (1996), Ozkul et al. (2002) e Claes et al. (2015). Para ambos os litotipos houveram adaptações quando necessário.

Foram descritas onze lâminas petrográficas de tufas de amostras provenientes de diferentes depósitos, abrangendo pelo menos duas vezes cada uma das fácies identificadas em escala macro; e 26 lâminas petrográficas de travertinos, com espaçamento de cerca de um metro no testemunho entre cada amostragem, buscando abranger toda a extensão do poço e todas as fácies descritas. As seções delgadas foram analisadas em microscópio óptico de luz polarizada Zeiss Axio, modelo Imager.A2m, no iLAMIR.

O refinamento da determinação das fácies, bem como a investigação das microtexturas e microrganismos associados foram possíveis através da análise por Microscopia Eletrônica de Varredura. Em relação aos estudos geoquímicos, foram coletadas cerca de 3,0 g de amostra em pó de rocha total, sendo 15 de travertinos e 15 de tufas, para análise das técnicas de difratometria de raios X, fluorescência de raios X e isótopos estáveis de C & O.

3.2 MICROSCOPIA ELETRÔNICA DE VARREDURA

O refinamento das fácies de tufa e travertino identificadas anteriormente em amostra de mão e por lâmina petrográfica, se deu através da análise por Microscopia Eletrônica de Varredura (MEV), capaz de analisar em alta resolução a superfície, morfologia, estrutura e a composição química semiquantitativa do material analisado.

O microscópio eletrônico de varredura tem como princípio a incidência de um feixe de elétrons sobre a superfície da amostra, podendo ser pontual ou por linhas sucessivas (varredura), resultando na emissão de elétrons retroespalhados e secundários, que vão gerar informações do material em uma escala de detalhe de até aproximadamente dez nanômetros (Dedavid, et al., 2007).

A análise de MEV das tufas foi realizada em microscópio da marca JEOL, modelo 6010LA, acoplado com sistema de análise química EDS marca JEOL, modelo EX-94410T1L11, no iLAMIR. Enquanto que as amostras de travertinos foram analisadas no equipamento TESCAN VEJA3 LMU acoplado com software AZ Tech, detector tipo SDD de 80 mm², do Centro de Microscopia Eletrônica da UFPR.

3.3 DIFRATOMETRIA DE RAIOS X

A Difratometria de Raios X (DRX) consiste na técnica de identificação das fases minerais presentes no material analisado, portanto, foi utilizada para determinar a composição mineralógica das amostras de tufas e travertinos, no que diz respeito à distinção dos minerais de carbonatos.

A técnica de DRX consiste no processo pelo qual o feixe de raios X é disperso pelos elétrons dos átomos dos cristais, sem que haja uma mudança do comprimento de onda (dispersão coerente) quando as condições geométricas são satisfeitas (Formoso, 1984). A difração de um cristal corresponde a uma propriedade física fundamental da substância, uma vez que compreende a posição e intensidade das linhas de difração desse cristal, por isso acaba servindo para a identificação e também o estudo de dimensões da cela unitária (Klein & Dutrow, 2009).

A análise foi realizada no iLAMIR, através do equipamento Malvem PANalytical, modelo EMPERYAN, com detector X'Celeratore com tubo de cobre. Os difratogramas foram interpretados com base na porcentagem semiquantitativa dos minerais pelo método RIR (Reference Intensity Ratio), com auxílio do software HighScore Plus, com banco de dados PAN-ICSD.

3.4 FLUORESCÊNCIA DE RAIOS X

A Fluorescência de Raios X (FRX) é uma técnica de alta sensibilidade que foi utilizada com objetivo de determinar a composição química das amostras de tufas e travertinos, em relação aos principais óxidos presentes no material.

A técnica de FRX é a excitação dos átomos dos elementos químicos a partir da emissão de um feixe de raios X sobre a amostra, que em condições adequadas vai gerar uma radiação secundária denominada de fluorescência (Dutra & Gomes, 1984). Através dos ângulos de reflexão e das intensidades dessa radiação é possível identificar e quantificar os elementos presentes na amostra.

A análise de FRX foi realizada no iLAMIR, através do espectrômetro Malvern PANalytical Axios-mAX, com tubo de ródio, cujos dados são obtidos a partir do software SuperQ 5.3. O equipamento foi calibrado com padrões nacionais e internacionais, sendo possível a leitura dos seguintes óxidos para amostras de rochas carbonáticas: CaO, MgO, SiO_2, Al_2O_3, Fe_2O_3, Na_2O, K_2O, SrO, TiO_2, MnO e P_2O_5.

3.5 ISÓTOPOS ESTÁVEIS DE CARBONO E OXIGÊNIO

A análise de isótopos estáveis de C e O foi realizada visando a interpretação das condições geoquímicas de formação das tufas e travertinos, como a paleotemperatura do fluido formador, e também a influência biológica na precipitação mineral.

Essa análise é obtida através da comparação relativa da razão isotópica (R) do $\delta^{18}O/^{16}O$ e $\delta^{13}C/^{12}C$ da amostra em relação a um padrão de referência internacional, de acordo com a equação a seguir:

$$\delta\ em\ ‰\ (per\ mil) = \frac{R\ (amostra) - R\ (referência)\ x\ 1000}{R\ (referência)}$$

Os valores isotópicos padrões (referência) para carbonatos são o PDB (fóssil *Belemnite* da Formação Pee Dee de idade Cretácea, USA), para o oxigênio e o carbono; e o SMOW (Standard Mean Ocean Water), para o oxigênio. Portanto, valores isotópicos de δ positivo refere-se às amostras ricas em isótopos pesados em relação ao padrão; valores de δ zero, quando a amostra apresenta um valor igual ao padrão; e δ negativo, se a amostra estiver enriquecida em isótopos mais leves que o padrão (Rodrigues & Fauth, 2013).

A análise isotópica foi realizada no iLAMIR, através do espectrômetro de massa Thermo Fischer Scientific, modelo Delta V Advantage, acoplado a um sistema Gas Bench II de fluxo continuo, sendo a leitura dos dados feita a partir do software Isodat 3.0 Gas Isotope Ratio MS.

CAPÍTULO 4 – RESULTADOS E DISCUSSÕES

A análise e discussão dos resultados, bem como as conclusões desta pesquisa, serão apresentados a seguir em formato de artigo que será submetido à publicação na revista científica *Sedimentary Geology*.

PETROGRAPHIC AND GEOCHEMISTRY CRITERIA FOR DISTINGUISHING TUFAS AND TRAVERTINES: CASE STUDY OF BODOQUENA PLATEAU, BRAZIL, AND DENIZLI BASIN, TURKEY

ABSTRACT

Tufa and travertine are continental carbonates precipitated in fluid conditions rich in calcium carbonate, however, there is a difficulty of distinguishing these rocks existed specially in ancient deposits. This work aims to characterize the carbonate facies of modern environments of tufa and travertine, seeking to understand the genesis and formation processes of these lithotypes, in addition to investigating the organic influence on mineral precipitation and its relationship within the fabrics and microfabrics. The study area of the tufas was the Mimoso River, located in Bonito city, Brazil, and the travertine area was the Faber quarry, located in the northeast of Denizli, southwestern Turkey. The main similarity found between tufa and travertine is the wide variation of facies in these systems, as well as their associations, which reflects the high dynamics of the deposition environments. Reed Travertine and Bryophyte Phytoherm Tufa can be correlated due to the preservation of organic vegetable material in their framework, however, in travertine, the reed facies corresponds to the one with the highest presence of organic matter, whereas in the tufa, all facies have effective influences of plants. In addition, tufa fabric is controlled by the material that composes it, allochthonous or autochthonous, unlike travertine whose fabric is probably controlled by the type of deposit. The main difference between tufa and travertine lithotypes is related to the presence of micrite in the rock matrix. Travertine facies have both primary and secondary micrite, this one filling pores by micritization, ensuring less porosity for travertine compared to tufa. In addition, two types of micrites have been recognized for travertine facies: massive micrite and granular peloidal. In all tufa facies, organomineral features were identified as a product of organomineralization, such as smooth rhombohedral microcrystals and fibrous triads. However, for travertine, only caliche and reed travertine showed biogenic structures associated with organomineralization. These micro and nanostructures vary in size and shape according to the EPS content present in the facies. In conditions of low EPS, only nanometric spheroids and fibrous triads were formed; the more EPS, the more developed the products of organomineralization, such as smooth rhombohedral calcites. Therefore, it is suggested that EPS production is much more effective in tufa systems than in travertine. Concerning the tufa forming-fluid, the isotopic values of $\delta^{18}O$ were found to be of exclusively meteoric origin. The isotopic values of $\delta^{13}C$ suggest control of photosynthesis in this system, given the

predominance of cyanobacteria, algae and bryophytes, in addition to the influence of C3 plants. Travertine $\delta^{18}O$ values suggest that the fluid was meteoric water heated through fracture and fault infiltration, generating a thermo-meteogenic fluid. The $\delta^{13}C$ negative values of travertines are attributed almost exclusively to Caliche facies, suggesting a greater influence of organic matter in this system, or even, the action of photosynthesis related to the pedogenic process. Finally, XRF and XRF data showed a pure and restrict composition in both systems, which only calcite and quartz were identified, and the main oxides presented were CaO and SiO2. Tufa and travertine systems represent important producers of carbonate sediments in the context of continental deposits.

Keywords: continental carbonates, organomineralization, carbonate systems, spring deposits, calcite, phytoherm framestone.

INTRODUCTION

Tufas are carbonates precipitated from water at environmental temperature, usually around 20º C, while travertines are commonly referred to as precipitates within hot water (temperatures above 30°C) representing carbonates of hydrothermal origin (Pedley, 1990; Ford & Pedley, 1996; Pedley, 2009; Capezzuoli et al. 2014). Tufas and travertines are terms widely used to designate lacustrine and fluvial freshwater carbonates, however, the difficulty of distinguishing between these rocks remain for decades (Pentecost & Viles, 1994; Claes et al., 2015). Variations in lithological precipitate results when the temperature of the fluid decreases as it moves away from the water source, thus resulting in proximal travertine deposits and distal tufa deposits in the same system (Claes et al., 2015).

The comparison of petrofacies and stable isotopic signatures from active deposits characterize the water and the system of origin, biota association, as well as the geomorphological context, which can provide criteria for unambiguous lithological identification even at field scale and applicable to the characterization of ancient deposits, revealing tufas, if controlled by climate, or travertines, controlled by tectonic processes (Gandin & Capezzuoli, 2008; Capezzuoli et al., 2014).

Tufa deposition is often related to the presence of macrophytes, cyanobacteria, heterotrophic bacteria, and algae, indicating a lower precipitation temperature when compared with travertine deposits (Guo & Riding, 1998; Capezzuoli et al., 2014). These biological components favor biologically induced/influenced mineral precipitation, a process in which mineral formation

occurs in an organic matrix, commonly exopolymeric substances (EPS), serving as substrate for the nucleation of the crystals (Dupraz et al., 2009). In addition, the deposition rate is relatively lower, the deposits are poorly laminated and layered, with high porosity, predominantly composed of calcite, with a low and strongly negative $^{13}C/^{12}C$ isotope ratio (Capezzuoli et al., 2014).

The tufa facies classification was proposed by Pedley (1990), in which the author presented a scheme based on petrographic and environmental observations, classifiying deposits into autochthonous: Phytoherm framestone and Phytoherm boundstone; and allochthonous: Phytoclast tufa, Cyanolith oncoid tufa, Intraclast tufa, Microdetrital tufa, and Palaeosoils facies. Ford & Pedley (1996) updated this classification by adding shrub-type tufas to autochthonous deposits, with factory associated with bacteria activity; and for the allochthonous deposits category, they added lithoclastic tufas, composed of polymitic lithoclasts within carbonate cement.

Travertine deposits generally have a high deposition rate, range between 1 and 1000 mm per year; regular banding and thin millimetric lamination; low porosity; low permeability; inorganic crystalline factory; content of aragonite higher than calcite; and a fairly high $\delta^{13}C$ isotope ratio, with positive or slightly negative values (Chafetz & Folk, 1984; Pedley, 1990; Pentecost, 2005; Gandin & Capezzuoli, 2008; Capezzuoli et al., 2014). The organic influence on travertine precipitation is lower than in tufas, once microorganisms, within hydrothermal vents live in extreme conditions, so the organisms are mostly colonies of thermophilic bacteria, in microhabitats and low energy niches, where they play a passive role in the bioprecipitation by incorporating mineral particles within biofilms (Gandin & Capezzuoli, 2008). Fouke (2011) demonstrated that active travertine deposits from Mammoth Hot Spring (USA) are dominated by a wide variety of bacterial communities, once there is a relationship among the diversity of microbiota associated with travertine facies according to deposit type, temperature, geochemistry, and fluid flow.

As travertines precipitate in different depositional contexts, different characteristics are expressed in relation to color, bedding, porosity, texture, and composition. Ozkul et al. (2002) defined nine main lithofacies in travertines from the

Denizli region of Turkey, based on field-scale and petrographic characteristics: Crystalline crust travertine, Shrub travertine, Pisolith travertine, Paper-thin raft travertine, Coated bubble travertine, Reed travertine, Lithoclast travertine, Pebbly travertine, and Paleosoil. Claes et al. (2015) refined the classification of lithofacies by adding: dark-colored peloid travertine, whose composition is peloid micrite surrounded, intercalated, or covered by other micrites and/or microsparites; and monomictic travertine, in which the framework lithoclasts consist exclusively of travertine fragments, usually in a peloidal micritic carbonate matrix.

Tufas and travertines have been of great importance for paleoclimatic studies over the last decades (Capezzuoli et al., 2014), as well as remarkable geotouristic relevance due to their landscape value (Boggiani et al., 2002). Continental carbonates can also constitute important reservoirs for oil and gas due to their high porosity and permeability, therefore, the understanding of modern carbonate precipitation systems is applicable in the interpretation of the environments and the distribution model of these deposits (Terra et al., 2010; Wright, 2012; Della Porta, 2015).

Since the discovery of the Pre-salt section on the Brazilian continental margin, the interest in better understanding the genesis and distribution of these carbonate rocks precipitated in modern systems has expanded for use as analogous to subsurface petroleum reservoirs (Wright, 2012). The characterization of continental carbonate reservoirs is challenging once samples are punctual localized and may present similar lithological characteristics in macro and mesoscale. Therefore, a detailed comparative study, in micro and nanoscale, contribute to the distinction and improvement of knowledge about continental carbonate lithotypes.

This paper aims to characterize the carbonate facies from modern tufa and travertine environments, aiming to understanding the differences and similarities between both systems regarding the depositional environments; facies; microfabrics; biological components; the biogenic precipitation influence; and geochemical depositional conditions.

LOCATIONS AND GEOLOGICAL SETTING

The study area of tufas is a segment of the Mimoso River, located at the Estancia Mimosa Ecotourism farm (Figure 24A), in the municipality of Bonito, Central-Eastern Brazil (20°58'57.45" S / 56°30'57.96" W). Within 2 km distance where the Mimoso River runs in Estancia Mimosa, with 150 m uneveness, the rugged relief provides the occurrence of cascades and waterfalls with active deposits of tufas, formed from water-rich in carbonate ions originated from the underlying Proterozoic carbonate rocks of the Corumba Group (Sallun Filho et al., 2009). The Mimoso River runs to the southeast as the main tributary of the Formoso River, and it lies on karst relief of the Bodoquena Plateau (Sallun Filho & Karmann, 2007). The Formoso River basin belongs to the large Paraguay River Hydrographic Basin, which drains the Pantanal wetlands.

The tufa deposits of the Mimoso River were first described by Almeida (1965) and the Bodoquena Plateau tufa deposits were registered as one of the geological and paleontological sites of Brazil (Boggiani et al., 2002). Later, these deposits were studied by Sallun Filho et al. (2009) which presented a proposal to define the Serra da Bodoquena Formation. Recently, work carried out in the tufas of the Mimoso River focused on palynological and chemostratigraphic characterization (Oste et al., 2018); in addition to the investigation of environmental and depositional controls in the formation of these deposits (Oste et al., 2021).

The Bodoquena Plateau is a geomorphological feature located southeast of the Pantanal Plain, with elevation up to 800 m, and a length of about 200 km with north-south elongation (Boggiani et al., 2002; Sallun Filho et al., 2004; Sallun Filho et al., 2009). The Bodoquena relief, is characterized by cliffs to the west and a slight slope to the east, reaching the floodplain of the River Miranda influenced by tectonic structures of the Paraguay Belt (Boggiani et al., 2002; Sallun Filho et al., 2004). The Plateau also presents superficial occurrences of recent continental carbonates (Boggiani et al., 2002). This is a region where drainages present crystal-clear water, high dissolved calcium and carbonate content, autogenic recharge of the karst system, and absence of siliciclastic sediments, thus favoring biological activity and a wide deposition of tufas (Sallun Filho et al., 2009).

Boggiani et al. (2002) described two main types of tufas in Serra da Bodoquena, according to the type of deposit: layered tufa that form dams and waterfalls; and unconsolidated micrites. Oliveira et al. (2017) recognized a succession of carbonates with two depositional stages, being the basal part in the Late Pleistocene, with ages around 118 thousand years BP and 75 to 51 thousand years BP; and the top within the Holocene, with ages ranging from 5,600 to 2,100 years BP and from 800 years to the present.

The Serra da Bodoquena Formation was proposed by Sallun Filho et al. (2009). It is subdivided into the Formoso River Member, the uppermost unit, with deposits of dams and waterfalls, either active or not; and the São Geraldo Member composed of inactive micrites. The sediments of the Bodoquena Formation are little or not lithified. The tufa samples used in this work have been identified as belonging to the stratigraphic unit Member Formoso River of the Serra da Bodoquena Formation.

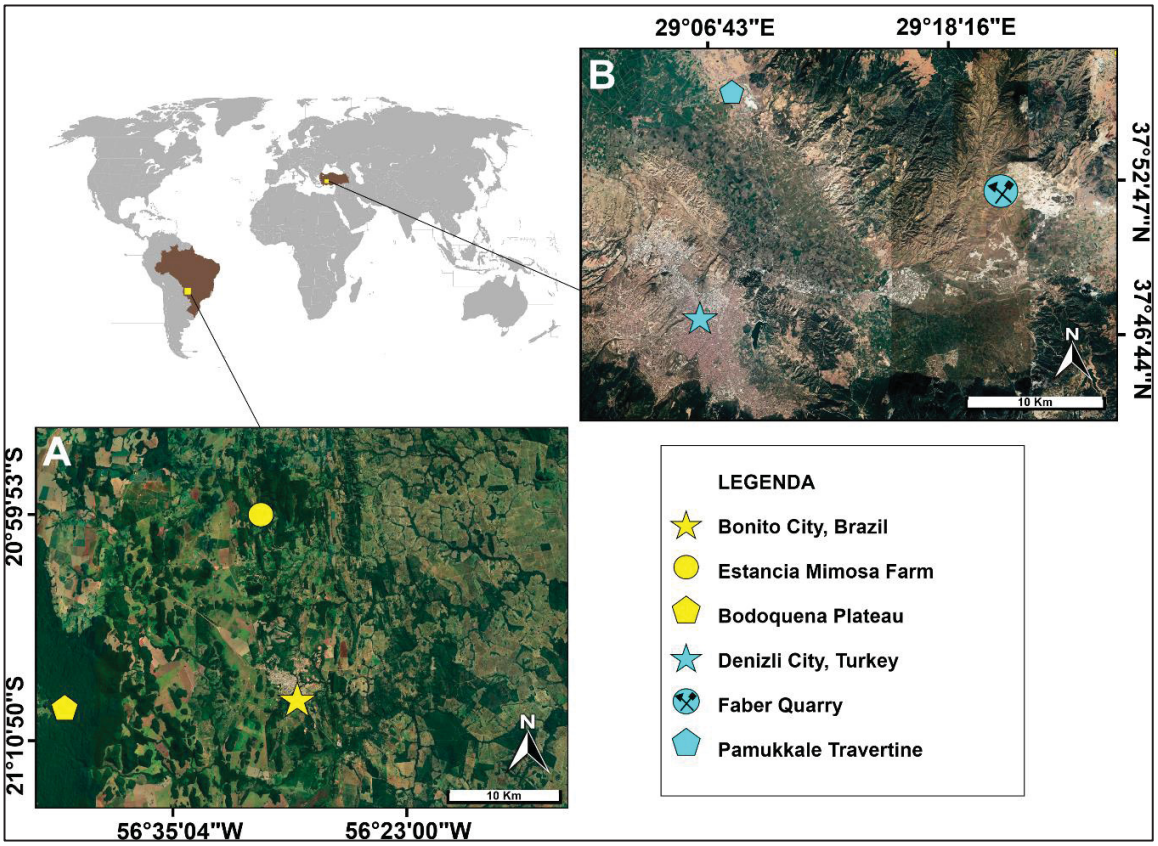


Figure 24 - Localization maps of the study areas. A) Image showing the Bodoquena Plateau and Estancia Mimosa, Brazil; B) Denizli city and the location of Faber quarry and Pamukkale travertine, Turkey.

The study area of travertines is the Faber quarry (Figure 24B), the sampling site of the cores used in this work, which is located northeast of the city of Denizli, homonymous province, in southwestern Turkey (37º51'56" N; 29º20'20" L). The travertine deposits from the Faber Quarry are part of the depositional system of the Denizli Basin, which occupies a total area of about 100 km^2 of ancient and recent deposits, whose thickness can reach up to 60 m (Ozkul et al., 2002). Travertines from Denizli province are recognized worldwide mainly for the world heritage of Pamukkale, where tourism is developed because of the extraordinary white carbonate deposits in pools, terraces and cascades (Altunel & Hancock, 1993; Erten et al., 2005), within warm waters with temperature around 35 °C and pH 6.67.

In the Faber Quarry, scientific works started with the discovery and dating of mammal fossils (Erten et al., 2005). Recently, the quarry has been extensively

studied with characterization of lithofacies and sedimentological reconstructions (Claes et al., 2015); generic controls over depositional architecture (De Boever et al., 2016); petrophysical responses and porosity classification (Claes et al., 2017). Also, tectonic reconstructions of the region were based on the structural analysis of the brittle deformation features of the quarry deposits (Van Noten et al., 2013; 2018).

The Denizli Basin is a depression 50 km long and about 25 km wide, with a WNW-ESSE trend, characterized as a small asymmetrical graben, formed to the east of the Buyuk Menderes graben, in southwestern Turkey, located about 250 km from the coast of the Aegean Sea (Westaway, 1993; Ozkul et al., 2002; Westaway et al., 2005). The basin is limited by scarps associated with normal faults of N-S direction. The Denizli Basin is part of the large Extensional Province of Western Anatolia, from western Turkey, to the Aegean Sea to part of Greece, making up one of the largest active crustal extension zones in the world, accommodated by normal faults that form horst-graben systems as a result of the increase in the subduction angle of the North African oceanic plate under the Anatolian plate in the post-Middle Miocene period (Westaway, 1993; Alçiçek et al., 2007; Ozpolat et al., 2007; Ozpolat et al., al., 2020).

According to Ozkul et al. (2002), quaternary travertine deposits accumulated along extensional fissures and normal faults over Neogene sediments from north to south of the basin. Carbonate enriched substrate served as a source of carbonate ions for the formation of overlying travertines. Ozkul et al. (2013) and Van Noten et al. (2013) demonstrated that the quaternary faults and fractures that occur along the banks of the graben are the natural paths by which meteoric water infiltrates and percolates underground, where it mixes with the hydrothermal fluid that ascends to the surface through different faults and fractures. The generated fluid, commonly acidic, re-emerges on the surface and, due to a decrease in temperature and pressure, loses CO_2 rapidly in the degassing process, which increases the pH and promote precipitates as travertine (Ozkul et al., 2013). This process is favored by the regional shallow and deep geothermal systems, which is influenced by the high local seismicity of the Denizli Basin (Westaway et al., 2005; Alçiçek et al., 2007).

METHODS

The sampling of tufa was performed in September 2019, at Estancia Mimosa farm, Central-Western Brazil, when 42 samples were collected from eight active and one inactive deposit. While for the travertine samples, a field campaign was carried out in 2011 by Petrobras company, in partnership with the University of Pamukkale and the Catholic University of Leuven, where three continuous drill cores were collected in different active quarries, including Faber quarry, in the Denizli region, southern Turkey. The Faber core has about 40 m, with 28.5 m recovered (71%). All tufas and travertines samples were stored at the Institute Laboratory of Minerals and Rocks Analysis (iLamir) of the Federal University of Parana (UFPR).

The field campaign permitted the general geomorphological and geological description and contributed with the advance in the comparative study between the two localities. Eleven petrographic thin sections of tufa samples from different deposits were described, covering at least twice each of the facies identified; and twenty-six petrographic sections of travertines, with a spacing of about 1 m in the core between each sampling, aiming to cover the entire length of the core and all the facies available. The thin sections were analyzed in a Zeiss Axio polarized light optical microscope, model Imager.A2m, at iLAMIR. The refinement of the determination of facies, as well as the investigation of microfabrics and associated microorganisms, were possible through the analysis by Scanning Electron Microscopy (SEM). Regarding the geochemical studies, about 5 g of total rock powder samples were collected, fifteen of travertines and fifteen of tufas for the following analytical techniques: X-ray diffraction (XRD), X-ray fluorescence (XRF), and carbon and oxygen stable isotopes. SEM analysis of the tufas was performed in a JEOL brand microscope, model 6010LA, coupled with a JEOL brand EDS chemical analysis system, model EX-94410T1L11, at iLAMIR. While the travertine samples were analyzed in a TESCAN VEJA3 LMU equipment coupled with AZ Tech software, 80 mm² SDD detector, at the Electron Microscopy Center of the UFPR. The XRD analysis was carried out at iLAMIR, using the equipment Malvem PANalytical, model EMPERYAN, with X'Celeratore detector with copper tube, and the diffractograms were interpreted based on the semiquantitative percentage of

minerals by the RIR (Reference Intensity Ratio) method, using the HighScore Plus software, with a PAN-ICSD database. The XRF analysis was performed at iLAMIR, using the Malvern PANalytical Axios-mAX spectrometer, with a rhodium tube, whose data are obtained from the SuperQ 5.3 software, and the equipment was calibrated with international standards, making it possible to read the following oxides for samples of carbonate rocks: CaO, MgO, SiO_2, Al_2O_3, Fe_2O_3, Na_2O, K_2O, SrO, TiO_2, MnO and P_2O_5. The stable isotope analysis was performed at iLAMIR, using a Thermo Fischer Scientific mass spectrometer, model Delta V Advantage, coupled to a Gas Bench II continuous flow system, and the data were read using the Isodat 3.0 Gas Isotope Ratio MS software.

RESULTS

The following results are presented based on three different approaches according to the working scale. A field-scale description was performed to define the differences between tufa and travertine deposits from the two sites. The determination of the facies of both systems was described based on macro and microscopic scale, using petrographic parameters, micro fabrics and organomineralization process and products. Finally, a detailed study was carried out using analytical techniques, considering the geochemical proxies.

SITE DESCRIPTIONS

The Mimoso River tufa deposits were described based on their morphologies into pools, dams, cascades, waterfall, and ramps (Figure 25) according to the classification of Pedley (1990).

Tufa sites are controlled by asymmetric pools controlled by the bedrock orientation of the substrate rock. The pools are asymmetric with deeper portions below the waterfalls, and the shallowest located at the edges, where leaves, mineral products, bacteria, and bryophytes accumulated. The transported material calcifies mainly near the edges of the pools to become more resistant and to stand out in the

relief as dams, keeping the pools stable and forming, on the outside, cascades, whose height varies from 1 to 2 m; or waterfalls ranging from 5 to 10 m. The sites progress through areas with holes and small caves near the edges of the waterfalls, where roots and tree trunks stand out, which often connect with the substrate below and form a tufa facies. There are also ramps, which are the inner part of the larger pools, close to the dams, with dip angle lower than 10º. In this case, the deposited material is mostly micrite brought in suspension by river water. Filamentous green algae also developed in the ramps trapping and agglutinating the micrite, calcifying and forming tufa facies.

The tufa sequence of the active deposits are slightly layered, with a predominantly dendriform internal structure, with variable growth directions. Bryophytes are responsible for the formation of about 80% of the facies, despite of the massive presence of calcified superior plants, such as trees, and bacterial activity with a high rate of carbonate precipitation. While inactive tufa deposits are found in abandoned channels on the sides of the actual course of the river or isolated as small islands. These sequences have the same facies of active deposits, including the predominance of dendriform structures of bryophytes.

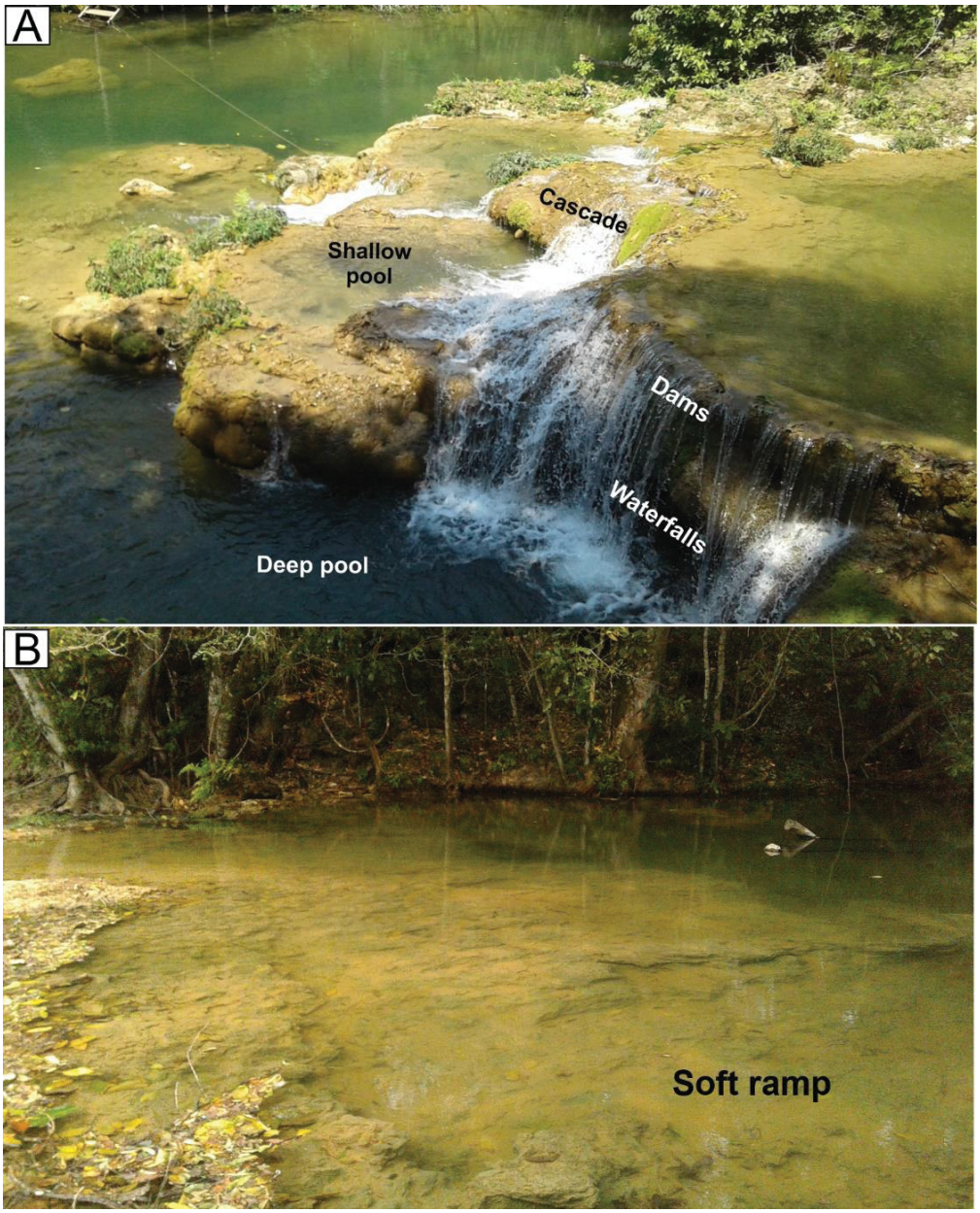


Figure 25 - Different tufa morphologies in the Mimoso River. A) cascades, waterfalls, dams, and pools of different sizes in the same site, showing the deeper portions in the center of the pools, and shallow portions close to the edges; B) ramp deposit with carbonate mud deposition in the shallow portion of larger pools.

The travertine system of Faber quarry, exhibit features characteristic of certain types of deposits recognized on the walls of the quarry based on the classification proposed by Ozkul et al. (2002): ramp, depression, mounds, fissured hill, and self-built channel, all with their sub-environments (Figure 26). Travertine

facies reflect in their fabrics the distinct characteristics of the deposits where they were formed.

Pisolith travertine facies are deposited in terraces and pools; at the edges of the pools, crystalline crusts grow perpendicular to the vertical walls. On smooth slopes (up to 40º), laminated deposits are generated, due to the velocity changes of the water flux, consisting of crystalline crusts (high fluid velocity) and thin crusts with shrubs (low velocity).

The deposits in waterfalls are crystalline crusts that form in semi-vertical walls, such as curtains, and may involve plants that grow in protected spaces, within caves with pseudo speleothems. The sb-environmental flat depression with shrubs layers is responsible for the horizontal and sub-horizontal travertine deposits of light colors and thin lamination. While the sub-environmental marsh-like depression corresponds to deposits of dark beige to brown color and rich in situ preserved vegetation, such as reeds and gastropod shells. Since the environment experiment periods of exposure and partial erosion the formation of caliches is part of the system. Paleosols are generated by pedogenetic processes derived from episodic flooding. Mounds are positive carbonate features observed in depressions with a high density of aquatic vegetation, predominantly reeds, a bamboo species found in the region, also called reed mounds. Fissured hills are open fractures, in which crystalline crusts fill the fracture walls perpendicularly. The self-constructed channels are naturally constructed by walls up to seven meters high, constituted by a crystalline crust of calcite and layers of micrite, and pisoliths generated by the agitation of the water.



Figure 26 - Travertine deposits identified within the quarries of the Denizli Basin. A) quarry wall showing deposits such as smooth ramps, waterfalls, and caves with stalactites (red narrows) formed by calcification of plant walls; B) the high-slope ramps with > 40º of slope, preserved pools and waterfalls; C) highlight the paleosol layer between the travertine layers; D) reeds that are common in the region and responsible for the formation of travertine reed lithofacies.

TUFAS FACIES

The tufas from Mimoso River were defined in six distinct facies, divided into two systems according to their depositional model namely: **autochthonous**, corresponding to the calcified tufas in situ, with no evidence of transport of the compounds; and **allochthonous** composed of material transported and deposited

at the site of calcification. The autochthonous facies are bryophyte phytoherm tufa, tree phytoherm tufa, algal tufa, and bioherm tufa. In contrast, the allochthonous facies are the micrite tufa and phytoclast tufa. Different facies were frequently associated so that more than one facies occur in the same deposit, showing a very dynamic depositional environment. Furthermore, the same facies were recorded both in the tufa active precipitation environments and in the inactive deposits.

The main characteristic of the autochthonous facies is the preservation of the original morphologies of the biological elements that compose the framestone. In the classification of tufas proposed by Pedley (1990), the name phytoherm tufa refers to plants formed by macrophyte plants in general, colonized by microorganisms. Here phytoherm was subdivided based on the preservation of two different plant frameworks described in tufas from Mimoso River (Table 3): bryophytes phytoherm (avascular framework) and tree phytoherm (vascular framework). Green algae (Characeae) are also avascular, like bryophytes, however, this group presents distinct morphological and depositional characteristics that defined another facies: algal (phytoherm) tufa.

Allochthonous facies are mainly recognized by the trapped clast material that composes the tufa framework and does not reflect its morphologies directly in the structure of the rock. Therefore, the phytoclast tufas and laminated tufa correspond directly to the phytoclast tufas and microdetrital tufa of Pedley (1990).

Table 3 - Classification of tufa facies by Pedley (1990) and its adaptations related to the present study, including the bioherm facies of Leggitt & Cushman (2001).

Pedley (1990)	**This study**
Phytoherm tufa	Bryophyte phytoherm tufa
	Tree phytoherm tufa
	Algal tufa
Microdetrital tufa	Laminated tufa
Phytoclast tufa	Phytoclast tufa
Leggitt & Cushman Jr. (2001)	
Caddisfly-dominated bioherm	Bioherm tufa

Bryophyte Phytoherm Tufa

This facies is associated with in situ calcification of bryophytes, small avascular plants whose original morphology is preserved in the tufas (Figure 27A). The bryophyte phytoherm tufa is brownish, sometimes greenish. The rock fabric varies from dendriform to palisade, between 2.0 and 5.0 cm in length, showing excellent preservation of the phyllodes (leaves) of the bryophytes. Micrite grains were trapped by the plant preserving its structure. The rhizoids (roots) of the bryophytes are also preserved in the tufa structure, occurring as hollow tubes, smaller than 1.0 mm in diameter, whose walls are massively calcified, and grow perpendicular to the phylloid branch. Calcified phylloid have varied directions, probably due to growth toward sunlight. This facies presents high porosity of the phytoporosity type and it is intercalated with plane levels of the laminated tufa facies (Figure 27B) that succeed one another, forming metric sequences in the outcrops, commonly horizontal to sub-horizontal. In thin sections the presence of micrite as a matrix range between 30 and 40%. The phylloids are calcified by sparite calcite, forming a light fringe up to 0.2 mm thick, growing perpendicular to the organic filament; or by micrite, probably by trapping the grains by the moss, so that the

original plant structure is preserved as fine dark filaments (Figure 27C). The association of facies with laminated tufa occurs by a thin layer of micrite, slightly grading to sparite, deposited perpendicular to the growth of bryophyte phylloids.

Tree Phytoherm Tufa

This facies associates with in situ calcification of trunks and roots of superior vascular plants, such as trees (Figure 27D). Usually located on the edge of drainages, the tree phytoherm tufa is formed by autochthonous carbonate tubes that cover roots and trunks or as a mold of those plants that have already been decomposed, presenting diversified forms. The tree phytoherm tufa has lengths ranging from centimeters to meters, and millimeter to centimeter diameters. The tufa fabric is related to the mineral growth around the original trunks, generally concentric, in layers, similar to the growth of stalactites; or dendritic, like shrubs, of the organic surface of the tree (Figure 27E). The color varies from light brown to greenish and the porosity varies from high to medium. Furthermore, this facies may be associated with bryophyte phytoherm tufa, considering the development of bryophytes around the calcified trunks and roots. In the thin sections, it is observed the variation in mineral growth forms around plant trunks and roots. In contact with the plant structure, the mineral growth occurs by concentric layers and nanometric thickness, but they grate slightly for growth of the palisade sparite, with millimeter sizes in a direction perpendicular to the center. Another form of mineral growth in these facies are the shrubs, growing directly from woody organic material or after the development of concentric laminae (Figure 27F). The shrubs grow on top of each other, as layers, and may appear as acicular crystals forming dendritic to radiated structures.

Algal Tufa

Algal Tufa correspond to the calcification of green algae, Characeae, found in the shallower portions of pools (Figure 27G). Consists of filamentous algae that

trap micrite transported in suspension on the water, promoting the calcification of the tallus (filaments), preserving as tufa fabric. The Algal Tufa shows a greenish-brown color and high porosity of the phytoporosity type (Figure 27H). The constituent tallus of green algae are thin tubes, lengths greater than 10 cm (Figure 27I). This facies have the minor occurrence in the studied deposits and was described in only three waterfalls. Furthermore, due to the fragility of the algal tufa, it was not possible to make specific thin sections of this facies, but there was petrography occurrences of the Algal Tufas in association with other facies.

Bioherm Tufa

The Bioherm Tufa facies is formed by an agglomeration of tubes with diameters varying on average from 2.0 to 4.0 mm, corresponding to in situ calcified cases of insect larvae (Figure 27J). The larval tubes are formed by very thin inner walls in layers (up to 6 layers) probably because of calcification of the silk excreted by the organisms to build their protective cases. The tubes differ from bryophyte root tubes by their size in diameter, for the sizes found in the roots are smaller than 1.0 mm, and also by the layered shown on the case larvae walls (Figure 27K). The larval case carbonates stand out in the Bryophyte Phytoherm facies, as evidenced in the field by the active deposits, showing the association of these facies. The waterfalls where bryophytes grow, record the presence of aquatic larval insects living attached to the substrate, suggesting the current in situ calcification of their cases. In thin sections, the larvae cases occur as perfect circles of preserved organic matter, such as microsparite and sparite, with very low presence of micrite matrix, about 5 to 10%, and very high porosity, greater than 80%. The various layers of silk that form the walls of the cases are preserved as well, showing the original morphology of these structures, that can be circular when in a basal cut, or elliptical, in a longitudinal cut (Figure 27L).

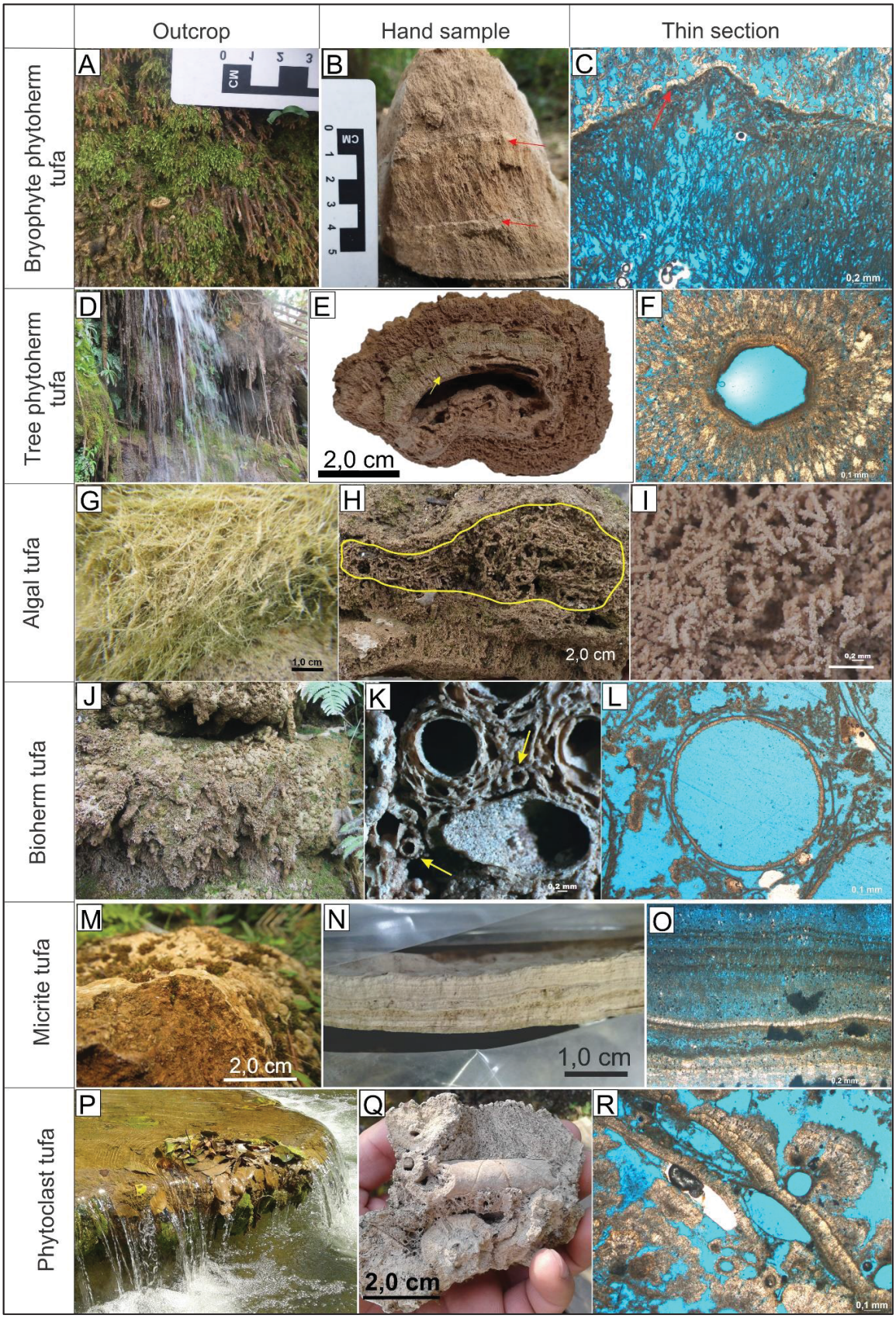

Outcrop
Hand sample
Thin section
Bryophyte phytoherm tufa
Tree phytoherm tufa
Algal tufa
Bioherm tufa
Micrite tufa
Phytoclast tufa
A
B
C
D
E
F
G
H
I
J
K
L
M
N
O
P
Q
R
2,0 cm
1,0 cm
0,2 mm
0,1 mm

Figure 27 - Tufa facies in the Mimoso River, Bonito, Brazil. A) bryophyte phytoherm tufa, active and in situ precipitation of bryophytes; B) tufa fabric reflecting the dendriform plant structure, interleaved with millimeter layers of micrite (red arrow); C) preservation of phylloides as original fine plant structure (dark organic matter) and the association of the laminated facies; D) tree phytoherm tufa, in situ precipitation of roots and trunks of superior vascular plants, located at the edge of rivers and waterfalls; E) mineral growth around woody material, that occurs as concentric layers or as shrubs (yellow arrow); F) thin concentric laminar growth around the woody material that decomposes, the thickness of the laminae may vary, followed by spatic palisade growth in a perpendicular direction; G) algal tufa, in situ occurrence of Characeae green algae which was calcified in shallow pools; H) algal tufa level lithified, showing excellent porosity; I) calcified Characeae algae tallus with evident micrite trapping; J) bioherm tufa facies, outcrop showing the bioherm facies as a cluster of calcified larval tubes; K) the facies fabric with thin layers forming the tube walls, showing the difference in sizes of the larval cases in relation to root tubes or branches of bryophyte structure (yellow arrow); L) precipitation of organic tissues as sparite and microsparite, showing the exceptional preservation of the layered walls of the larval cases; M) laminated tufa, outcrop with micrite deposition on calcified bryophyte, forming a micrite crust; N) thick laminated tufa layer showing continuous internal lamination; O) sub-horizontal to horizontal laminar inner structure, with continuous and localized levels of palisade sparite growth; P) phytoclast tufa, active deposit of woody material where the facies formation occurs; Q) sample showing phytoclastic material, such as leaves, small trunks, and roots, trapped and calcified as phytoclast tufa facies; R) examples of phytoclasts such as fragments of bryophytes and other small calcified plants, leaf molds, basal sections of small trunks, roots, and associated organic matter.

Laminated Tufa

Laminated Tufa facies is generated by the deposition of light brown carbonate micrite, present at the bottom of pools and ramps or above the Bryophyte Phytoherm Tufa (Figure 27M). The Laminated Tufa presents millimetric to centimetric thick and, generally, with a continuous internal lamination, alternating light and dark colors, suggesting a stromatolitic inner structure (Figure 27N). In active deposits it was possible to identify micrite deposition above the bryophytes, forming a carbonate crust, justifying the effective association between such facies. In thin sections, the layers occur as sub-horizontal to plane-parallel or wavy, but the inner lamination remains continuous. In addition to micrite deposition, it was possible to recognize some submillimetric to millimetric levels of microsparite calcite growth, forming palisade fringes up to 0.2 mm in length and shrubs around 1.0 mm (Figure 27O).

Phytoclast Tufa

The facies is composed of leaves and woody material such as allochthonous trunks and roots calcified in a micritic matrix or even associated with other facies. This phytoclastic material is fragmented and transported to the deposition site where precipitation takes place, (Figure 27P). Commonly composed with leaves of trees twisted and curled, associated with pieces of trunks and branches. The Phytoclast Tufas are light brown and do not have a defined structure (Figure 27Q). In the preserved leaf molds, it is possible to notice that the calcification occurred by trapping or massive microcrystalline precipitation. They are usually in the cascades and dams formed on the edge of pools where the phytoclastic material accumulates and for this reason, this facies is massively associated with the Bryophyte Phytoherm Tufa. Thin sections showed fragmented and entire phytoclasts, with sizes submillimetric to centimetric, in a sparse matrix of micrite, about 5 - 10%. Leaves, root tubes, branches and small trunks are common in the basal section, in addition to small plants and pieces of bryophytes, all predominantly calcified by calcite sparite (Figure 27R). Larger leaves molds showed palisade sparite calcification that grows perpendicular to the leaf (dark organic material) in its inner portion. In addition, detrital material of non-carbonate composition mixes with organic matter and micrite.

TRAVERTINES FACIES

The travertine carbonates of Faber quarry were described and characterized by six facies, in which the carbonate facies represents about 84% of the composition of the core, corresponding to: micrite travertine, granular travertine, reed travertine, caliche, pisolith travertine and breccia. Such facies occur several times along the core, interspersed between them, with centimetric to metric thicknes. At the bottom of the core, was registered siliciclastic facies: sandstones, conglomerates, and paleosol, representing 16% of the lithological composition, and were considered in the present work.

With regard to lithofacies characterizationall facies of the travertine system were defined as autochthonous deposition. Even breccias which in carbonate system are influenced in situ by a soil formation process where they are involved in

weathering, erosion, dissolution, expansion, and contraction in arid and semi-arid climates, as proposed by Ozkul et al. (2002). Therefore, we based the descriptions on the travertine classifications from two different works, as presented in the Table 4.

The caliche, pisolith and reed travertine facies correspond directly to those proposed by Ozkul et al (2002). Claes et al. (2015) presented a classification of travertine facies called dark-colored peloid travertine, referring to that facies composed of dark peloid micritic carbonate associated with micrite and microsparite. Here it was used two different facies that are remarkable in the Faber quarry: micrite travertine and granular travertine. Besides that, the breccia facies were also adapted from the name proposed by Claes et al (2015) as monomitic travertine.

Table 4 - Travertine classifications from literature, and adaptations related to this study.

Claes et al. (2015)	**This study**
Dark-colored peloid travertine	Micrite travertine
	Granular travertine
Monomitic travertine	Breccia
Ozkul et al. (2002)	
Reed travertine	Reed travertine
Caliche	Caliche
Pisolith travertine	Pisolith travertine

Micrite Travertine

The Micrite Travertine Facies is composed of light beige limestone, occasionaly slightly pink to whitish, with a massive structure and matrix with a predominant composition of calcite micrite (Figure 28A), constituting more than 90% of the rock. It is the most common facies with thickness ranging from 15 cm to 2.15 m. The Travertine Micrite has generally low porosity, locally with high reed

phytoporosity; gastropod molds, up to 1.5 cm in diameter; and vugs reaching 1 cm. It is observed manganese oxides in fractures.

In thin sections, the Travertine Micrite is massive commonly varying in dark (Figure 28B) and light cream-color, with preservation of ostracod and gastropod molds (Figure 28C). Locally, there is matrix dissolution forming pores that are partially filled by calcite sparite, forming cement with a mosaic structure at the edges of the pores, and dog-tooth calcite that grows mainly in the moldic pores of gastropods.

Granular Travertine

Granular Travertines are light and dark beige, massive structure and granular texture (Figure 28D). This facies differentiates from Micrite Travertines because of the majority presence of peloid micrite and microsparite in the Granular facies, besides the interparticle pores filled with calcite cement, producing sub-rounded sparite granules in a granular micrite matrix. The thickness variation of this facies in the core is about 20 to 65 cm. The porosity increases in relation to the anterior facies, being of the vugular types, with vugs of up to 1.0 cm; phytoporosity of reeds in living position; gastropod molds, with valves up to 0.5 cm in diameter; and fenestral porosity. Locally, this facies shows a slight bedding due to the intercalation of light and dark layers along the core. There is evidence of fluid percolation recorded by reddish coloration, hardening of the rock, and reduced porosity.

In thin sections, the peloid micrite is dark brown and forms sparse sub-rounded and elongated grains (Figure 28E), with sizes about 0.01 mm, sometimes presenting a lumpy texture. The peloids are spaced apart by the microsparite that forms the rock cement (Figure 28F). When a microsparite is dissolved, it forms large irregular pores that are completely filled with sparite calcite, forming a mosaic and dog tooth cement.

Reed Travertine

Reed Travertine are dark beige limestone, with a massive structure and granular texture, the intraclasts being mostly composed of reeds and charophytes (above 75%) supported by the micritic or fine granular matrix. It is possible to distinguish intraclasts from reeds in living position (verticalized) with sizes up to 3.0 cm in length, or reworked, with horizontalized and broken plant tubes (Figure 28G). The medium to high porosity is predominantly phytoporosity of reeds in situ or not, and secondarily, molds from gastropods with valves of up to 0.8 cm.

Under optical microscopy, phytoclasts, such as plant residues of charophyte algae and reeds, are presented in a micritic matrix and microsparite cement. Phytoclasts have a dark brown color, due to the presence of preserved organic matter, making it possible to visualize the organic layers that compose them (Figure 28H). Reeds and charophytes are sometimes fragmented, sometimes with the rings of their stems intact. In the case of charophytes, it is the reproductive organs called oogonia, which calcifies and is preserved, being easily identified petrographically, and occurring in large numbers. Oogonia are recognized as ovoid or circular bodies 0.5 to 1 mm in diameter, with tubules arranged in spiral forming outer rings (Figure 28I). The porosity is medium to high (about 20 – 30%), of the phytoporosity type whose phytopores of charophytes and reeds vary from circular, showing the basal section of their stems, and elliptical, when in the longitudinal sections. Reed phytopores are almost always hollow, whereas charophyte phytopores are partially or completely filled with microsparite or sparite calcite, in this case, forming a mosaic-type cement. There are also vugular and dissolution porosity, which is partially filled with equant calcite cement.

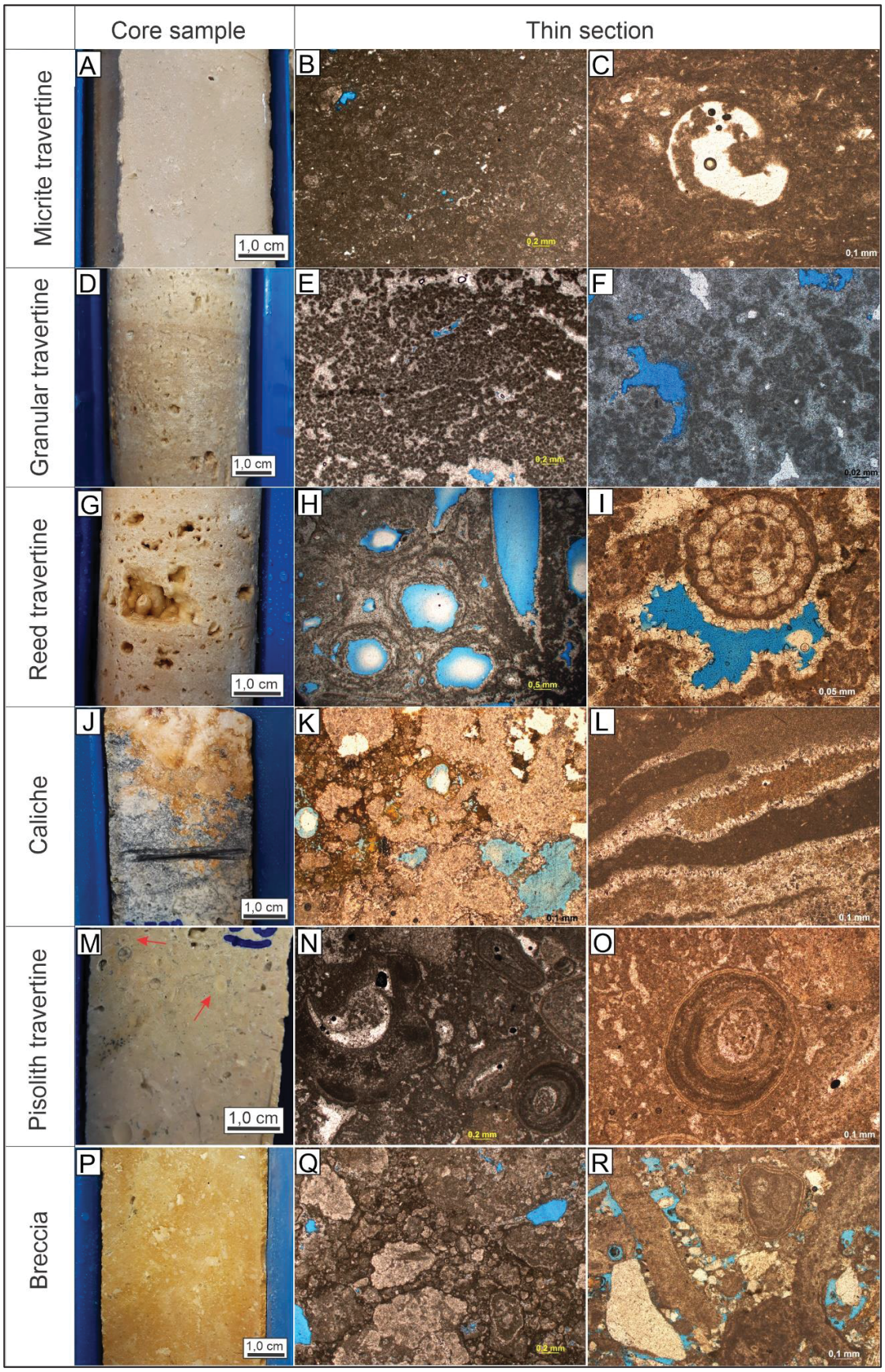

Core sample
Thin section
Micrite travertine
Granular travertine
Reed travertine
Caliche
Pisolith travertine
Breccia
A
B
C
D
E
F
G
H
I
J
K
L
M
N
O
P
Q
R
1,0 cm
0,2 mm
0,1 mm
0,02 mm
0,5 mm
0,05 mm

Figure 28 - Travertine facies described from Faber quarry, Denizli, Tukey. A) micrite travertine, core sample showing the massive structure and predominant composition of micritic calcite; B) thin section overview of the facies showing dark and massive micritic calcite; C) gastropod mold porosity preserved in micritic calcite matrix; D) granular travertine, core sample showing a granular facies texture with calcite granules created by filling pores; E) photomicrograph of overview showing the composition of dark peloid micrite as a rock framework and with microsparite surrounding, as a pore-filling cement; F) another type of micrite with a lumpy appearance and microsparite cement filling the dissolution pores totally or partially; G) reed travertine, core sample with phytoporosity represented by fragments of reeds in a living position (sub-vertical) and other round pores, possibly of charophytes or even reed roots, highlighting the calcified reed tube and preserved in a porous cavity; H) photomicrograph with an overview of the rock whose reed phytoclasts occur in a dark micritic matrix and microsparite cement, forming high phytoporosity of basal and longitudinal sections of their stems; I) highlighting oogonia phytoclasts, the reproductive organ of charophyte algae, whose mold was completely filled with sparite calcite, forming a mosaic cement, in addition to a pore by dissolution partially filled with calcite equant cement; J) caliche, in a core sample distinguishing micrite travertine lithoclasts reworked and cemented by a granular matrix with intense oxide percolation; K) photomicrograph with an overview of the rock composed of reworked material, with percolation of yellowish oxides within irregular pores; L) emphasis on vadose silt infiltrations, which are intercalated with dark micrite and sparite films filling fractures; M) pisolith travertine, core sample with glass lithoclasts of rounded and laminated circular pisoliths (red arrow); N) photomicrograph of the general view with a framework consisting of pisoliths and ooids, in a dark micrite matrix; O) emphasis on spherical pisolith with continuous internal laminae and carbonate lithoclast core; P) breccia, core sample whose framework is composed of angular clasts and supported by the granular micritic matrix; Q) photomicrograph showing a micritic and massive matrix supporting the framework of angular grains of carbonate lithoclasts from other facies or reworked; R) framework composed of angular lithoclasts of varying sizes, the interparticle porosity is preserved without effective posterior cementation, in addition to the preservation of the pisolith clast, in a matrix-supported by the framework, an occurrence located in the facies.

Caliche

Brown caliche with yellowish portions, massive structure, and framework composed of subangular and reworked carbonate lithoclasts. Also, calcitic crusts with shrubs and an intense percolation of oxides, filling fractures (Figure 28J). The porosity is medium (20 – 30%) ranging from reed phytoporosity to gastropod and vugular mold (vugs up to 2.0 cm).

In thin sections, the reworked carbonate lithoclasts showed vadose silt infiltrations, fractures filled by micrite and microsparite. The carbonate lithoclasts originated from other facies, composed of granular micrite, interconnected by microsparite cement and oxide films (Figure 28K). In the matrix, there are also shrub-type structures, up to 1.5 mm. The porosity increases with matrix dissolution. There is partial filling of the pores with mosaic equant sparry calcite. Locally there are

geopetal structures with vadose silt and micrite infiltration, forming films that are intercalated with mosaic of sparry calcite cement (Figure 28L).

Pisolith Travertine

The Pisolith Travertine are light beige color and massive structure, with micritic to granular matrix. The intraclasts are formed by pisoliths (Figure 28M), varying from 4.0 to 6.0 mm in diameter. The shape of the pisoliths is subspherical and the nucleus is mostly composed of carbonate, originating from the reworking of other facies. The Pisolith Travertine facies occurs in just 20 cm along the core, displaying, moldic porosity by dissolution of gastropod shells, reaching 5.0 mm.

In thin sections, it is possible to recognize that the constitution of the lithoclasts of the framework is about 50% pisoliths, and subordinately ooids (smaller than 2.0 mm), in a massive and dark micrite matrix (Figure 28N). Pisoliths are rounded to subrounded, larger than 2.0 mm in diameter, and have a concentric lamination formed by growth lines around their nucleus that vary from carbonate (Figure 28O) to siliceous. The porosity is low (approximately 5 – 10%), moldic by dissolution of gastropod, and interparticle, totally or partially filled with sparry calcite cement (dog toot and mosaic). Locally, the pisolith grows around the gastropod mold, so that the bioclast works as the nucleus.

Breccia Travertine

The Breccia Travertine facies is massive, brown-colored, locally reddish (Figure 28P). The matrix is granular micritic with marl composition, and the framework is composed of angular to sub-rounded carbonate lithoclasts, varying in sizes from 0.2mm to 1.0 cm, supported by the matrix (Figure 28Q). The carbonate clasts are formed by dissolution during pedogenetic processes where reddish matrix infiltrations are common, as well as meteoric and vadose calcite cement. The Breccia Travertine varies between 15 and 45 cm, porosity is very low to medium (10 - 25%), predominantly molds of gastropods and minor dissolution partially filled with

sparry calcite. The interparticle porosity is generally preserved. Locally, there are gastropod bioclasts and also pisoliths (Figure 28R).

MICROFABRICS

Under SEM scale, it is possible to observe several micro and nanometric mineral features, such as organomineralization products, for both tufas and travertines, allowing the definition of specific microfabrics for the facies. In the Tufa Facies, the identification of EPS associated with filaments in all of the samples, indicates the main type of organic matrix for that facies. On the other hand, in the Travertine Facies, only the Reed Travertine and Caliche facies presented a rich content of organic matter associated with mineral precipitation. All the other facies analysed, display inorganic mineral features from secondary precipitation.

Tufas from the Mimoso River commonly present a granular microfabric composed of microcrystals of micritic calcite subhedral to euhedral with shapes of soft rhombohedrons trapped or precipitated by biological influence in an organic matrix. All facies in this system are closely associated with fossil remains of filamentous bacteria and EPS (Figure 29A), suggesting that micrite grains nucleate and grow on the bryophytes, tree trunks and roots, larval cases, and wood material fragments calcifying these structures and preserving their frameworks.

Well-developed calcite microcrystals occur pervasively in the bioherm, algal, and laminated tufa facies, where the grains vary from 5 to 25 μm, assuming well-defined polyhedral forms, normally rhombohedral or triangular (Figure 29B). While in the bryophyte phytoherm, tree phytoherm, and phytoclast tufa facies, the neoformed grains are anhedral to subhedral, assuming a not completed development of the crystals (Figure 29C), usually in these cases, smaller mineral features are noticeable, such as nanocrystals calcite tetrahedrons, ranging from 20 to 800 nm, in a coalescence process to form a larger rhombohedral crystal (Figure 29D), showing an in situ organomineral precipitation.

In the Bryophyte Phytoherm Tufa facies, the phylloids and roots of the bryophytes are calcified as microtubes ranging from 20 to 150 μm thick, with an

average of 60 μm. The Figure 29E shows a basal section displaying hollow microtubes in the center, most likely due to decomposition of organic matter vegetable. Even though well-developed euhedral crystals have not been identified in the tree phytoherm facies, these facies have a rich content of fossil EPS and mucus-like material (Figure 29F), in which it is possible to identify the in-situ growth of carbonate crystals. The Algal Tufa Facies has calcified algal tallus recognized by trapping neoformed rhombohedral micrite crystals or by organomineralization of the algae organic tissue (Figure 29G). The Laminated Tufa Facies is characterized by bacteria moldic imprint on microsparite crystals, and hollow microtubes with thicknesses between 2.2 and 6.7 μm (Figure 29H), an evidence of the activity of filamentous bacteria, and green algae, in the pools where this facies is currently been deposited.

The Bioherm Tufa Facies displays calcification of larval cases by trapping micrite grains by the silk that forms the case walls, or by biological influence on mineral precipitation indicated by filaments with EPS. Besides, it is suggested that the silk excreted by the organism when forming the cases also serves as an organic matrix for organomineralization, considering that its inner layers are exceptionally well preserved (Figure 29I). The calcite grains that form the layers of the case walls are equigranular subhedral to euhedral rhombs, with an internal triangular structure, (Figure 29J). Another structure identified in the Bioherm Tufa Facies are microcolumns up to 1 μm thick and up to 5.7 μm long, formed by coalescence of calcite nanospherulites (Figure 29K). These microcolumns coalesce to form larger crystals of triangular polyhedral calcite.

The occurrence of trapped diatoms between calcite micrite grains are ubiquitous recorded in the Bioherm Tufa Facies (Figure 29L), where two different species of diatoms are identified based on the difference in the ornamentation of their carapaces. In addition, there is the incipient presence of diatoms traps between calcite grains in the bryophyte phytoherm, algal and laminated tufa facies.

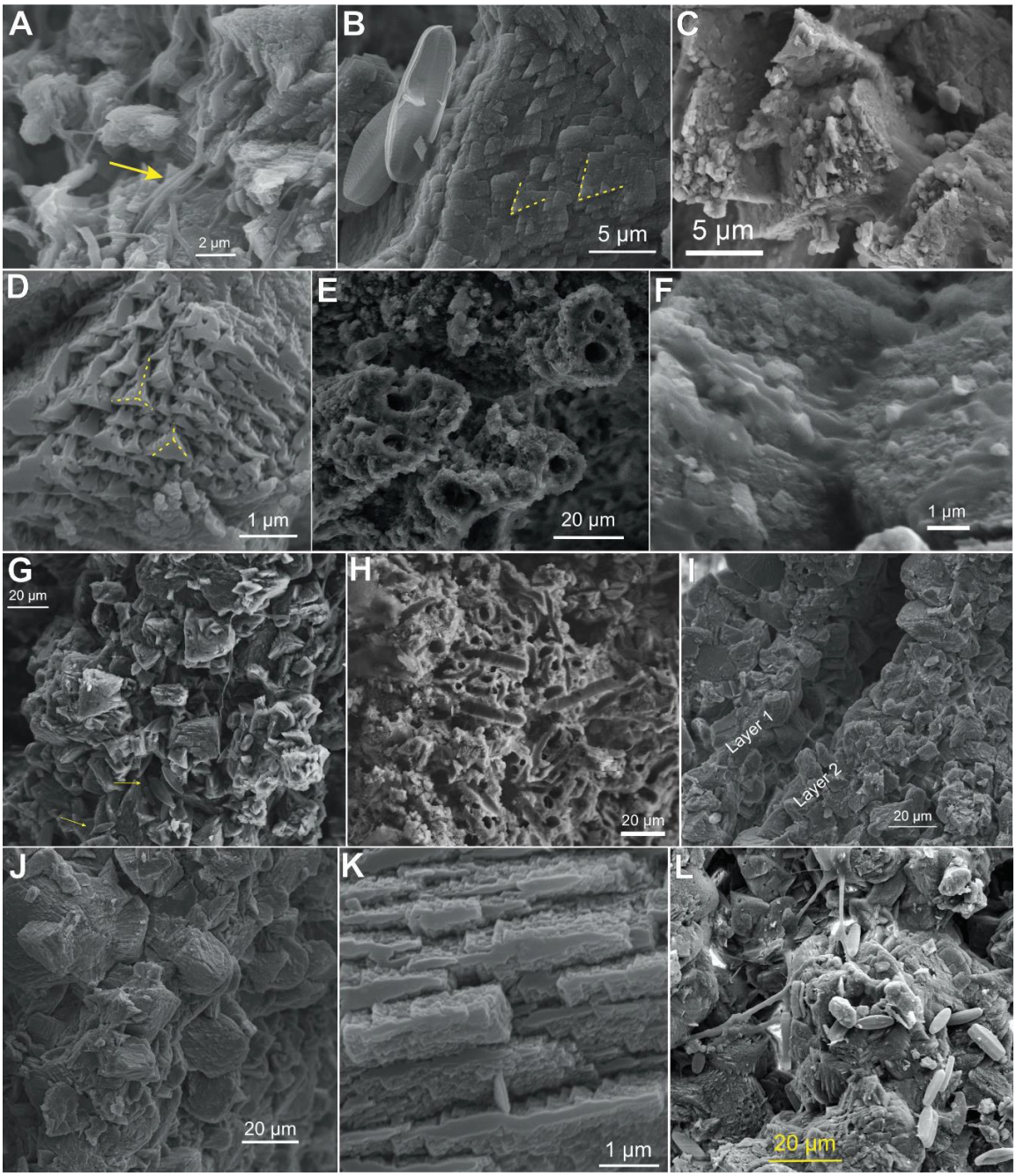


Figure 29 - SEM images from tufas facies microfabrics and biological contents associated. A) fossil remains of filamentous bacteria (yellow arrow) and EPS largely disseminated in the tufa facies; B) well-developed calcite microcrystal as triangular polyhedral shape, neoformed by the coalescence of nanocrystals (yellow line highlighted), and the association of this facies with diatoms in the Bioherm Tufa; C) anhedral calcite grains showing not completed development of the crystal in the tree Phytoherm Tufa; D) nanocrystals of tetrahedrons (yellow highlight) in a coalescence process to form a larger rhombohedral crystal in the Bryophyte Phytoherm Tufa; E) basal section of the microtubes in Bryophyte Phytoherm Tufa, due to the probable decomposition of organic matter vegetable; F) tree phytoherm facies showing a rich content of fossil EPS and mucus-like material; G) calcified Characeae algal tallus in Algal Tufa, with organominerals formed by on the algae organic tissue, besides the trapping neoformed rhombohedral micrite crystals and diatoms (yellow arrow); H) imprint

of cyanobacteria on microsparite crystals and hollow microtubes in the Laminated Tufa, an evidence of the activity of filamentous cyanobacteria in pools where this facies was deposited; I) larval cases with its inner layers preserved in the Bioherm Tufa Facies, suggesting that the silk excreted by the organism also serves as an organic matrix for organomineralization; J) calcite grains forming the layers of the larval cases, with similar sizes and subhedral to euhedral shapes of soft rhombohedrons with an internal triangular structure; K) microcolumns formed by coalescence of calcite nanospherulites in the Bioherm Tufa Facies; L) trapped diatoms between calcite micrite grains as an ubiquitous content in the bioherm tufa, but they also occur on other facies.

Based on SEM images of travertines in the Faber quarry, it was possible to recognize microfabrics distinct from tufas, both in relation to those associated with organomineralization, and the features formed by inorganic precipitation. The micritic matrix content in the travertines of the Faber quarry is higher in all of the facies, compared to the tufas of the Bonito area. The Breccia facies samples were not analyzed in scanning electron microscopy.

In the Travertine Micrite facies, it was possible to differentiate two microfabrics corresponding to two distinct types of micrite: a densely packed massive micrite, cryptocrystalline, assuming an aphanitic to sub-aphanitic texture, slightly laminated (Figure 30A), grading to a granular micrite with grain sizes ranging from 1 to 2 μm, that occurs also, in the Travertine Pisolith Facies (Figure 30B). Another type of micrite, as peloids, occurs in the Granular Travertine Facies, whose rounded grains reach up to 222 μm in diameter (Figure 30C).

In the Granular Travertine Facies, the pores are partially filled with secondary crystals of calcite equant with sizes above 130 μm (Figure 30D) and dog-tooth calcite, sizes from 28 to 50 μm in the long axis; and total filling pores with mosaic sparry calcite cement (Figure 30E). Locally, there are acicular calcite crystals of about 5 μm long, corresponding to microsparites (Figure 30F). Incipiently, evidence of carbonate dissolution was recorded in clusters of initially acicular calcite crystals, as well as in euhedral equant calcite crystals filling pores, in this case only the crystal cores were dissolved.

In relation to microfabrics of organominerals, small variations were observed for the travertine facies in relation to the tufas. The best-developed organominerals occur in the Reed Travertine Facies, as are euhedral crystals of rhombohedral calcites, with sizes ranging from 5 μm to 6.7 μm on the long axis (Figure 30G),

neoformed by the junction of smaller triangular polyhedrons, which are identified as the internal structure of larger crystals. The rhombohedral calcites are associated with EPS and filamentous organic material, showing an effective organomineralization process in the Reed Travertine. In addition, structures of calcified charophyte algae are identified, such as the tallus and the oogonia, the algae reproductive organ, showing exceptional preservation (Figure 30H).

The Caliche Facies presents the initial products of biologically influenced mineralization, closely associated with EPS, filamentous microorganisms, and mucus-like material. Clusters of neoformed calcite nanospheres in an organic matrix predominate in the Caliche Facies (Figure 30I), which coalesce to form structures in the form of pinnacles, pseudo microcolumns, and fibrous triads, but without the formation of larger, well-defined crystals (Figure 30J). In larger neoformed calcite crystals, it was noted the occurrence of possible fossils of coccoid bacteria, characterized by colony-like aggregates of ovoid and spherical carbonate nanocrystals, with sizes from 4 to 17 μm, forming a distributed granular viscous texture irregularly on the crystal surface (Figures 30K). Bacterial rods characterized by isolated solid calcite tubes and associated with mucus-like structures of the honeycomb type were also recognized (Figure 30L).

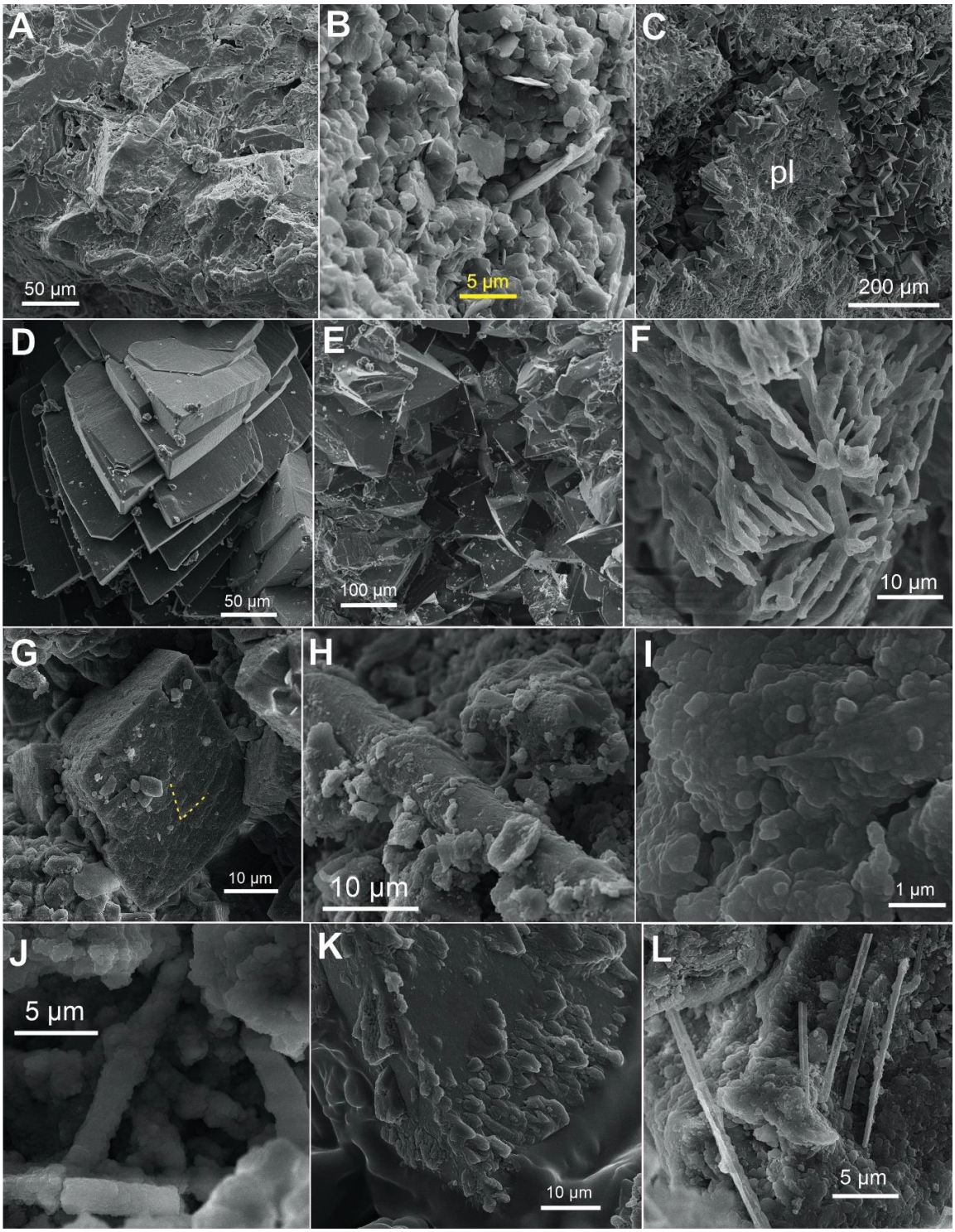


Figure 30 - SEM images from travertine facies microfabrics and some biological contents associated. A) densely packed cryptocrystalline micrite aphanitic to sub-aphanitic slightly laminated texture, in the Micrite Travertine Facies; B) granular micrite, with grain size ranging from 1 to 2 µm, that occurs in the micrite and pisolith travertine; C) peloid as another type of micrite (pl) in Travertine Facies, occurring in the Granular Travertine, as rounded grains reaching up to 222 µm in diameter, surrounded by sparry calcite filling the pore spaces; D) pores partially filled with secondary crystals

of calcite equant in the Granular Travertine Facies; E) total filling pores with mosaic sparry calcite cement, also in the Granular Travertine Facies and in the Micrite Travertine; F) acicular microsparry calcite crystals of about 5 µm long, in the Granular Travertine Facies; G) best-developed organomineral in the Reed Travertine Facies as euhedral crystal of rhombohedral calcite neoformed by the junction of smaller triangular polyhedrons, identified as the internal structure of the larger crystals (yellow highlighted); H) structures of calcified charophyte algae, such as the tallus and the algae reproductive organ, showing exceptional preservation in the Reed Travertine Facies; in the Caliche Facies there is the occurrence of I) clusters of neoformed calcite nanospheres in an organic matrix, which will coalesce to form larger structures, such as pinnacles, J) pseudo microcolumns, and fibrous triads, but without the formation of larger and well-defined crystals; K) possible fossils of coccoid bacteria, characterized by colony-like aggregates of ovoid and spherical carbonate nanocrystals, forming a distributed granular viscous texture irregularly on the crystal surface; L) bacterial rods as isolated solid calcite tubes and associated with mucus-like material.

GEOCHEMICAL ANALYSIS

The tufa facies have a homogeneous chemical composition, with CaO being the main oxide found, ranging from 49.86 to 53.07% (Figure 31A). Some facies have a less expressive SiO_2 content up to 3.88% as in the Larval Bioherm Tufa Facies, and also significant MgO contents with values above 1.09% in all facies, except for the Phytoclast Tufa around 0.96%.

The Travertine Facies also present a homogeneity in the chemical composition, marked by the predominance of CaO (50.72 to 54.92%) and effective silica content in some facies, reaching 4.92% in the Breccia Facies (Figure 31B). Unlike tufas, in travertines the MgO content is not significant, showing values less than one per cent. On the other hand, the presence of Al_2O_3 was recorded in travertine facies where the silica content is high, showing an association of these oxides.

Volatile oxide contents measured by loss to fire for tufas and travertines were obtained by X-ray fluorescence. Finally, the samples have trace compositions of Fe_2O_3, Na_2O, K_2O, TiO_2, MnO, P_2O_5, and SrO, with values less than 1.00%.

The mineralogical composition of tufas and travertines was analyzed by X-ray diffraction and only two mineral phases, calcite and quartz, were determined in both lithotypes. The XRD data can be correlated with the chemical composition obtained by XRF, as both analyzes showed homogeneity in the systems. Calcite and quartz minerals have an inversely proportional relationship, so that calcite occurs mostly in all facies, reaching 100% in some cases, while quartz occurs more

significantly in those facies where there is a decrease in calcite content. The contents of MgO in the tufas and Al_2SiO_3 in the travertines obtained by XRF were not enough to change the mineral chemistry.

In the tufa system, the Tufa Phytoclast Facies, of allochthonous origin, presented all samples composed of calcite and quartz (Figure 31C), the same happened for the Caliche and Pisolith facies in the travertine system (Figure 31D). The other facies from both sites demonstrated either an exclusionary composition of calcite in some samples, but also an association of calcite and quartz.

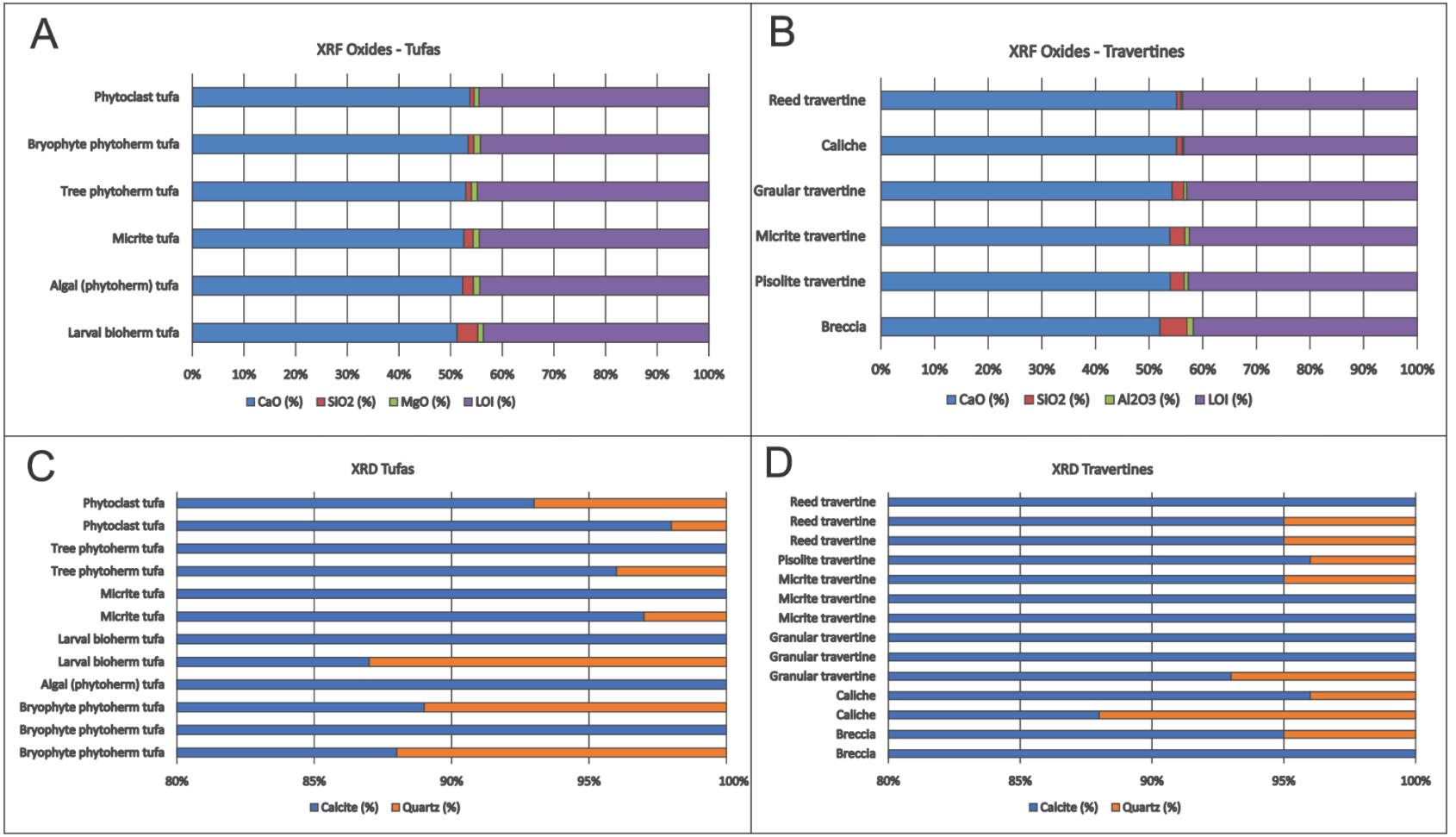


Figure 31 - Geochemical analysis data. A) and B) graphs with the oxide contents obtained by X-ray fluorescence, with values presented in an ascending order of the CaO content, the main chemical component found in both tufa and travertine samples, and the volatile content was calculated based on the loss to fire, and the composition of trace oxides was not considered; C) and D) X-ray diffraction results, with the main mineral phases found in the samples of both lithotypes, calcite and quartz, which have an inversely proportional relationship, so that calcite occurs mostly in facies where there is a decrease in quartz content.

The travertines show negative to slightly positive trend for $\delta^{13}C$, whereas both, the travertine and tufas, show negative trend for $\delta^{18}O$. Thus, both systems are enriched in light isotope and depleted at the heavy ones (Figure 32). The tufas from the Mimoso River show isotopic values ranging between -7.10 and -8.91 ‰ VPDB for the $\delta^{13}C$, indicating associations with microbes and plants, and probably photosynthetic influence; while the $\delta^{18}O$ signatures varies between -7.02 and -7.98 ‰ VPDB, corresponding to the meteoric water contribution. The stable isotope ratios of travertines in the Faber core have values of negative $\delta^{18}O$, ranging from -6.65 to -8.00‰ VPDB, which also may indicate the influence of meteoric water in the system; whilst values of $\delta^{13}C$ vary from 1.20 to -4.00‰ VPDB, and when correlated with facies, the negative values are attributed exclusively to caliche, thus suggesting a greater influence of organic matter in this facies, or still, photosynthetic process action.

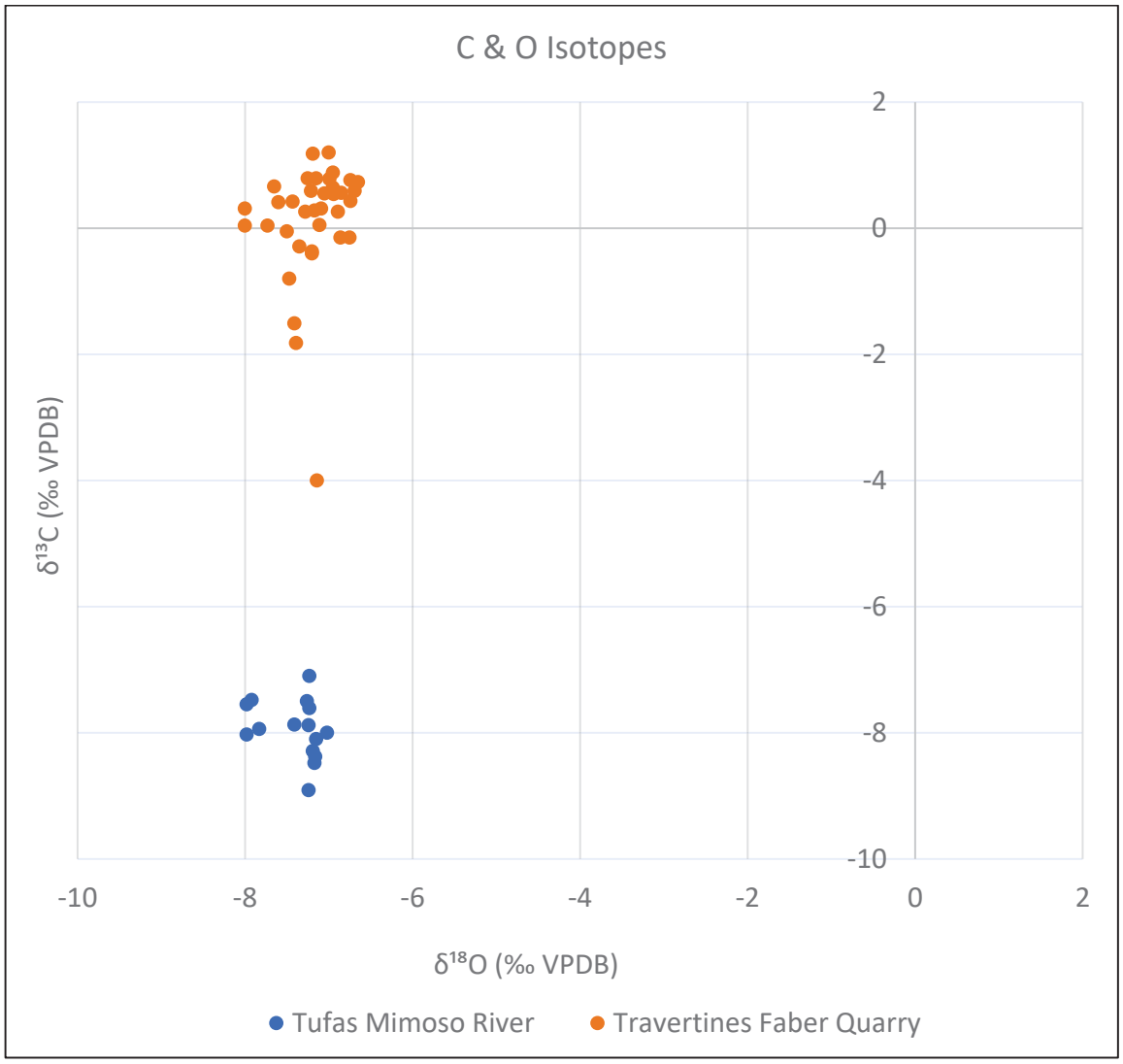


Figure 32 - Carbon and oxygen stable isotope data. Tufas from the Mimoso river showed negative ranges for either $\delta^{13}C$ and $\delta^{18}C$ values; whilst travertines from the Faber quarry presented $\delta^{13}C$ signature lightly enrichment only in the caliche facies, and also a negative range for $\delta^{18}O$.

DISCUSSIONS

MORPHOLOGY OF THE ACTIVE DEPOSITS

The most notable difference in an outcrop scale of tufa and travertine refers to the size of the deposits. For purposes of comparing active deposits, we decided to use in this topic the current Pamukkale deposits, which are also located in the

Denizli Basin, northwest of the Faber quarry. Capezzuoli et al. (2014) argued that the most common manifestations of continental carbonate deposition are terraces, soft sloping surfaces that cover several square kilometers, either in hot springs or in tufa terraces composed of lacustrine, paludal, and dam deposits. This assumption is confirmed in the case of the Denizli travertine deposits; however, it does not apply to the tufa deposits of the Mimoso River. The tufa deposits in the Mimoso River occur as scattered patches in the landscape, with dozens of meters, while the Pamukkale travertine deposits occur as extensive terraces covering hundreds of meters.

The active tufa deposits of the Mimoso River present a geometry concordant with the river bed, so the width of the bed also corresponds to the width of the deposits, varying from 8.20 m to 18.60 m for the deposits of the Mimoso River, occurring predominantly as cascades, dams and pools (Figure 33A). In this system, the thickness of the deposits does not exceed ten meters due to the prograding fluvial dynamics. Tufa constructions cause an increase in the weight of newly built deposits that collapse and self-destructs. The eroded material is transported and deposited downstream as tufa lithoclasts from adjacent deposits. Thus, active tufa deposits in the Mimoso River present a cyclical formation character, for the constant flow of drainage promotes the deposition and precipitation of tufa-building sediments, and subsequent washout, culminating in the erosion of the deposits, this causes tufas to have small preservation potential in the geological record (Capezzuoli et al., 2014).

The Pamukkale travertine deposits are not limited by the river bed, but by the resurgence pulses of the forming fluid and by changes in the source area. The relief controls the geometry of the deposits (Guo & Riding, 1998). There is a huge difference between the geometry of the Pamukkale deposits and their sizes in relation to the tufa deposits studied in the Rio Formoso. In the Pamukkale system, deposits vary from tens of meters in pools and waterfalls, reaching more than a hundred meters in extension for terraces (Figure 33B). In addition, these deposits have thicknesses of tens of meters due to the vertical stacking of the precipitated layers according to the successive pulses of water, therefore, it is a constructive

system. Such deposits can present a great variation of facies laterally, unlike tufas where the variation occurs both laterally and vertically.

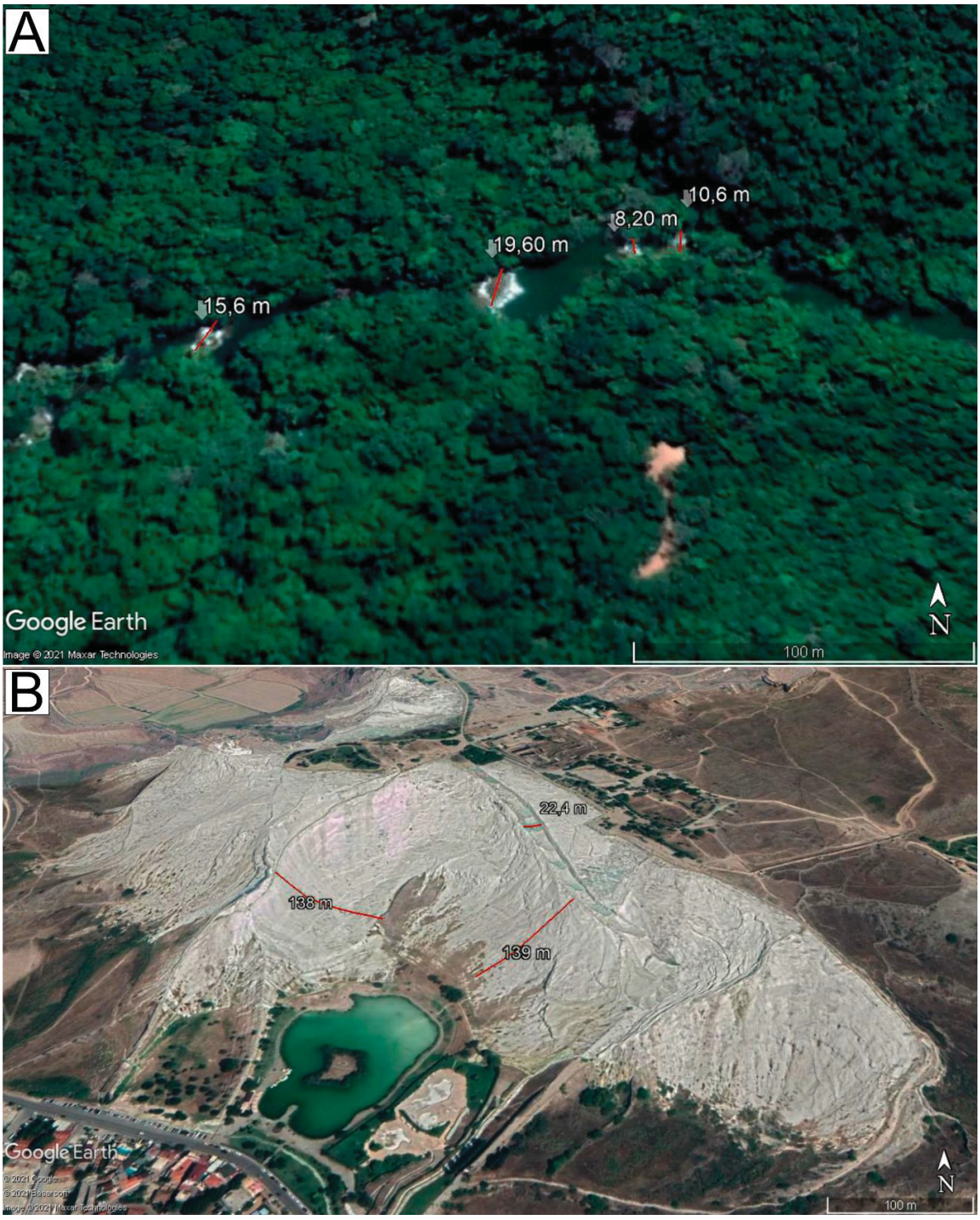


Figure 33 - Comparison between tufa and travertine active systems. Tufa deposits in the Mimoso River are controlled by the river bed geometry, showing a width of tens of meters, while the travertine deposits in Pamukkale correspond to the pre-existing relief, covering hundreds of meters in extension.

The tufas of the Mimoso River present a greater association of facies both horizontally and laterally, due to the small dimensions of the deposits compared to the Faber travertine system in Denizli, where the facies association is more common vertically. In the Mimoso River deposits, it is possible to identify, in centimetric scales, the calcification of bryophytes, forming the Phytoherm Facies, associated with the local deposition of micrite, which serves as a fixed substrate for the proliferation of aquatic insect larvae, constructors of the Bioherm Facies (Figure 34). The Denizli travertines present associations of facies laterally, but in a more spaced way, considering that the deposits have dimensions of hundreds of meters, as there is no limitation on the width of the river bed, as in the tufas. The Faber core shows a high varied vertical intercalation of facies within the 28.5 m length (Figure 35), suggesting depositional variations in the system, possibly due to the migration of the source area.

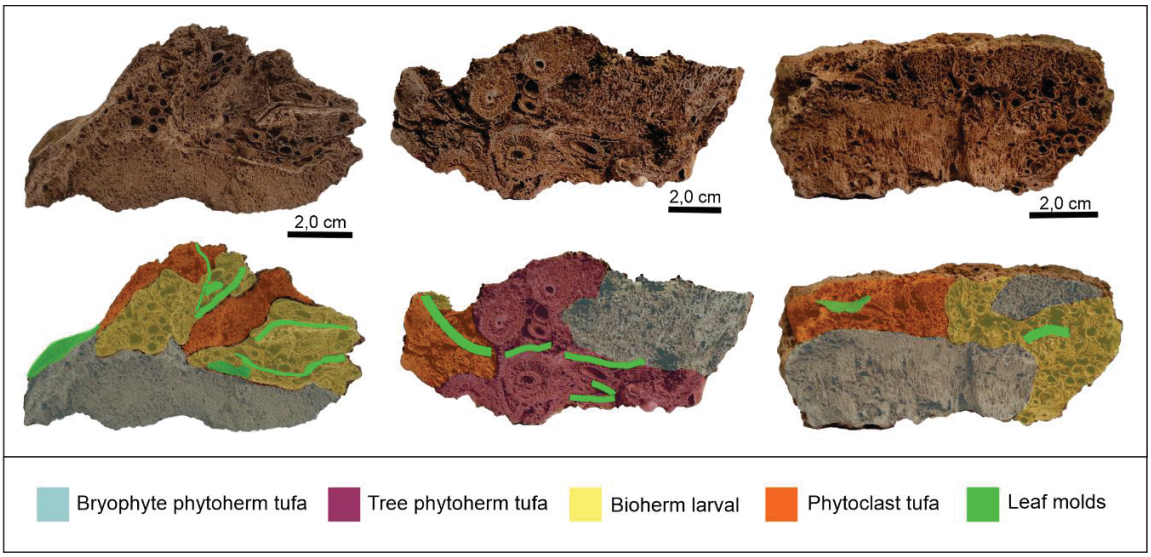


Figure 34 - Hand samples of tufas from the Mimoso River showing the massive association of facies on centimeter scales, identified in most of the collected samples.

According to Arenas-Abad et al. (2010), the tufa system might be grouped into two depositional sedimentary contexts: one in low-gradient, non-stepped fluvial, and fluvio-lacustrine conditions; another in high-gradient and stepped fluvial conditions. Both situations may exist in a single system, but one will usually be

dominant. For the tufas of the Mimoso River, the high-gradient and stepped fluvial model is suggested, which develops in rivers with steep slopes or topographical ruptures along with the longitudinal profile, with narrow transversal profiles and a limited extension of flood plains. Under these conditions, they form in tufa deposits as an agglutination of steps, occurring sub-environment with distinct facies and morphologies, such as waterfalls, cascades, dams, caves behind overhangs. In addition, Bryophyte Phytoherm Tufas are the most common buildups in cascade and dammed deposits. In relation to the proximity to the resurgence area, the tufas of the Mimoso River is arranged as the proximal and, on a smaller scale, intermediate models proposed by Capezzuoli et al., (2014). In the proximal model, carbonate deposition is a combination of physicochemical processes of supersaturation of groundwater rich in CO_2 and calcium ions, which, when flowing away from the resurgence point, promotes the degassing of CO_2 into the atmosphere, and also biomediation by biofilms and macrobiota, which is extremely important in this system, where the Phytoherm Facies are formed. On the other hand, intermediate environments has generally a lower flow velocity profile, and the colonization of biofilms and aquatic plants more effectively will encourage carbonate precipitation, such as the Algal Tufa facies.

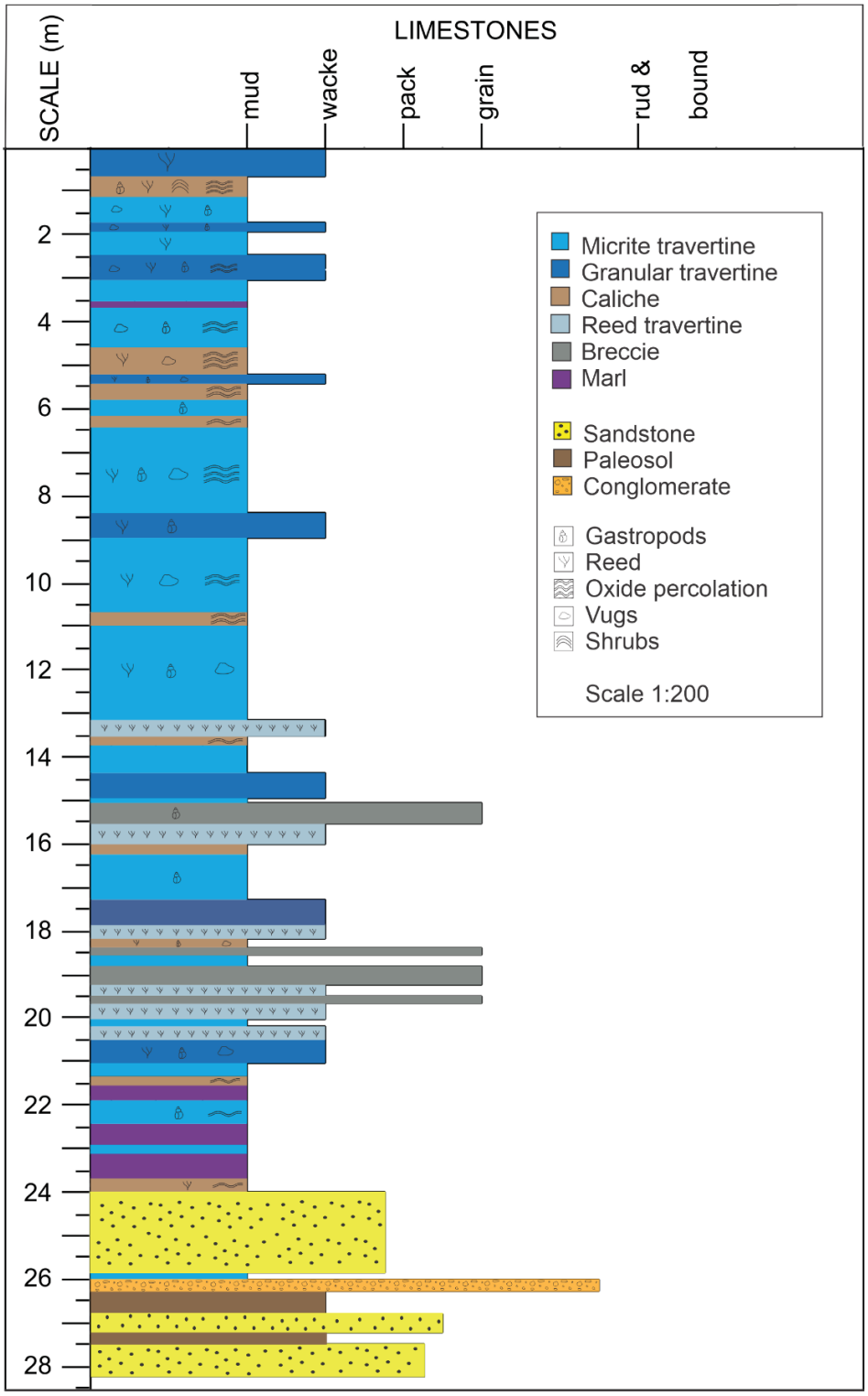


Figure 35 - Representative vertical section of the Faber core, in the scale of 1:200, showing the great intercalation of the travertine facies described in the quarry.

Based on previous studies, Capezzuoli et al. (2014) separated the travertine systems into three depositional models according to the proximity of the source area: vent environments (proximal), slope environments (intermediate), and distal environments. For the Faber quarry travertines, it is suggested that the deposits were formed in shallower conditions of sloping and distal environments. In the slope environments, thermal waters flow and cool rapidly by degassing, and the final shape of the deposits will be controlled in the short term by the morphology of the underlying relief, which will be quickly buried. The depositional facies will be products of the interactions between the pre-existing relief, the flow velocity, and the biological components, for example, reed bushes (Guo & Riding, 1998). However, due to fluctuations in fluid discharge, portions of the deposits can be exposed to sub-aerial conditions and, depending on the period of exposure, may undergo pedogenic changes (Flugel, 2010), forming brecciated sheets and paleosol horizons, as seen in the Faber quarry deposits. In the distal environments, the deposits settle on a low relief topography, where water temperature is close to the environment and there may be a mixture with meteoric water, forming configurations of paludal, shallow lakes, and alluvial plains, which will form material facies reworked and breccia (Guo & Riding, 1998).

COMPARISON BETWEEN TUFAS AND TRAVERTINES FACIES

The great variation of tufas and travertines facies are the main similarity found in these systems, as well as their associations, which reflects the dynamics of the deposition environments, but also provide great different characteristics between the systems (Table 5). Six distinct facies were recognized for both systems representing different components, fabrics, textures, porosities and biological influence.

In tufas deposits, all facies present effective influences of bacteria, algae, and avascular or vascular plants as proposed by Ford & Pedley (1996); Pedley (2009). Whereas in travertine deposits, the reed and caliche facies correspond to those with the greatest presence of organic matter, with reeds being the only vegetal example. In addition, the tufa fabrics of the Mimoso River are controlled by the framework

material, allochthonous or autochthonous, that sustains the rock, unlike the travertines which factory is probably controlled by the type of deposit, and the micritic matrix that supports the clasts of the framework.

Table 5 - Comparison of tufas from Mimoso River and travertines from Faber quarry, according to the parameters analyzed in this study, following a decreased scale.

	TUFAS OF THE MIMOSO RIVER	**TRAVERTINES OF THE FABER QUARRY**
Deposits	Cascades, dams, waterfalls, pools, and soft ramps	Terraces, soft and high-sloped ramps, cascades, pools, waterfalls
Facies	Bryophyte Pphytoherm Tufa Tree Phytoherm Tufa Algal Tufa Bioherm Tufa Laminated Tufa Phytoclast Tufa	Micrite Travertine Granular Travertine Reed Travertine Caliche Pisolith Travertine Breccia
Framework components	Bryophytes, algaes, larvae cases, and woody fragments (phytoclasts)	Massive micrite, peloids, reeds, pisoliths, and litoclasts
Biological content	Cyanobacteria, characeae algae, EPS, microphyte, macrophyte, insect larvae, diatoms	Reeds, charophyte algae, EPS, coccoid bacteria, and cyanobacteria
Organomineralization products	Soft rhombohedral calcite, filamentous remains, fossil EPS, cyanobacteria imprint, fibrous triads, nanospheres, triangular polyhedrons, microcolumns, and mucus-like structures	Nanospheres, pinnacles, microcolumns, fossil EPS, mucus-like structures, and calcite needles
Mineralogical composition	Calcite and quartz	Calcite and quartz
Main oxides	CaO, SiO_2 and traces of MgO	CaO, SiO_2 and traces of Al_2O_3
$\delta^{13}C$	-7.10 to -8.91 ‰ (VPDB)	-4.00 to 1.18 ‰ (VPDB)
$\delta^{18}O$	0.48 to -7.98 ‰ (VPDB)	-6.65 to -8.00 ‰ (VPDB)
Fluid of the active deposits	T: 24ºC pH: 8.1 to 8.5	(Pamukkale deposits) T: 35.20ºC pH: 6.67

The main difference found between tufa and travertine lithotypes is related to the presence of micrite in the rock matrix and microsparite cement. Even in the most porous Faber travertine facies, such as Reed Travertine, the micrite content in the matrix is high compared, for example, with the Bryophyte Phytoherm Tufa facies, in which the main component of the framework is also plant material. However, a similar feature was noted between these facies. The organic tissue of the plant is commonly preserved as dark filaments remains from which calcite develops as microsparite crystals (Figure 36A). In the Phytoherm Tufas of the Mimoso River there is no micrite matrix, only the microsparitic cement filling the spaces among the phylloids of the bryophytes (Figure 36B), whereas in the Reed Travertines it was noticed that sometimes occurs only the microsparitic cement (Figure 36C) or also micrite associated (Figure 36D). Reid et al. (2003) proposed that cyanobacteria commonly promote microsparite and sparite micritization from crystal edge boring. The same process was suggested by Rodríguez-Berriguete (2020) for travertines in Spain. Considering a deactivation of the Mimoso River precipitation system, it is suggested that the tufas would probably have their pores partially or totally obstructed by sparitic cement, without the increase of micrite as a rock matrix, but there could be micritization by microbial activities or else through inorganic processes in diagenesis.

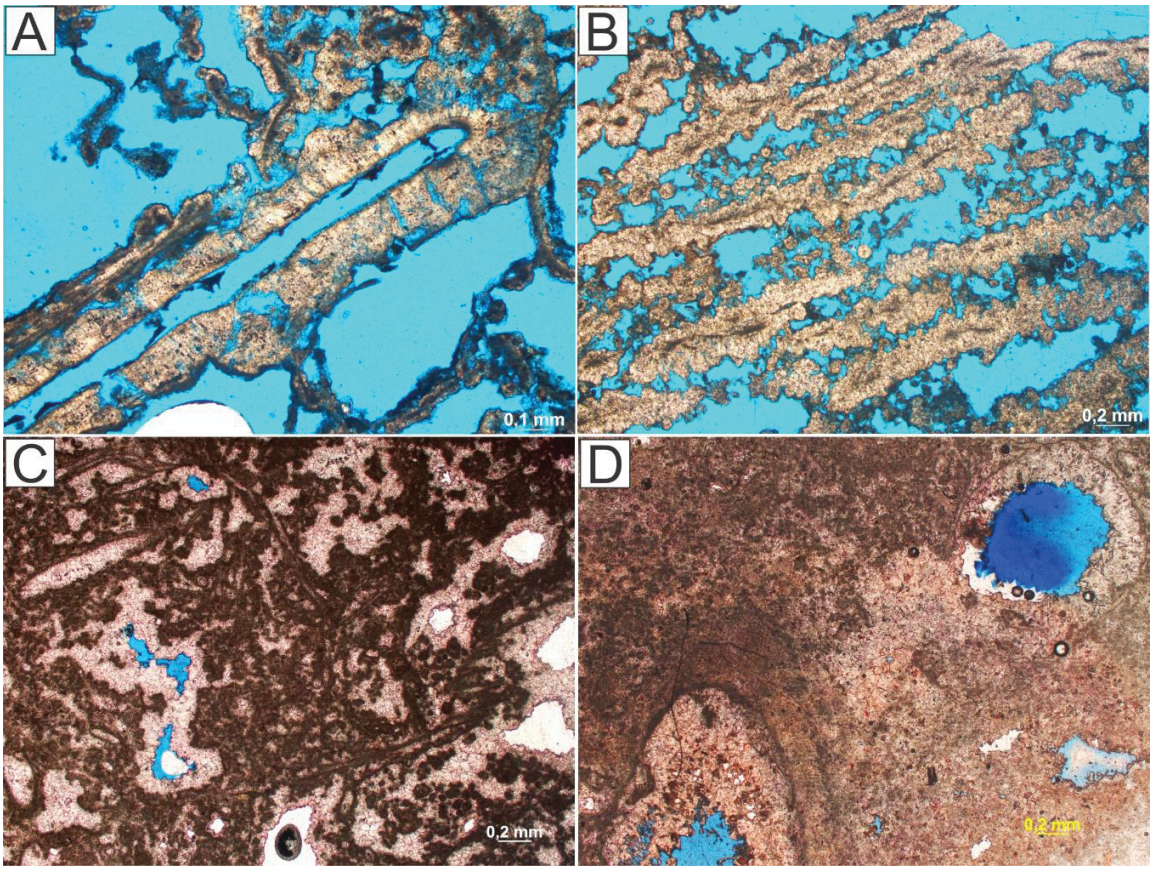


Figure 36 - Tufas from the Mimoso River showing plant material such as A) leaf mold, from which microsparite crystals grow; and B) bryophytes calcified also by precipitation of microsparite from the remaining organic filaments, slightly obliterating the porosity of the rock. Travertine facies reed from Faber quarry with C) reed and charophyte algae remain surrounded by microsparitic cement completely filling the pores; and D) travertine facies with reed mold in basal and transversal cut, partially filled with microsparite, in addition to micrite forming the rock matrix (upper left portion of the thin section).

The travertine facies have both deposited primary micrite and filling pores by micritization, ensuring lower porosity for travertines in relation to tufas. Furthermore, two types of micrites were recognized for the travertine facies: the rigid and massive micrite; and the granular peloid micrite, both precipitated in an autochthonous way, corresponding respectively to the facies Travertine Micrite and the Granular Travertine.

For the peloid micrite of the Granular Travertine Facies, Spadafora et al. (2010) argues that the peloid texture is formed by aggregates of oval nanocrystals

forming assemblages of small trigonal polyhedrons about 20 to 80 nm, corresponding, therefore, to biological origin.

The Travertine Micrite Facies described in the present work may correspond to the massive micritic fabric defined by Reid et al. (2003) for stromatolites from Hamelin Pool, Australia. The authors presented the massive micrite facies as a dense and mottled haze of light brown to reddish-brown limestone, formed by equant agglomerates with sizes of 20-50 μm, constituted by homogeneous and dense micrites. Dense micrite can graduate to a granular appearance, whose granules show degrees of micritization, and when strongly micritized they fuse with the micritic matrix and become unrecognizable. Based on observations in SEM Reid et al. (2003) showed that the growth of massive micrite can start within an organic matrix, suggesting a biologically influenced primary deposition once the initial precipitates are amorphous, a typical characteristic of carbonates formed in biological systems. However, no apparent EPS has been identified in the Travertine Micrite Facies in the Faber quarry, therefore, a biogenic origin cannot be proven. Pedley (2009) suggested that in addition to microbial biomediation, micritic mud is precipitated in the water column due to evaporation and degassing at the water/air interface, depositing on the bottom of pools.

Another distinguishing factor between the tufa and travertine systems is diagenesis. In the travertines of the Faber quarry, several diagenetic features are recognized, such as pore fillings by spatic calcite; formation of microsparitic cements; dissolution; percolation of oxides and vadose silt and geopetal structures, suggesting pedogenetic processes described by Flugel (2010). Such features are not registered in the tufas of the Mimoso River, since this system is in an active context of precipitation, while the Denizli travertines have already been buried and several facies have undergone eodiagenesis processes. It is suggested, however, that an initial diagenetic process occurred immediately after the deposition as shallow burial (Rodríguez-Berriguete, 2020), not being able to obliterate the original features of the rock.

Symmetrical cements forming borders around the pore walls were identified in all facies of the Faber travertines, as the most common being dog-tooth crystals

(Figure 37AB) and fibrous to acicular (Figure 37CD), arranged perpendicularly to the pore walls; and equidimensional calcite mosaic (Figure 37EF). Rodríguez-Berriguete (2012) reported the same occurrences of cement in travertines of the Canary Islands, Spain. The author suggests that fibrous to acicular cement are initially composed of aragonite and subsequently neomorphised to microsparite, through the thickening of primary fibrous crystals into shrubs and crusts consisting of radially grown fibers. The Tree Phytoherm Tufa facies from Mimoso River showed, incipiently, thick radial calcite crystals form shrub structures (Figure 38A) and radial fiber crusts growing from the organic plant substrate (Figure 38B). Rodríguez-Berriguete (2012) also argues that micrite-to-microsparite aggregation neomorphism usually occurs in low-slope sub-environments to fluvial and perched cascades, hence, it can occur in both tufas and travertines, once according to Pentecost (2005) the neomorphism is controlled by the stability of the mineral phases and the size of the crystal as well as the availability of water.

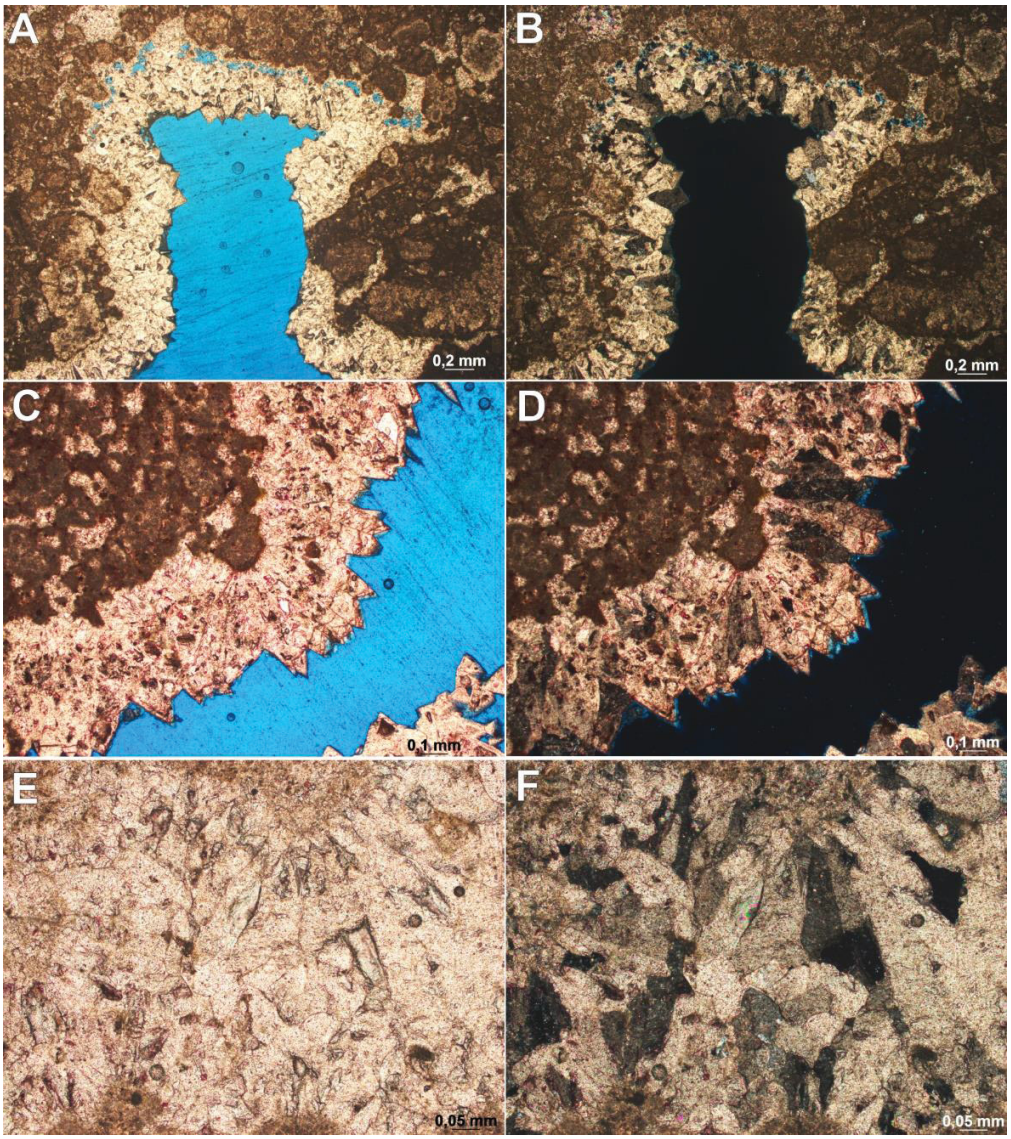


Figure 37 - Types of cement in the Faber travertine facies. A) dog-tooth cement, in which equant calcite crystals grow perpendicular to the pore wall surface, in plane-polarized light; B) image with crossed polarizers; C) fibrous to acicular calcite cement partially filling pores of the Travertine Reed Facies, in plane-polarized light; D) image with crossed polarizers; E) pore completely filled with mosaic-type cement, in Granular Travertine Facies, in plane-polarized light; F) image with crossed polarizers.

Chafetz & Guidry (1999) defined three types of shrub structures according to genesis: *bacterial shrubs*, those that have the typical dendritic shape of woody shrub or bush; *crystal shrubs*, those with regular geometric patterns; and *ray-crystal crusts*, for those formed by crystalline calcite fans. The shrub structures described in the Tree Phytoherm Tufa facies correspond to ray-crystal crusts, while the structures

identified locally in the Caliche Facies of the Faber travertines correspond to bacterial shrubs (Figure 38CD). For Chafetz & Guidry (1999) bacteria act as catalysts in the mineral precipitation of bacterial shrubs, while ray-crystal crusts may be associated with the presence of organic matter, however, an environment with high supersaturation is necessary for their formation. Erthal et al. (2017) suggested that shrub structures form in flooded and very shallow environments, in flat areas with a slight slope. The occurrences of bacterial shrubs in the Caliche Facies corroborated this premise, as Ozkul et al. (2002) demonstrated that Denizli travertines with shrub facies develop in depression depositional environments, such as marsh-pools and flat sub-environments. In the case of tufas of the Mimoso River, shrubs occur in the Tree Phytoherm facies, which receive percolation of supersaturated water, in sub-aerial areas at the edges of the waterfalls, so that precipitation is probably controlled by physicochemical processes, justifying the development of shrubs of the type ray-crystal crusts.

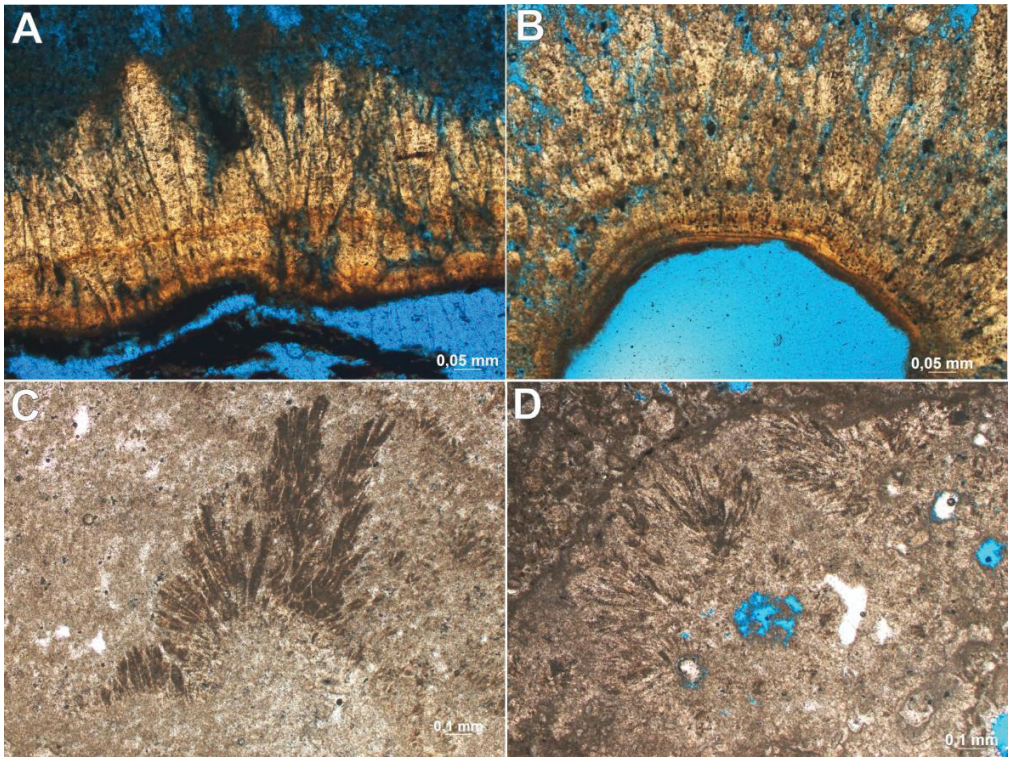


Figure 38 - Occurrences of shrub structures in tufas and travertines of the present study. A-B) examples of tree phytoherm tufa facies shrubs in the Mimoso River as ray-crystal crusts, in which the radial development of the crystals takes place on remain organic matter; C-D) in Faber travertines

only the Caliche Facies present the incipient occurrence of bacterial shrubs, with precipitation mediated by microbes.

Another common diagenetic feature in travertine is dissolution, which occurs due to the presence of subsaturated water of different compositions, for example, vadose and phreatic, producing vugs in the matrix and cement or dissolving intraclasts (Rodríguez-Berriguete, 2012). In all the facies of the Faber travertines, dissolution features of size from micrometers to millimeters were recognized. Pentecost (2005) suggests that the decomposition of organic matter of plant origin is one of the processes commonly responsible for carbonate dissolution, as seen in the Reed Travertine Facies.

Diagenetic features in the Faber travertines suggested a high fluid circulation through the rock pores, forming symmetrical cement, thus it is inferred that in an active travertine system, the facies porosity is as high as in the Mimoso River's tufa system.

The presence of the Bioherm Tufa Facies is a peculiarity of tufas in the Mimoso River in relation to the travertines of the Faber. Drysdale et al. (2003) argue that these constructions are related to the development of the insect and its ecological behavior, that is, whether the construction of the cases was for predation, housing, or feeding. Aquatic insects at immature stages may live freely, attached to the substrate or inhabiting retreats that can be portable cases or anchored to the substrate (Drysdale, 1999). According to this author, case-building insects in tufa deposits are predominantly associated with three families: *caddisflies* (Trichoptera), *midges* (Diptera), or aquatic *moths* (Lepidoptera). Each family has distinctive characteristics of larval constructions. For the tufa deposits of Mimoso River, we suggest that the bioconstructions of larval cases correspond to those formed by *caddisfly insects* of the Trichoptera family. As described by Ahmed et al. (2018), the larval stage of the caddisflies live fixed in the substrate (Figure 39AB) and their cases are densely compacted (Figure 39C) and, occasionally arranged transversely to the water flow, forming a spare volume in the tufa deposit (Figure 39D). Furthermore, the fixed tubes of the caddisflies are interpreted as the larval dwelling and feeding retreats, composed of sediments and organic debris welded together by silk and

anchored in the substrate. Leggit & Cushman (2001) described similar structures in the Green River Formation, USA, attributed to caddisflies, and proposed that larval retreats are a stable substrate for microbial communities to settle and contribute to the calcification of cases through biomineralization. The constructions of these aquatic larval insects present an important contribution to the formation of tufa deposits, as it increases the primary porosity and the deposit accumulation rate, in addition to the constructions physically interrupting the water flow, thus increasing the local turbulence and promoting a greater loss of CO_2 by degassing and accelerating carbonate precipitation (Carthew et al., 2002; Drysdale et al., 2003).

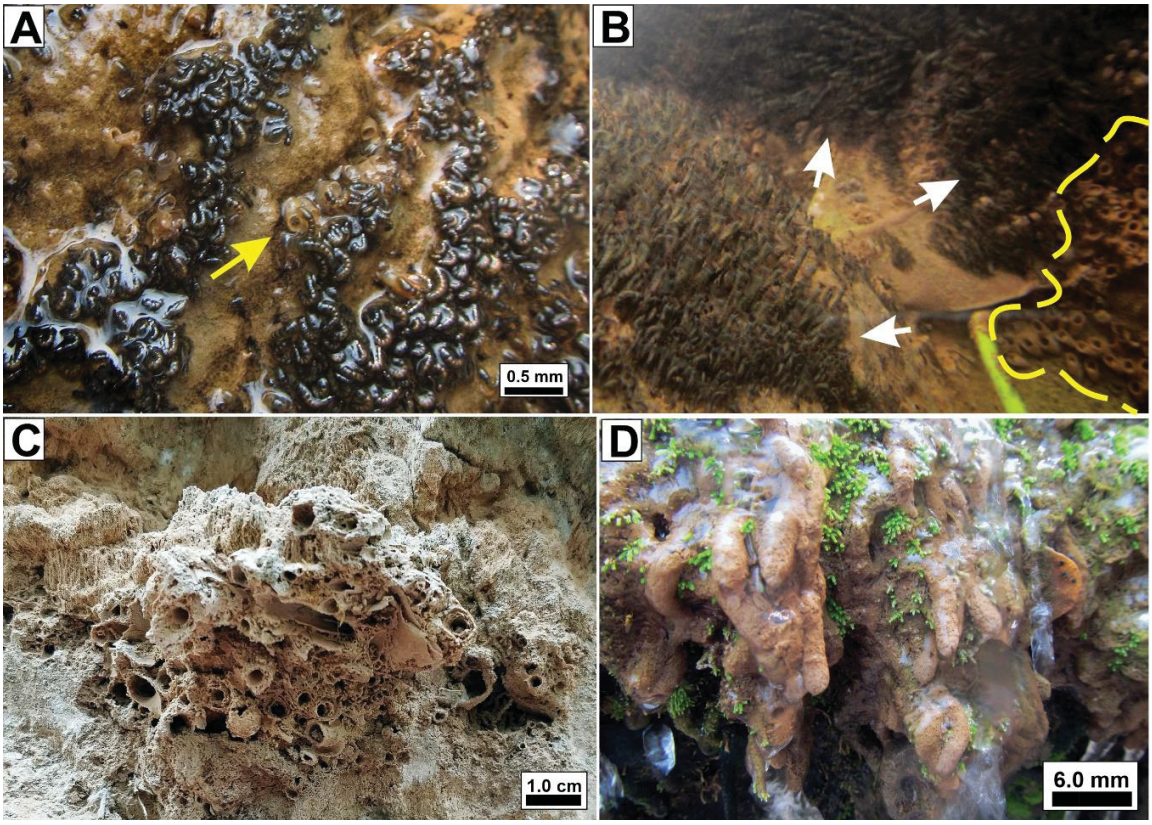


Figure 39 - Bioherm Tufa Facies of the Mimoso River. A-B) aquatic insects in their immature stage as larvae that live fixed in the substrate, the yellow arrow indicates the beginning of the construction of a single larval case; the white arrows show the dense community of larval insects living fixed and submerged in waterfalls, with emphasis on cases in early stages of formation in the area demarcated with a dashed line; C) inactive deposit in the Mimoso River with densely compacted Bioherm Tufa; D) active occurrence of Bioherm Tufa in waterfall showing a spare arrangement.

ORGANOMINERALIZATION PROCESSES AND ITS INFLUENCE IN THE TUFAS AND TRAVERTINES MICROFABRICS

The tufas and travertines in the present study showed a wide variety of microfabrics associated with biologically influenced precipitation, closely associated with EPS. Manzo et al. (2012) demonstrated through a biologically influenced mineral precipitation experiment in tufas of southern Italy, that neoformed crystals in an organic matrix, usually EPS, present four successive precipitation scales with their respective features: a) subspherical nanocrystals; b) polyhedral and fibrous triads; c) tetrahedrons; and d) microcolumns. Pedley et al. (2009) recognized nanospheres as the first product of organomineralization, which are developed in clusters composed of micropeloids in tufas. Nanospheres coalesce early to form crystal aggregates that represent the building blocks of microcolumns and pinnacles (Manzo et al., 2012), which in turn will coalesce to form larger structures, such as fibrous triads and polyhedral microcrystals. However, for the development of larger crystals such as tetrahedrons and microcolumns, a great production of organic matrix is necessary (Pedley, 2014), so that the presence of certain types of neoprecipitates may suggest conditions with more or less organic matrix (Manzo, 2012).

The variation of well or poorly-developed crystals, neoformed closely associated with EPS, may also be related to the fluid flow velocity, as suggested by Pedley & Rogerson (2010) based on laboratory experiments. According to the authors, in the initial development of crystals through the aggregation of nanospheres in fast flow and in autumn, a random stacking of nanospheroids is observed, with incipient development of rhombic crystals. While in slow flow development and summer conditions, nanospheres form micropeloids that clump together to form well-formed calcite rhombohedrons associated with dehydrated EPS.

In the tufa facies of the Mimoso River, the presence of EPS associated with filaments has been identified in all samples analyzed. Manzo et al. (2012) observed that EPS substrates of live cyanobacteria commonly mineralize through polyhedral

microcrystals and fibrous triads. Both, in the bioherm tufa facies, and in the Bryophyte Phytoherm Tufa, subhedral to euhedral neoformed crystals have been identified, in the form of well-defined carbonate rhombohedral crystals. In this case, the crystals present inner structures of smaller tetrahedrons, corroborating the hypothesis that the precipitation process in an organic matrix happens with the junction of smaller crystal until forming larger neoformed crystals (Figure 40A). Dupraz et al. (2009) reported that, carbonate organocrystals with morphology resembling smooth rhombohedra, are the final products of physico-chemically forced precipitation in an EPS matrix, with or without the presence of bacterial cells (Figure 40B).

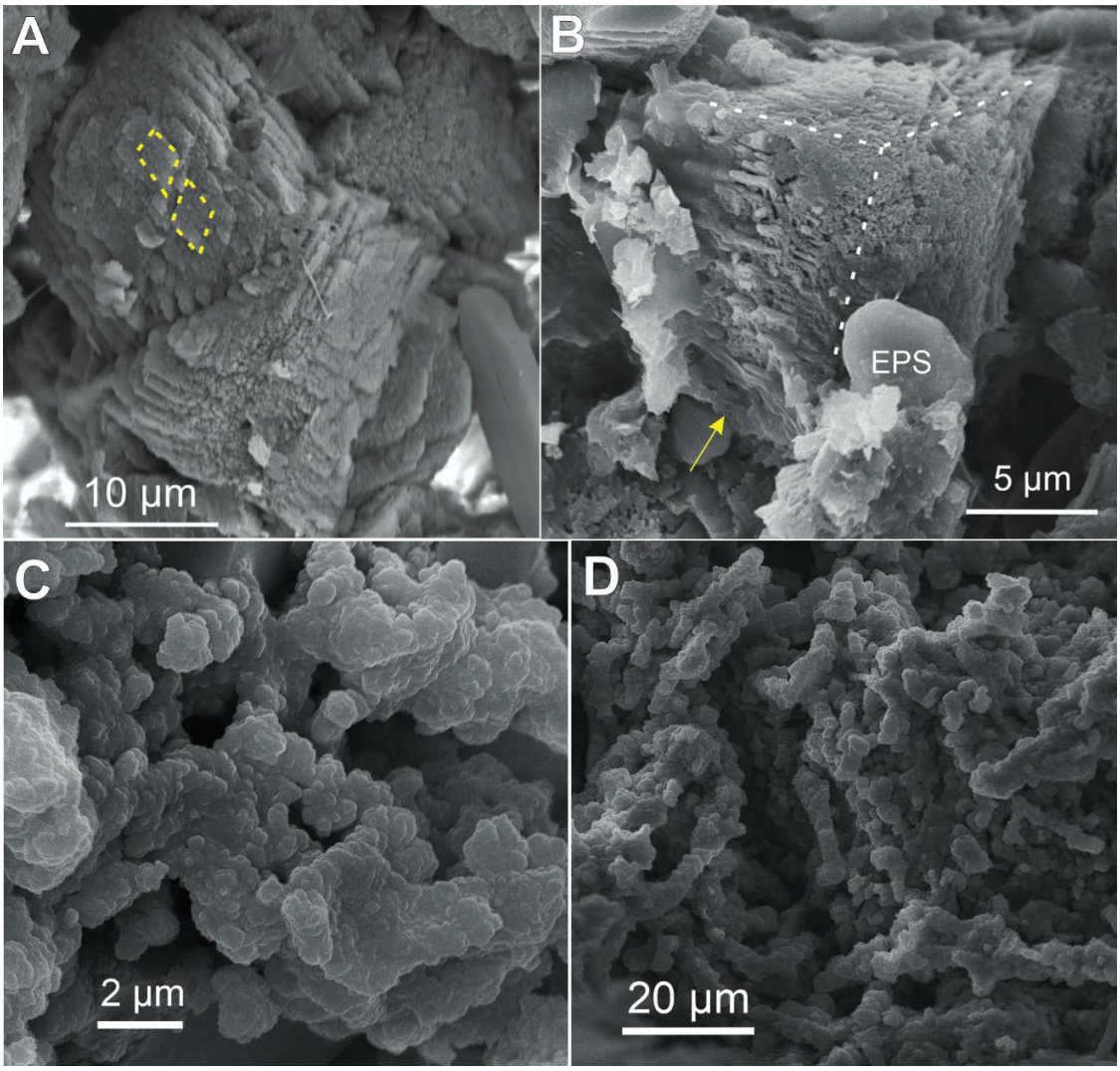


Figure 40 -Comparison of the main organomineralization products of the tufas and travertines facies. A) gentle rhombohedral calcite formed in Bioherm Tufa Facies, showing tetrahedrons (highlighted) as a remnant structure of grain coalescence; B) neoformed crystal in Bryophyte Phytoherm Tufa Facies, in which, despite being large, it is not well developed as a polyhedron; highlighting the association of EPS and filaments (yellow arrow) around the crystal; C) calcite nanospheres in caliche facies, as the initial product of organomineralization in an organic matrix; D) pseudo fibrous triads neoformed by the coalescence of nanospheres also in the travertine Caliche Facies, but without forming larger crystals.

Nanostructures called pinnacles by Manzo et al. (2012), neoformed by the coalescence of carbonate nanospheres, were identified in the Bryophytes Phytoherm, Trees Phytoherm and Bioherm Tufa Facies. The morphologies of the neoprecipitated nanocrystals are related not only to the content of the organic matrix, but also influenced by seasonal environmental change (Manzo et al., 2012). These

authors demonstrated that abundant precipitates of polyhedral microcrystals were observed in the coldest season; during the intermediate seasons they are gradually replaced by short triads and finally by long triads in warmer conditions.

In addition to biologically influenced mineral precipitation, as occurs excessively in the Bioherm Tufa facies, another form of biogenicity involved in the mineral precipitation process were identified in the Mimoso River tufa system: the biologically induced mineralization, as evidenced especially in the Algal Tufa facies. In this case the Characeae algae alkalinize the system through their effective photosynthesis, and the organic material of the algae itself serves as a substrate for mineral precipitation to occur (Dupraz et al., 2009).

For the Faber travertines, only the Reed Travertine Facies presented well-developed crystals in the final stages of rhombohedral calcite. In the Reed Travertine, as in the Phytoherm Tufa Facies, organomineralization products such as polyhedrons and fibrous triads coalesced to form larger tetrahedron crystals, and the stages of this biomineralization have been recognized in the internal structures of the newly formed crystals. The rich content of EPS in Reed Travertine is probably related to the massive plant presence of reeds and also charophyte algae, since the preservation of tallus and the reproductive structure of these algae have been identified, as well as filament remains and fossilized EPS.

Meanwhile, the Caliche Facies presented only initial organomineralization products (Figure 40C), linked to less EPS conditions, such as nanospheres and pseudo fibrous triads that disperse without forming larger crystals (Figure 40D). The formation of the Caliche Facies, as discussed above, is linked to diagenetic processes and water level fluctuation, therefore, providing time for the development of EPS-producing microbial communities. Based on an experiment with calcite precipitating biofilms in freshwater. Pedley (2014) found low viscosity EPS in small cloud-like bodies, associated with coccoid bacteria as bean-shaped clusters. However, similar structures were identified in the Caliche Facies of the Faber travertines, possibly suggesting that the fluid temperature during the formation of this facies was already close to the depositional environment temperature.

In fluvial systems, such as in the tufas of the Mimoso River, cyanobacteria and algae are the most important EPS producers, therefore they are the organisms responsible for creating microenvironments favorable to carbonate precipitation (Arp et al., 2001; Arenas-Abad et al., 2010). Nevertheless, exclusively in the Bioerma Tufa Facies, larval cases calcification occurs by mineral growth in the silk itself that forms the case walls, suggesting this as the organic matrix of organomineralization. It is visible that the case layers are composed of grains of gently rhombohedral calcite. The SEM images show that this facies is the one with the highest organic content. There are localized filaments associated with EPS, but the pervasive presence of diatom microfossils associated with Bioherm Tufa is notable. Underwood et al. (2004) demonstrated that diatoms are efficient producers of EPS, thus, we suggest that the contribution of EPS as an organic matrix from diatoms further favored the high organomineral development of this lithofacies.

In the active carbonate precipitation systems, factors such as the water saturation index and hydrodynamic conditions may influence the size and morphology of newly precipitated calcite crystals (Arenas-Abad et al., 2010). Normally, according to that study, well-developed rhombohedral calcites happen biologically induced, close to the source area where the saturation index is low; in contrast, the formation of crystals of more varied and smaller shapes is linked to a high saturation index located further downstream from the source. We hence suggest that the Mimoso River tufa system has a more proximal characterization, while the Faber quarry travertines are in a more distal context.

GEOCHEMICAL CONDITIONS OF THE TUFAS AND TRAVERTINES FORMATION

Both in tufa and travertine systems, the mineralogical composition corresponds only to two mineral phases: calcite between 87 to 100% in tufas, and between 88 to 100% in travertines; and quartz, ranging from 0 to 13% in tufas, and from 0 to 12% in travertines. The XRF results are compatible with the mineralogical composition, so that the large amount of CaO and SiO_2 correspond, respectively, to

the massive presence of calcite and quartz. The MgO identified in the tufa samples is in low quantity, but due to the Ca/Mg ratios, temperature and the carbonate saturation index (Manzo et al., 2012), its content was not enough to change the mineral chemistry and form carbonate mineral phases different from calcite. Furthermore, SiO_2 in the travertine system is related to Al_2O_3 to form clay minerals associated with pedogenesis processes, considering that the highest content of Al_2O_3 recorded in Faber travertines was in the breccia facies.

In continental carbonate systems, a low-Mg content is expected, showing no marine influence in these environments (Flugel, 2010). Boggiani et al. (2002) propose that the source of Ca and Mg ions that form the Serra da Bodoquena tufas is the underlying carbonate rocks of the Corumba Group (Neoproterozoic III). The probable sources of silica in this system are detrital quartz, transported by drainage or even associated with flood events; siliceous diatom shells; and pedogenic processes associated with infiltration of vadose silt (Oste et al., 2018). Whereas the source of calcium carbonate, SiO_2 and Al_2O_3 for the Denizli Basin travertines are the Neogene basement rocks, which consist of the Menderes Massif composed of marbles and schist, (Ozkul et al., 2002).

The isotopic values presented in this study, both for tufas and for travertines, corroborate the values obtained by previous works in the same regions. Arenas-Abad et al. (2010), showed that common isotopic values of tufas in fluvial systems are between -4 and -12 ‰ (VPDB) for $\delta^{13}C$, and between -8 and -5 ‰ (VPDB) for $\delta^{18}O$. Oliveira et al. (2017) reported the isotopic compositions of Serra da Bodoquena tufas of Pleistocene and Holocene ages, ranging between -9.26 ‰ and -1.39 ‰ (VPDB) to $\delta^{13}C$, and between -9.44 ‰ and -4.20 ‰ (VPDB) to $\delta^{18}O$. Oste (2017) analyzed the isotopic values of tufas from two locations in Bonito: for the Taika site the values found were -7.33 to -8.57 ‰ (VPDB) for the $\delta^{13}C$, and -6.52 to -8.42 ‰ (VPDB) for the $\delta^{18}O$; while at Estância Mimosa the values ranged from -6.16 to -9.52 ‰ (VPDB) for $\delta^{13}C$, and -6.35 to -9.05 ‰ (VPDB) for $\delta^{18}O$.

The isotopic values $\delta^{18}O$ presented here for the tufas of the Mimoso River, -7.02 to -7.98 ‰ (VPDB), are slightly depleted in $\delta^{18}O$ isotope and enriched in $\delta^{16}O$, corresponding to the isotopic signal of meteoric water in the Bonito-Campo Grande

region, of -7.36 ‰ (VPDB), as presented by Paula (2012). Occurrences of tufas in the Denizli region of Turkey were analyzed by Ozkul et al. (2013), with values ranging from -2 to -12 for the $\delta^{18}O$. Therefore, it is suggested that the fluid that forms the tufas of the Mimoso River comes from the recharge of the system by meteoric water, as it is a hydrologically open karstic system, with high rates of evaporation or degassing of CO_2 (Andrews, 2006).

Regarding the $\delta^{13}C$ values of the Mimoso River tufas, -7.10 to -8.91 ‰ (VPDB), it was demonstrated by Schidlowski (2000) that negative trends of $\delta^{13}C$ may be associated with the photosynthetic processes or also with the influence of superior plants (C3 plants) on the ground. This could suggest that in the tufas of the Mimoso River, photosynthesis is massively produced by the action of cyanobacteria and bryophytes, but with a high influence of trees biodiversity, including C3 plants, since the metabolism of fixation of this type of plant presents calcites with $\delta^{13}C$ values below -8 ‰ (VPDB) in a temperate climate (Andrews, 2006). Oliveira et al. (2017) argued that the mean values for Pleistocene tufas of the Bodoquena region are more negative than Holocene samples, possibly due to increased rainfall and vegetation in the more recent period. However, Chen et al. (2004) divided the effects of macro and microorganisms associated with the formation of tufas into physical and chemical ones: the physical effects do not result in the supersaturation of calcite in the water, for instance, as encrustation, trapping and binding, assimilation, nucleation and secretion of crystals; while chemical effects remove CO2 from the water and cause supersaturation, like photosynthesis. Chen et al. (2004) found through experiments that the consumption of CO_2 by organisms is much lower than the CO_2 lost by degassing in waterfalls, and therefore suggest that organisms such as bacteria, algae, macrophytes and microphytes cannot be the main cause of the formation of tufas in turbulent flow and high-velocity environments.

The isotopic results of Faber travertines are within the range expected for the Denizli Basin travertines. Ozkul et al. (2013), based on the comparison of occurrences of quaternary travertines in Denizli, defined $\delta^{13}C$ values between -1.0 to 10 ‰ (VPDB) as the standard for that region. Oste (2014) found values between -7.41 to -8.74 ‰ (VPDB) for $\delta^{18}O$ and -1.3 to 0.71 ‰ VPDB for $\delta^{13}C$, in the Çinkaya

quarry; França et al. (2017), analyzing the travertines of the Simersan quarry, found values of $\delta^{18}O$ between -6.6 to -8.9 ‰ (VPDB), and for $\delta^{13}C$: -2.4 to 2.4 ‰ (VPDB). The values of $\delta^{13}C$ in Faber travertines vary from -4.00 to 1.18 ‰ (VPDB), however, only the Caliche Facies presents values depleted in $\delta^{13}C$, ranging from -1 to -5 ‰ (VPDB), probably associated with the concentration of ^{12}C by the action of microorganisms as a function of photosynthesis, which justifies the higher organic influence on carbonate precipitation in this facies, as seen in SEM structures.

Forizs et al. (2011), presented the value of -9.5 ‰ (VPDB) as a standard for the $\delta^{18}O$ of meteoric water in the Denizli locality. The $\delta^{18}O$ values of the Faber travertines presented here, -6.65 to -8.00 ‰ (VPDB) are slightly more positive than the value proposed by Forizs et al. (2011), suggesting that it is not a purely meteoric fluid. Gandin & Capezzuoli (2008) exposed stable isotopic data obtained from calcite precipitated from warm or thermal waters, where the $\delta^{18}O$ ranges from -4 ‰ to -30 ‰, suggesting an influence of high temperatures and water supersaturation levels; while the typical range of -2 ‰ to +8 ‰ of values of $\delta^{13}C$, is interpreted as a reflection of meteoric origin and partly of recycled juvenile geothermal or magmatic provenance. Rodriguez & Fauth (2013) demonstrated that warm water carbonates tend to incorporate the lighter oxygen isotope. Hence, it is suggested that the fluid which formed the Faber travertines was meteoric water heated through infiltration by fractures and faults, generating a thermometeogenic fluid (Ozkul et al., 2013). Works such as Ozkul et al. (2013) and Van Noten et al. (2013) demonstrated that the quaternary faults and fractures that occur along the grabens are the natural paths through which meteoric water infiltrates and percolates underground, where it mixes with the hydrothermal fluid that ascends to the surface through the same fissures. The generated fluid, commonly acidic, re-emerges in the surface and, due to a decrease in temperature and pressure, loses CO_2 rapidly in the degassing process, which lowers the pH and precipitates as travertine (Ozkul et al., 2013). This process is favored by the local shallow and deep geothermal systems, which influence the high local seismicity of the Denizli Basin (Alçiçek et al., 2007).

The distributive variation of carbon and oxygen isotope values is commonly greater in travertines than in tufas, due to the wider range of temperature, degree of

circulation, volcanic or underground water sources (Gandin & Capezzuoli, 2008). While in tufa river systems, the isotopic values have a low covariance, as the $\delta^{18}O$ reflects the isotope ratio of the oxygen in the meteoric water that feeds the drainage system, reflecting more uniform climatic conditions (Arenas-Abad et al., 2010).

CONCLUSIONS

- The present study has demonstrated how continental carbonate precipitation systems are quite dynamic. The related variables encompass both, the physicochemical processes of fluvio-lacustrine dynamics, in the case of tufas, and the tectonic aspects of fault reactivation and fissures, in the case of travertines. All these factors, together with the action of organisms that influence precipitation, make these systems important producers of carbonate sediments in the context of continental deposits.
- Differences and similarities were listed for two modern tufa and travertine systems, using variables at different scales. Concerning the depositional environments analyzed, in both systems, there is a similar variation in deposits: cascades, waterfalls, dams, and pools. However, extensive terraces are associated only with travertine deposits.
- The tufa deposits of the Mimoso River have their geometries controlled by the river bed, so their sizes vary according to the width of the drainage, whereas, in the travertines of the Faber quarry, the formation of the deposits was controlled by the surge pulses of the fluid that was deposited in large areas, molding the existing pre-relief, which was later buried, as seen currently in the Pamukkale deposits.
- Six different facies were defined for the Mimoso River tufas and six for Faber travertines, however, there is no direct correlation between them, due to framework components that are different between the systems.
- Tufas have less presence of micrite in the rock matrix, whereas, in travertines, micrite is the main component in all facies, making it possible to define different types of micrite: massive, granular, and peloid. Even if the tufas are

later buried after the inactivation of this precipitation system, it is suggested that the microsparite or sparite content should increase, by diagenetic processes, therefore, the micrite may be a distinguishing feature between these two systems.

- The tufa deposits of the Mimoso River display a greater diversity of biological components compared to the travertines of the Faber quarry. While travertine facies are only associated with microbial components and reeds, tufa facies are related to microbes such as cyanobacteria, but also to algae, bryophytes, trees, woody fragments, and activities of aquatic insect larvae.
- Because the biologically influenced mineralization is linked to the presence of an organic matrix, the biological variety found in the tufas justifies this system as a more effective producer of biogenic carbonate sediments in relation to travertines. Thus, the mineral products of organomineralization are suggested as another possible distinguishing factor between these systems.
- The Bioherm Tufa facies described in the Mimoso River deposits demonstrates how biological processes can increasingly influence geological processes and their products. The formation of facies formed by the calcification of aquatic insect cases increases the porosity of the deposit, contributes to the construction of waterfalls and the degassing process, accelerating carbonate precipitation.
- Stable isotopic signals of carbon and oxygen, which have been extensively investigated in previous works, continue to be an important proxy for helping to characterize tufa and travertine deposits, especially from ancient occurrences.
- The carbonate precipitation in tufa and travertine systems is linked to the input and output of CO_2, which can be controlled either by abiotic processes, as the mechanical agitation in waterfalls, or by biotic processes, such as photosynthesis.

ACKNOWLEDGMENTS

This research was supported by the MICROBIAL Research Project Nº 2016/00141-1 (SIGITEC Process), a partnership among iLAMIR, UFPR, and PETROBRAS company, in Brazil. Special thanks to the Estância Mimosa Ecotourism team which gave all the assistance in the fieldwork.

CAPÍTULO 5 - CONSIDERAÇÕES FINAIS

A partir desse estudo de caso das tufas do Rio Mimoso, no Brasil, e dos travertinos da pedreira Faber, na Turquia, foi possível compreender como os sistemas geológicos ativos podem ser dinâmicos e correlacionáveis em diferentes escalas.

A maior escala de trabalho refere-se aos tipos de depósitos e suas morfologias. No sistema de tufas, o tamanho e tipos de depósitos está condicionado ao leito do Rio Mimoso, de modo que seus tamanhos não ultrapassam cerca de vinte metros, correspondente à largura da drenagem; enquanto que no sistema de travertinos da Bacia de Denizli, os depósitos alcançam centenas de metros, sendo dispostos ao longo do relevo acidentado até que o escoamento do fluido termine.

Em uma escala macroscópica e petrográfica foi possível delimitar seis diferentes fácies para as tufas do Rio Mimoso: *Bryophyte Phytoherm Tufa, Tree Phytoherm Tufa, Algal Tufa, Laminated Tufa, Bioherm Tufa* e *Phytoclast Tufa*; e seis diferentes fácies para os travertinos da pedreira Faber: *Micrite Travertine, Granular Travertine, Reed Travertine, Caliche, Pisolith Travertine* e *Breecia*. A principal diferença entre os litotipos de tufas e travertinos diz respeito aos componentes do arcabouço, pois nas tufas predomina o material biológico como algas, briófitas e fragmentos vegetais; já nos travertinos, encontra-se comumente micrita, litoclastos, pisólitos e fragmentos de juncos.

Em última escala, levou-se em consideração os parâmetros geoquímicos, nos quais tanto as tufas quando os travertinos apresentam uma composição mineralógica restrita de calcita e quartzo, revelando se tratar de sistemas autorreguláveis. Além disso, as assinaturas isotópicas do carbono e oxigênio demonstraram que a água meteórica possuí uma forte contribuição na recarga desses sistemas, mesmo no caso dos travertinos onde ocorre o aquecimento e mistura desta com fluidos hidrotermais.

A ampla diversidade de componentes biológicos encontrada nas tufas do Rio Mimoso sugere uma maior produção de matriz orgânica, como EPS, necessária para a precipitação efetiva de organominerais maiores e bem desenvolvidos; ao passo que a presença restrita de juncos e microorganismos nos travertinos da

pedreira Faber, demonstrou uma menor produção bioinfluenciada de minerais em detrimento da presença massiva de cristais de microesparita provenientes de processos inorgânicos diagenéticos. Portanto, sugerimos que estudos cujo foco sejam as microtexturas carbonáticas possam corresponder à escala diagnóstica de tufas e travertinos quando se trata da caracterização de reservatórios carbonáticos continentais.

Por fim, os diferentes depósitos e fácies de tufas e travertinos analisados neste estudo comprovaram que os sistemas ativos de precipitação de carbonatos continentais são altamente dinâmicos devido a intrínseca relação existente entre os parâmetros hidrológicos e geomorfológicos com a precipitação mineral, seja ela físico-química ou mediada biologicamente.

REFERÊNCIAS

Ahmed, W. B., Henchiri, M., Mastouri, A., & S'himi, N. S. (2018). Calcified aquatic insect larval constructions in the Pleistocene tufa of Jebel El Mida, Gafsa, southern Tunisia: recognition and paleoenvironmental significance. *Journal of African Earth Sciences, 140*, 256-266.

Alçiçek, H., Varol, B., & Özkul, M. (2007). Sedimentary facies, depositional environments and palaeogeographic evolution of the Neogene Denizli Basin, SW Anatolia, Turkey. *Sedimentary Geology, 202*(4), 596-637.

Almeida, F. F. M. (1965). Geologia da Serra da Bodoquena (Mato Grosso). DNPM.

Altunel, E. R. H. A. N., & Hancock, P. L. (1993). Morphology and structural setting of Quaternary travertines at Pamukkale, Turkey. *Geological Journal*, *28*(3-4), 335-346.

Andrews, J. E. (2006). Palaeoclimatic records from stable isotopes in riverine tufas: synthesis and review. *Earth-Science Reviews*, *75*(1-4), 85-104.

Arenas-Abad, C., Vázquez-Urbez, M., Pardo-Tirapu, G., & Sancho-Marcén, C. (2010). Fluvial and associated carbonate deposits. *Developments in Sedimentology*, *61*, 133-175.

Arp, G., Wedemeyer, N., & Reitner, J. (2001). Fluvival tufa formation in a hard-water creek (Deinschwanger Bach, Franconian Alb, Germany). *Facies*, *44*(1), 1-22.

Assine, M. L. (2004). A bacia sedimentar do Pantanal Mato-Grossense. *Geologia do Continente Sul-Americano: evolução da obra de Fernando Flávio Marques de*

Almeida (V. Mantesso-Neto, A. Bartorelli, CDR Carneiro & BB Brito-Neves, orgs.). Beca, São Paulo, 61-74.

Assine, M. L., & Soares, P. C. (2004). Quaternary of the Pantanal, west-central Brazil. *Quaternary International*, *114*(1), 23-34.

Boggiani, P. C. (1997). *Análise estratigráfica da Bacia Corumbá (Neoproterozoico)-Mato Grosso do Sul* (Doctoral dissertation, Universidade de São Paulo).

Boggiani, P. C. (1999). Geologia da Bodoquena: Por que Bonito é Bonito? *Nos jardins submersos da Bodoquena: guia para identificação de plantas aquáticas de Bonito e região*. (p. 83). ECOA-Ecologia e Ação.

Boggiani, P. C., Coimbra, A. M., Gesicki, A. L., Sial, A. N., Ferreira, V. P., Ribeiro, F. B., & Flexor, J. M. (2002). Tufas calcárias da Serra da Bodoquena. *Sítios Geológicos e Paleontológicos do Brasil.* 249–259.

Boggiani, P. C., Gaucher, C., Sial, A. N., Babinski, M., Simon, C. M., Riccomini, C., ... & Fairchild, T. R. (2010). Chemostratigraphy of the Tamengo Formation (Corumbá Group, Brazil): a contribution to the calibration of the Ediacaran carbon-isotope curve*. Precambrian Research*, 182(4), 382-401.

Campanha, G. A. da C., Boggiani, P. C., Sallun Filho, W., de Sá, F. R., Zuquim, M. D. P. S., & Piacentini, T. (2011). A faixa de dobramento Paraguai na Serra da Bodoquena e depressão do Rio Miranda, Mato Grosso do Sul. *Geologia USP. Série Científica*, *11*(3), 79-96.

Capezzuoli, E., Gandin, A., & Pedley, M. (2014). Decoding tufa and travertine (fresh water carbonates) in the sedimentary record: the state of the art. *Sedimentology*, *61*(1), 1-21.

Carthew, K. D., Drysdale, R. N., & Taylor, M. P. (2003). Tufa deposits and biological activity, Riversleigh, northwestern Queensland. In *Advances in Regolith: Proceedings of the CRC LEME Regional Regolith Symposia. CRC LEME, Bentley, Australia* (pp. 55-59).

Chafetz, H. S., & Folk, R. L. (1984). Travertines; depositional morphology and the bacterially constructed constituents. *Journal of Sedimentary Research*, *54*(1), 289-316.

Chafetz, H. S., & Guidry, S. A. (1999). Bacterial shrubs, crystal shrubs, and ray-crystal shrubs: bacterial vs. abiotic precipitation. *Sedimentary Geology*, *126*(1-4), 57-74.

Chen, J., Zhang, D. D., Wang, S., Xiao, T., & Huang, R. (2004). Factors controlling tufa deposition in natural waters at waterfall sites. *Sedimentary Geology*, *166*(3-4), 353-366.

Claes, H., Erthal, M. M., Soete, J., Özkul, M., & Swennen, R. (2017). Shrub and pore type classification: Petrography of travertine shrubs from the Ballık-Belevi area (Denizli, SW Turkey). *Quaternary International*, *437*, 147-163.

Claes, H., Soete, J., Van Noten, K., El Desouky, H., Marques Erthal, M., Vanhaecke, F., ... & Swennen, R. (2015). Sedimentology, three-dimensional geobody reconstruction and carbon dioxide origin of Pleistocene travertine deposits in the Ballık area (south-west Turkey). *Sedimentology*, *62*(5), 1408-1445.

De Boever, E., Foubert, A., Lopez, B., Swennen, R., Jaworowski, C., Özkul, M., & Virgone, A. (2016). Comparative study of the Pleistocene Cakmak quarry (Denizli Basin, Turkey) and modern Mammoth Hot Springs deposits (Yellowstone National Park, USA). *Quaternary International*, *437*, 129-146.

Dedavid, B. A., Gomes, C. I., & Machado, G. (2007). *Microscopia eletrônica de varredura: aplicações e preparação de amostras: materiais poliméricos, metálicos e semicondutores*. EdiPUCRS.

Della Porta, G. (2015). Carbonate build-ups in lacustrine, hydrothermal and fluvial settings: comparing depositional geometry, fabric types and geochemical signature. *Geological Society, London, Special Publications*, 418(1), 17-68.

Drysdale, R. N. (1999). The sedimentological significance of hydropsychid caddis-fly larvae (order; Trichoptera) in a travertine-depositing stream; Louie Creek, Northwest Queensland, Australia. *Journal of Sedimentary Research*, *69*(1), 145-150.

Drysdale, R. N., Carthew, K. D., & Taylor, M. P. (2003). Larval caddis-fly nets and retreats: a unique biosedimentary paleocurrent indicator for fossil tufa deposits. *Sedimentary Geology*, *161*(3-4), 207-215.

Dupraz C., Reid R. P., Braissant O., Decho A. W., Norman R. S., Visscher P. T. (2009). Processes of carbonate precipitation in modern microbial mats. *Earth-Science Reviews, 96*, 141-162.

Dutra, C. V. & Gomes, C. B. (1984). A fluorescência de raios X na Geologia. *Técnicas analíticas instrumentais aplicadas à geologia* (No. 550.84 TEC).

Erten, H., Sen, S., & Özkul, M. (2005). Pleistocene mammals from travertine deposits of the Denizli basin (SW Turkey). In *Annales de Paléontologie* (Vol. 91, No. 3, pp. 267-278). Elsevier Masson.

Erthal, M. M., Capezzuoli, E., Mancini, A., Claes, H., Soete, J., & Swennen, R. (2017). Shrub morpho-types as indicator for the water flow energy-Tivoli travertine case (Central Italy). *Sedimentary Geology*, *347*, 79-99.

Flugel, E. (2010). *Microfacies of carbonate rocks: analysis, interpretation and application*. 2nd Ed. (p. 1005). Springer Science & Business Media.

Ford, T. D., & Pedley, H. M. (1996). A review of tufa and travertine deposits of the world. *Earth-Science Reviews*, *41*(3-4), 117-175.

Fórizs, I., Kele, S., Deák, J., Gökgöz, A., Özkul, M., Baykara, M. O., & Alçiçek, M. C. (2011). Comparison of the isotope hydrogeological features of thermal and cold

karstic waters in the Denizli Basin (Turkey) and Buda Thermal Karst (Hungary). *Central European Geology*, *54*(1-2), 115-119.

Formoso, M. L. L. (1984). Difratometria de Raios X. *Técnicas analíticas instrumentais aplicadas à geologia* (No. 550.84 TEC).

Fouke, B. W. (2011). Hot-spring Systems Geobiology: abiotic and biotic influences on travertine formation at Mammoth Hot Springs, Yellowstone National Park, USA. *Sedimentology*, *58*(1), 170-219.

França, A. B., (2012). *Travertinos da Bacia de Denizli – Turquia*. Relatório de Viagem. (p. 65).

França, A. B., Bahniuk, A. M., Erthal, M., Oste, J. F., Neto, J. M. R. (2017). *Projeto Microbial - 1º Relatório Técnico, Subprojeto Turquia Poço Simersan, Bacia Denizli*. (p. 181). Relatório de Projeto de Pesquisa.

Gandin, A., & Capezzuoli, E. (2008). Travertine versus calcareous tufa: distinctive petrologic features and stable isotopes signatures. *Italian Journal of Quaternary Sciences*, *21*(1B), 125-136.

Guo, L., & Riding, R. (1998). Hot-spring travertine facies and sequences, Late Pleistocene, Rapolano Terme, Italy. *Sedimentology, 45*(1), 163-180.

Hasui, Y. (2012). Sistema orogênico tocantins. *HASUI, Y. et alli. (Orgs). Geologia do Brasil. São Paulo: Beca*.

He, X., Chen, Z. Q., Lu, Z., Li, J., Hu, W., Li, S., & Xu, Z. (2015). Exceptionally preserved caddisfly larval cases (Insecta) from the Lower Cretaceous of the Liupanshan Basin, Western China. *Journal of Earth Science, 26*(2), 192-202.

Klein, C., & Dutrow, B. (2009). *Manual de ciência dos minerais*. Bookman Editora.

Leggitt, V. L., & Cushman Jr, R. A. (2001). Complex caddisfly-dominated bioherms from the Eocene Green River Formation. *Sedimentary Geology, 145*(3-4), 377-396.

Lips, A.L., Cassard, D., Sözbilir, H., Yilmaz, H., & Wijbrans, J.R. (2001). Multistage exhumation of the Menderes massif, western Anatolia (Turkey). *International Journal of Earth Sciences, 89*(4), 781-792.

Manzo, E., Perri, E. and Tucker, M. E., (2012). Carbonate deposition in a fluvial tufa system: processes and products (Corvino Valley–southern Italy). *Sedimentology, 59*(2), pp.553-577.

Oliveira, E. C. D. (2013). *Rochas carbonáticas continentais (Quaternário) do Pantanal Matogrossense e adjacências* (Doctoral dissertation, Universidade de São Paulo).

Oliveira, E. C., Rossetti, D. F., & Utida, G. (2017). Paleoenvironmental evolution of continental carbonates in West-Central Brazil. *Anais da Academia Brasileira de Ciências*, *89*, 407-429.

Oste, J. T. F. (2014). *Quimioestratigrafia e ambiente deposicional de travertinos: estudo de caso da Bacia de Denizli, Turquia*. (Monografia de Graduação, Universidade Federal do Paraná).

Oste, J. T. F. (2017). *Caracterização geoquímica dos depósitos tipo tufa do Quaternário da formação Serra da Bodoquena, Membro Rio Formoso, MS*. (Master dissertation, Universidade Federal do Paraná).

Oste, J. T. F., Arai, M., França, A. B., Cury, L. F., & Bahniuk, A. M. (2018). Geoquímica e palinologia de tufas calcárias da região de Bonito (MS): Implicações ambientais. *Geociências (São Paulo)*, *37*(4), 733-744.

Oste, J. T. F., Rodríguez-Berriguete, Á., & Dal'Bó, P. F. (2021). Depositional and environmental controlling factors on the genesis of Quaternary tufa deposits from Bonito region, Central-West Brazil. *Sedimentary Geology*, *413*, 105824.

Özkul, M., Kele, S., Gökgöz, A., Shen, C. C., Jones, B., Baykara, M. O., ... & Alçiçek, M. C. (2013). Comparison of the Quaternary travertine sites in the Denizli extensional basin based on their depositional and geochemical data. *Sedimentary Geology*, *294*, 179-204.

Özkul, M., Varol, B., & Alçiçek, M. C. (2002). Depositional environments and petrography of Denizli travertines. *Bulletin of the Mineral Research and Exploration*, *125*(125), 13-29.

Özpolat, E., Yıldırım, C., & Görüm, T. (2020). The Quaternary landforms of the Büyük Menderes Graben System: the southern Menderes Massif, western Anatolia, Turkey. *Journal of Maps, 16*(2), 405-419.

Paula, M. S. D. (2012). *Variabilidade do sistema de monções de verão durante os últimos 1500 anos na região de Bonito-MS com base em registros paleoclimáticos de espeleotemas* (Doctoral dissertation, Universidade de São Paulo).

Pedley, H. M. (1990). Classification and environmental models of cool freshwater tufas. *Sedimentary Geology*, *68*(1-2), 143-154.

Pedley, H. M. and Rogerson, M., (2010). In vitro investigations of the impact of different temperature and flow velocity conditions on tufa microfabric. *Geological Society, London, Special Publications, 336*(1), pp.193-210.

Pedley, M. (2009). Tufas and travertines of the Mediterranean region: a testing ground for freshwater carbonate concepts and developments. *Sedimentology*, *56*(1), 221-246.

Pedley, M., (2014). The morphology and function of thrombolitic calcite precipitating biofilms: A universal model derived from freshwater mesocosm experiments. *Sedimentology, 61*(1), pp.22-40.

Pedley, M., Rogerson, M., & Middleton, R. (2009). Freshwater calcite precipitates from in vitro mesocosm flume experiments: a case for biomediation of tufas. *Sedimentology*, *56*(2), 511-527.

Pentecost, A. (1981). The tufa deposits of the Malham district, North Yorkshire. *Field Studies 5*. 365-387.

Pentecost, A. (1993). British travertines: a review. *Proceedings of the Geologists' Association*, *104*(1), 23-39.

Pentecost, A. (1995). The quaternary travertine deposits of Europe and Asia Minor. *Quaternary Science Reviews*, *14*(10), 1005-1028.

Pentecost, A. (2005). *Travertine*. Springer Science & Business Media.

Pentecost, A., & Viles, H. (1994). A review and reassessment of travertine classification. *Géographie physique et Quaternaire*, *48*(3), 305-314.

Perri, E., Manzo, E., & Tucker, M. E. (2012). Multi-scale study of the role of the biofilm in the formation of minerals and fabrics in calcareous tufa. *Sedimentary geology*, *263*, 16-29.

Plant, A. R. (2019). Biomediation of tufa formation by silk capture nets of larval Philopotamidae (Insecta: Trichoptera). *Tropical Natural History, 19*(2), 113-116.

Reid, R. P., James, N. P., Macintyre, I. G., Dupraz, C. P., & Burne, R. V. (2003). Shark Bay stromatolites: microfabrics and reinterpretation of origins. *Facies*, *49*(1), 299.

Rodrigues, G. B., & Fauth, G. (2013). Isótopos estáveis de carbono e oxigênio em ostracodes do Cretáceo: metodologias, aplicações e desafios. *Terrae Didatica*, *9*(1), 34-49.

Rodriguez-Berriguete, A. (2020). Early diagenetic features in Holocene travertine and tufa from a volcanic setting (Azuaje, Gran Canaria, Spain). *Facies*, *66*, 1-16.

Sallun Filho, W., Karmann, I., & Boggiani, P. C. (2004). Paisagens cársticas da Serra da Bodoquena (MS). *Geologia do Continente Sul-Americano*, *1*, 423-433.

Sallun Filho, W., Karmann, I., Boggiani, P. C., Petri, S., de Souza Cristalli, P., & Utida, G. (2009). A deposição de tufas quaternárias no estado de Mato Grosso do Sul: proposta de definição da formação Serra da Bodoquena. *Geologia USP. Série Científica*, *9*(3), 47-60.

Schidlowski, M., (2000). Carbon isotopes and microbial sediments. *Microbial Sediments* (pp. 84-95). Springer.

Seard C., Camoin G., Rouchy, J. M., Virgone, A. (2013). Composition, structure and evolution of a lacustrine carbonate margin dominated by microbialites: Case study from the Green River formation (Eocene; Wyoming, USA). *Palaeogeography, Palaeoclimatology, Palaeoecology, 381*, 128–144.

Spadafora, A., Perri, E., McKenzie, J. A., & Vasconcelos, C., (2010). Microbial biomineralization processes forming modern Ca: Mg carbonate stromatolites. *Sedimentology, 57*(1), 27-40.

Terra, G. J. S., Spadini, A. R., França, A. B., Sombra, C. L., Zambonato, E. E., Juschaks, L. D. S., ... & Winter, W. R. (2010). Classificação de rochas carbonáticas aplicável às bacias sedimentares brasileiras. *Boletim de Geociências da PETROBRAS*, *18*(1), 9-29.

Torres, T. G., Paranhos Filho, A. C., Teruya Junior, H., Corrêa, L. C., Garcez, A. J. S., & Copatti, A. (2006). Utilização dos dados SRTM na geração dos limites da bacia hidrográfica do rio Formoso (Bonito, MS). *Anais 1º Simpósio de Geotecnologias no Pantanal, Campo Grande, Brasil*, 11-15.

Turner, E. C., & Jones, B. (2005). Microscopic calcite dendrites in cold-water tufa: Implications for nucleation of micrite and cement. *Sedimentology, 52*(5), 1043-1066.

Underwood, G. J., Boulcott, M., Raines, C. A., & Waldron, K., (2004). Environmental effects on exopolymer production by marine benthic diatoms: dynamics, changes in composition, and pathways of production 1. *Journal of Phycology, 40*(2), 293-304.

Van Noten, K., Claes, H., Soete, J., Foubert, A., Özkul, M., & Swennen, R. (2013). Fracture networks and strike–slip deformation along reactivated normal faults in Quaternary travertine deposits, Denizli Basin, western Turkey. *Tectonophysics*, *588*, 154-170.

Van Noten, K., Topal, S., Baykara, M. O., Özkul, M., Claes, H., Aratman, C., & Swennen, R. (2019). Pleistocene-Holocene tectonic reconstruction of the Ballık travertine (Denizli Graben, SW Turkey): (De) formation of large travertine geobodies at intersecting grabens. *Journal of Structural Geology*, *118*, 114-134.

Westaway, R. (1993). Neogene evolution of the Denizli region of western Turkey. *Journal of Structural Geology, 15*(1), 37-53.

Westaway, R., Guillou, H., Yurtmen, S., Demir, T., Scaillet, S., & Rowbotham, G. (2005). Constraints on the timing and regional conditions at the start of the present phase of crustal extension in western Turkey, from observations in and around the Denizli region. *Geodinamica Acta, 18*(3-4), 209-238.

Wright, V. P. (2012). Lacustrine carbonates in rift settings: the interaction of volcanic and microbial processes on carbonate deposition. *Geological Society, London, Special Publications*, 370(1), 39-47.